NEW SUBDWARFS. VI. KINEMATICS OF 1125 HIGH-PROPER-MOTION STARS AND THE COLLAPSE OF THE GALAXY

ALLAN SANDAGE
Mount Wilson and Las Campanas Observatories, Carnegie Institution of Washington, 813 Santa Barbara Street, Pasadena, California 91101-1292
and
Department of Physics and Astronomy, The Johns Hopkins University, Baltimore, Maryland 21218

GARY FOUTS
Mount Wilson and Las Campanas Observatories, Carnegie Institution of Washington, 813 Santa Barbara Street, Pasadena, California 91101-1292
and
Astronomy Programs, Computer Sciences Corporation, Space Telescope Science Institute, 3700 San Martin Drive, Baltimore, Maryland 21218
Received 1 August 1986; revised 22 September 1986

ABSTRACT

The *UVW* velocity components and the planar eccentricities and angular momenta are calculated for 878 stars from the radial-velocity catalog of Paper V using photometric distances from data in Paper IV. An additional 247 high-velocity stars from the literature bring the total sample to 1125 stars. The kinematic data are combined with ultraviolet-excess values $\delta(0.6)$ from the photometric catalog to study again the correlations of kinematics and metal abundance among stars of high proper motion. Two Lindblad kinematic components can be identified in the data. Nearly half the sample belongs to a low $\langle V\rangle$ velocity component that lags the local standard of rest by ~ 30 km s^{-1} in its rotation about the Galactic center. Its mean velocity dispersion perpendicular to the plane is $\sigma(W) = 42$ km s^{-1} (mean scale height ~ 1 kpc), intermediate between that of the old, thin disk with $\sigma(W) \simeq 20$ km s^{-1} (scale height ~ 350 pc) and that of the halo with $60 < \sigma(W) < 115$ km s^{-1}. This component, which we identify as part of the Gilmore-Reid-Wyse *thick disk*, has an intermediate mean metallicity of $\langle$[Fe/H]$\rangle \sim -0.5$, with a range of $\sim \pm 1$ dex. Stars belonging to it can be separated out of the complete sample kinematically using velocity limits of $V > -100$ and/or $|W| < 60$ km s^{-1}. There is a strong correlation of $\sigma(W)$ with [Fe/H] for stars belonging to this disk component, varying between $\sigma(W) = 27$ and 70 km s^{-1} as $\langle$[Fe/H]$\rangle$ varies from 0 to -1.7, indicating again a chemical gradient within the first ~ 2 kpc from the plane. The second component, comprising the other half of the sample, is composed of the extremely high-velocity *halo* stars whose kinematic distribution in W is a monotonic function of metallicity over the entire metallicity range of $0 \gtrsim$ [Fe/H] $\gtrsim -4$. From the well-defined variation of $\langle|W|\rangle$ and $\sigma(W)$ with [Fe/H] for the halo sample as well as for the thick-disk component, we conclude that collapse of the Galaxy occurred in the past and that there is a metallicity gradient in the halo (as well as in the thick disk) *in situ* to at least $z \sim 20$ kpc, albeit with a wide distribution of [Fe/H] at any given height; this distribution narrows as the height increases. The galactic rotation of the halo decreases systematically from the local standard of rest value of 220 km s^{-1} (assumed) to zero as Fe/H changes from the solar value to $\sim 10^{-4}$, suggesting that spin-up occurred as the collapse proceeded. These conclusions differ from those of Norris, who finds no variation of kinematic properties with metallicity for all Fe/H values less than 1/10 the solar from a different sample. We argue in two ways that our present contrary result is not due to a kinematic selection bias in our sample, provided that our distance scale has no systematic errors *that depend* on [Fe/H]. If our distance scale is correct, our data support a picture of formation of the Galaxy as a continuous, coherent process rather than by merger of disparate parts, each with their own enrichment history. Our data from the eccentricity-angular-momentum distribution show a lack of stars with eccentricity $e > 0.5$ and angular momenta $h \gtrsim 25 \times 10^2$ kpc km s^{-1}, putting a limit of ~ 40 kpc for the apogalacticum distances of stars in our sample. This lack of stars is real, suggesting an edge to the stellar distribution near this R_{max} for the Galaxy. The escape velocity at the solar circle is estimated to be ~ 450 km s^{-1} from our data, but a more detailed analysis star-by-star near the zero-energy surface is needed to assess effects of distance errors. Because our sample was not designed to find the highest-velocity stars, this value is expected to be a *lower limit*, giving a limit on the ratio of total mass of the Galaxy to the mass inside the solar circle to be $M_T/M_{R\odot} \gtrsim 3$.

I. INTRODUCTION

The purpose of the present paper is to study again various relations found by Eggen, Lynden-Bell, and Sandage (1962, hereafter referred to as ELS) between kinematics and the chemical compositions of high-proper-motion stars. The new radial-velocity data for 878 such stars have been set out in Paper V (Fouts and Sandage 1986, hereafter referred to as FS). The *UBV* photometry from which photometric parallaxes and metal abundances can be derived is from Paper IV (Sandage and Kowal 1986, hereafter referred to as SK).

Space velocities in *UVW* Galactic coordinates have been computed and are listed for the new, 878 star sample. Literature values for an additional 247 previously studied subdwarfs bring the total sample to 1125 stars. The data available to ELS contained only 109 such stars, taken from Eggen's (1964) high-velocity catalog which lists stars with space motions larger than 100 km s^{-1} relative to the Sun.

 0004-6256/87/010074-42$00.90

Only 50 of the ELS stars had metal abundances smaller than [Fe/H] = −1.4 as measured by ultraviolet excesses of $\delta(0.6) \geqslant 0.21$, the metallicity domain which is believed to contain most of the clues to the early formation history of the Galactic halo. Our present sample contains 248 of these stars, which is an increase over the ELS sample by a factor of 5.

The present data set spans the metallicity interval from $+0.4 > [Fe/H] \gtrsim -4$ again as inferred from UV-excess values. The distribution of the $\delta(0.6)$ values is given in Table I for the total sample and for a 796 star subset with colors bluer than $B - V = 0.8$.

This same metallicity range was also covered in the ELS sample but with an important difference in the selection criteria that has a crucial bearing on the distribution of the *highest*-metallicity stars in our sample. Stars in ELS with $+0.4 > [Fe/H] > -0.6$ (i.e., $-0.1 < \delta \lesssim +0.12$) were taken from a catalog of known *low-velocity stars* (Eggen 1962), whereas the present 1125 star sample contains only stars with *high proper motion*. This selection criterion means that the ELS data contain very few stars that have intermediate kinematic characteristics, i.e., space motions less than 100 km s^{-1} but larger than the entrance requirement for Eggen's (1962) low-velocity catalog, which contains mostly stars of the old thin disk. In particular, this means that the Gilmore-Reid-Wyse *thick*-disk component (Gilmore and Reid 1983; Gilmore 1984a,b; Gilmore and Wyse 1985) was almost completely missed by ELS. Our present sample is based on proper motion alone. The catalog limit of $\mu \geqslant 0.27$ arcsec yr^{-1} here is itself small enough to include *intermediate*-velocity stars of, say 50 km s^{-1}, if the stars are closer than 40 pc (with proportional scaling for larger distances).

As the present photometric data (SK) were becoming available in the 1960s, one of the early, great surprises of the work (and not understood by us until the work of Gilmore and Wyse) was that large numbers of *high-proper-motion* stars do indeed exist with moderately high to intermediate [Fe/H] values. This was shown from the fact that many stars in the photometric catalog lie close to the lower fiducial Hyades line in the $U - B, B - V$ two-color diagram (Fig. 5 of SK). The result might, in fact, have been anticipated by recalling the HR diagram of Keenan and Keller (1953) for what they called "high velocity stars" but which, it turns out, have the intermediate kinematic characteristics similar to the Wyse and Gilmore (1986) thick disk. The spectra of the Keenan and Keller stars show only very mild line weakening and do indeed lie close to the Hyades fiducial line in the $U - B, B - V$ diagram, unlike spectra of stars in the halo globular clusters and the very high-velocity subdwarfs (cf. Roman 1957; Greenstein 1965). Gilmore and Reid (1983) and Gilmore and Wyse (1985) estimate that this Lindblad (1925a,b, 1959) intermediate kinematic component (their thick disk) comprises ~2% of all stars in the solar neighborhood.*

We show in Sec. V that this intermediate stellar population comprises nearly half of our sample. Its metallicity distribution is in the intermediate range of $0.2 \gtrsim [Fe/H] \gtrsim -1.7$ as discussed later in Sec. VI. Its Strömberg (1924, 1925) asymmetric-drift velocity relative to the local standard of rest is $\langle V \rangle \simeq 30$ km s^{-1} (a lagging rotation) corresponding to a rotational velocity of 220 − 30 ~ 190 km s^{-1}, similar to rotating bulges in other galaxies (cf. Illingworth 1977; Kormendy and Illingworth 1982; Dressler and Sandage 1983) to which the old thick disk may be connected as an outer extension (Jones and Wyse 1983). The dispersion in W for this intermediate population is also higher than for the old disk, giving, perforce, a larger mean scale height of ~1 kpc compared with ~350 pc for the old cold disk.†

The remaining half of our sample contains the very high-velocity subdwarfs of low metal abundance (stars near the upper-envelope line in the two-color diagram of SK, Fig. 5)—the halo stars that have been the main focus of this series of papers.

The plan of the present paper is to set out in the next section the basic UVW velocity data for the complete 878 star sample of Paper V. Literature data for 247 previously known subdwarfs are given in Sec. III. The Bottlinger diagrams for the total 1125 star sample are in Sec. IV. The data are analyzed in various bins of $|W|$ velocity to trace kinematics of the thick disk with height in Sec. V. With this component removed, the subsample of stars in the extreme extended Population II halo is shown in the (W,δ) diagram in

TABLE I. Distribution of metallicity of the program stars.

		All B-V		B-V ≤ 0.8	
δ range	[Fe/H]	<δ>	n	<δ>	n
≤0.01	∿ +0.25	-0.040	110	-0.044	29
0.00 to 0.09	+0.17 to -0.32	0.049	399	0.053	245
0.10 to 0.15	-0.40 to -0.82	0.124	225	0.124	183
0.16 to 0.20	-0.91 to -1.30	0.179	144	0.179	134
0.21 to 0.31	-1.40 to -2.66	0.251	199	0.250	182
≥0.32	∿ -3.5	0.375	48	0.352	23
			1125		796

*It should be recalled that this thick-disk component is not present in the base model of Bahcall and Soneira (1980, 1984), but it is required not only by the data of Gilmore and Wyse but also by the direct Basel (Fenkart 1967; Becker 1970), Edinburgh (Gilmore and Reid 1983), and Tokyo (Yoshii, Ishida, and Stobie 1987) star counts. From these data we have obtained a normalization of ~10% (Sandage 1987), for the thick disk, which is ~5 times larger than that of Gilmore and Reid.

† Throughout this paper we shall be quoting scale heights that correspond to the particular values of $\sigma(W)$. The notion is based on the theoretical expectation of the run of density $D(Z)$ of test particles in a potential, not influenced by them, which produces an acceleration perpendicular to the plane of $g(Z)$ cm s^{-1}. For a Gaussian distribution of velocities, $D(Z)$ is given later by Eq. (2) of the text, derived by many authors, including Kapteyn (1922), Spitzer (1942), Woolley (1957), Lindbland (1959), and Jones (1962), with references therein. Close to the Galactic plane, $D(Z) \sim \exp \sigma^2(W) Z^2$ whereas beyond $Z \sim 1.5$ kpc, where $g(Z) \sim$ constant, $D(Z)$ is closely exponential in Z, with the scale height varying strictly as $\sim \sigma^2(W)$.

In this paper we define the scale height h as the e^{-1} folding length *counted from* $Z = 0$. Because $D(Z)$ is *not* exponential in Z near $Z = 0$, this value of h differs from some commonly quoted values that are scaled directly as $\sigma^2(W)$. Our quoted numbers in this paper are based on the calculation of Eqs. (1) and (2) here, using the assumptions given in a following paper (Sandage 1987, Fig. 1). From the quoted paper, we adopt the following relations: for a velocity dispersion of 17 km s^{-1}, $h = 270$ pc; for $\sigma(W) = 42$, $h = 940$ pc; and for $\sigma(W) = 90$ km s^{-1}, $h = 3.2$ kpc.

Sec. VII, giving evidence for a true chemical gradient in the high halo. Using (V,W) diagrams for different δ values, and the (V,δ) diagram, again with the thick-disk component removed, we show in Sec. VIII that V_{rot} of the halo decreases monotonically as the metallicity decreases. In Sec. IV, it is shown via the (U,δ) diagram that the effect is real, not due to a bias in our kinematically selected sample. The main point is that our present sample is not biased against *high*-velocity stars relative to the Sun. We shall argue that if our distance scale is correct for all [Fe/H] values, then our result here requires V_{rot} to vary monotonically (decreasing) with decreasing metal abundance, consistent with the result in Paper II (Sandage 1969). The present data, analyzed using our distance scale, suggest that spin-up occurred as the collapse proceeds, accompanied by a concurrent progressive chemical enrichment.

From the existence of the smooth kinematic correlations, the formation of the Galaxy is seen then as a continuous coherent process rather than a merger of disparate parts, each with their own enrichment history. Most of this picture is the same as in ELS, except for the presence of a rotating bulge (the Gilmore-Reid-Wyse thick disk) that is intermediate in its metallicity distribution and its kinematic properties between the old thin disk and the halo. The presence of this component is clearly an important additional clue to the formation history of the Galaxy (Sec. XII) not contained in ELS.

II. KINEMATIC DATA FOR THE NEW RADIAL-VELOCITY SAMPLE

Galactic UVW velocities have been calculated for the 878 star sample by combining the radial velocities and the adopted proper motions listed in Table II of FS (1986) with photometric parallaxes obtained from the UBV photometry by the method detailed in Paper II (Sandage 1969) and in Paper IV (SK, Sec. IV*a*). Positive U velocity is directed toward $l = 180°$, $b = 0°$ (note the opposite sign convention from the Gliese (1969) catalog), V is positive toward $l = 90°$, $b = 0°$, and W is positive toward $b = +90°$.

The velocity results, together with other data, are listed in Table II as follows. The star name and the 1950 coordinates are in columns 1–3. If other data for the star have appeared in the earlier literature (referenced in Sec. III), an asterisk precedes the name. If no asterisk appears, the kinematic data for the star are not contained in earlier literature. The $B - V$ colors from the SK catalog are in column 4. The ultraviolet excess normalized to $B - V = 0.6$ is in column 5. The photometric distance in parsecs determined as explained in Papers II and IV is in column 6. U, V, W and their gradients in km s^{-1} pc^{-1} are in columns 7–12. The velocities are relative to the Sun, not to the local standard of rest. The total space motion, also relative to the Sun, is in column 13. The tangent of the inclination angle to the galactic plane as seen from the Sun, given by $W/(U^2 + V^2)^{1/2}$, is in column 14, and the angle itself is in column 15. The eccentricity of the galactic orbit defined by $(R_{max} - R_{min})/(R_{max} + R_{min})$ as in ELS and calculated from their Eqs. (6), (14), and (15) is in column 16. The apogalactic distances (R_{max}) in kiloparsecs and the angular momenta in units of 100 kpc km s^{-1}, again as in ELS, are in the final two columns.

III. KINEMATIC DATA FROM THE LITERATURE FOR 247 PREVIOUSLY KNOWN SUBDWARFS

Data similar to those in Table II are given in Table III for the sample of subdwarfs that is available in the literature through approximately 1982 which we have not observed in this program and which therefore do not appear in Table II. The photometry in columns 4–6 is generally the literature values rather than values from SK if there is overlap with Paper IV, although the basic source for some of them was, in fact, a preliminary version of Paper IV that was used for Papers II and III (Sandage 1969, 1981) and for some of the stars in Eggen's (1964) high-velocity catalog (and therefore in ELS).

The radial velocity from the literature is in column 8, with its Wilson (1953) quality class, if available, in column 9. The final column gives the literature sources as follows: The symbol E is for Eggen (1964), E2 is from Eggen (1978a, 1979), SY is Saio and Yoshii (1979), S2 is Sandage (1969, Paper II), S3 is Sandage (1981, Paper III), and C is Carney (1979b).

The UVW values are those quoted in the literature. We have made no attempt to recalculate them from first principles to put them on the same photometric parallax system as in Table II. However, the distances from the S2 and S3 literature sources *are* on the Table II system here because the same method was used to calculate them. Slightly different precepts were used by E, E2, and C, which will cause a systematic difference, but these are expected to be well within the errors of the distance method (SK, Figs. 5 and 6).

IV. VELOCITY DISTRIBUTIONS AND BOTTLINGER DIAGRAMS

a) Velocity Distributions

The distribution of the radial velocities and the U, V, W velocities are shown in Fig. 1 for the 878 stars of all colors in Table II. The upper left-hand panel is the same as Fig. 6 in Paper V (FS).

The distribution of U and W velocities in the top and bottom right-hand panels are each nearly symmetrical about zero. The maximum $|U|$ velocities reach $\sim$400 km s^{-1}, while only a few stars have $|W| > 100$ km s^{-1}. The distribution in U, with $\sigma(U) \sim 100$ km s^{-1}, is wider than in W, where $\sigma(W) \sim 60$ km s^{-1} for this total sample. If we were dealing with a single Lindblad kinematic group, the difference in the dispersions would indicate considerable halo flattening.

The distribution of V velocities in Fig. 1 (lower left-hand panel) shows the strong Strömberg asymmetric drift. As previously mentioned, the distribution is made from two components—the thick disk and the extreme halo. The thick disk shows as the near Gaussian distribution peaked near $\langle V \rangle \sim -45$ km s^{-1}. The halo component shows as the shoulder in the V distribution beginning at $V \lesssim -100$ km s^{-1} and ranging to ~ -600 km s^{-1}. The presence of the halo is relatively inconspicuous in Fig. 1 because the number of stars is less than half our total sample, and $\sigma(V)$ for the halo component is so large as to spread the halo V distribution thinly. Nevertheless, the [Fe/H] distribution and the $\sigma(W)$ values are so different for the thick disk and the halo components that their separate existence seems well enough established, most easily seen in the (W,V), (V,δ) and (U,δ) diagrams discussed in Secs. V–IX.

Fig. 2, similar to Fig. 1, shows the distributions of radial velocity and of the U, V, W velocities for the 247 high-velocity stars from the literature, listed in Table III. The shapes of the respective distributions differ between Figs. 1 and 2 because of the different selection criteria between the two samples. Stars in Table III generally have higher velocities than in Table II, giving all distributions in Fig. 2 broader wings.

TABLE II. Kinematic data for the 878 program stars.

NAME	RA	DEC	B-V	EX(.6)	D	U	V	W	DU/DR	DV/DR	DW/DR	S	TAN I	I	ECC.	RMAX	H
G130-42	423	275712	0.74	0.04	78	98.8	-36.8	-5.3	1.251	-0.512	-0.040	105.6	-0.05	-2.9	0.29	12.6	22.82
G131-23	444	284118	0.74	0.04	47	-38.8	-54.6	-14.4	-0.616	-0.562	-0.852	68.5	-0.22	-12.1	0.23	10.6	21.04
G30-46	538	144348	0.89	-.07	103	91.1	-84.9	-18.4	0.931	-0.676	-0.343	125.9	-0.15	-8.4	0.39	11.1	18.01
G31-26	545	-53130	0.63	0.33	129	145.7	-247.9	128.3	1.198	-1.252	-0.504	314.9	0.45	24.0	0.94	11.7	1.71
G130-48	641	250018	0.65	0.03	33	16.9	-29.8	-20.8	0.556	-0.787	-0.720	40.1	-0.61	-31.3	0.07	10.0	23.52
G131-29	653	185012	0.66	0.04	34	31.2	-40.0	25.6	1.186	-0.412	0.006	56.8	0.50	26.8	0.13	10.2	22.50
G31-36	1141	-55130	0.82	0.08	82	80.3	-42.5	-53.0	0.951	-0.696	-0.232	105.2	-0.58	-30.3	0.25	11.6	22.25
G131-45	1407	203442	0.95	0.10	42	61.8	-32.7	-3.2	1.493	-0.725	-0.125	70.0	-0.05	-2.6	0.18	11.2	23.23
*G31-41	1520	600	0.54	0.08	64	104.2	-12.7	-47.3	1.532	-0.551	-0.070	115.1	-0.45	-24.3	0.30	14.5	25.23
G131-53	1632	203418	0.62	0.02	76	-87.3	-17.6	-5.9	-1.019	0.075	-0.371	89.3	-0.07	-3.8	0.31	14.3	24.74
G131-55	1832	201842	0.96	0.03	47	41.0	-44.1	-50.2	0.775	-1.161	-0.849	78.4	-0.83	-39.8	0.16	10.3	22.89
G131-58	2003	164600	0.86	0.09	102	39.7	-124.4	-15.8	0.547	-0.858	-0.561	131.5	-0.12	-6.9	0.48	10.1	14.06
G131-59	2023	220608	0.63	0.03	32	-2.0	-58.5	-0.6	0.342	-0.933	-0.845	58.5	-0.01	-0.6	0.21	10.0	20.65
G31-46	2043	-654	0.92	0.08	43	56.7	-23.6	0.8	1.330	-0.517	-0.045	61.4	0.01	0.7	0.15	11.3	24.14
G32-16	2123	175054	0.88	0.13	40	-88.6	-60.0	47.3	-1.506	0.104	-0.527	117.0	0.44	23.8	0.35	12.2	20.50
G130-71	2402	295524	1.00	-.09	54	32.1	-68.3	-20.7	0.794	-0.867	-0.663	78.3	-0.27	-15.3	0.25	10.1	19.67
G1-4	2506	43348	0.89	0.06	67	98.4	-58.4	26.1	1.563	-0.637	-0.006	117.4	0.23	12.8	0.33	11.8	20.66
G31-55	2653	-23724	0.56	0.22	108	38.2	-155.4	-33.9	0.389	-1.341	-0.534	163.6	-0.21	-12.0	0.60	10.1	10.96
G131-71	2753	222942	0.93	0.02	34	21.5	-13.6	-42.6	0.376	-0.912	-0.775	49.6	-1.67	-59.2	0.04	10.5	25.14
G32-27	2807	184736	0.92	-.05	79	11.3	-122.2	1.6	0.455	-0.912	-0.650	122.7	0.01	0.7	0.47	10.0	14.28
G69-3	3208	254730	1.00	0.09	31	44.8	-29.5	-9.1	1.426	-0.988	-0.262	54.4	-0.17	-9.6	0.13	10.7	23.55
G69-8	3608	304442	0.63	0.12	51	-88.8	-22.9	27.9	-1.170	0.550	-0.166	95.9	0.30	16.9	0.31	14.0	24.21
*G1-9	3637	25118	0.63	0.04	28	103.8	-40.2	54.7	4.046	-0.766	0.672	124.0	0.49	26.2	0.31	12.7	22.48
G132-15	3804	395512	0.94	-.02	15	-21.3	-79.1	-20.2	0.628	-1.836	-3.015	84.4	-0.25	-13.9	0.31	10.2	18.59
G32-40	3829	185854	0.93	-.05	54	57.2	-88.5	8.3	1.298	-1.070	-0.305	99.1	0.08	4.8	0.33	10.4	18.45
G33-8	4243	164242	0.96	0.00	47	33.2	-49.0	1.7	0.847	-0.805	-0.249	59.2	0.03	1.6	0.17	10.2	21.60
G32-46	4243	140524	0.76	0.08	57	61.7	-29.6	-29.0	0.930	-0.776	-0.171	74.3	-0.42	-23.0	0.17	11.3	23.54
*G33-9	4256	164200	0.57	0.16	114	-71.2	-156.0	-47.4	-0.359	-0.925	-0.948	177.9	-0.28	-15.5	0.62	10.7	10.90
G69-21	4357	333312	0.68	0.14	78	78.9	-58.8	5.2	1.069	-0.660	0.004	98.5	0.05	3.0	0.29	11.1	20.62
G32-49	4459	142212	0.89	0.04	79	4.8	-79.0	-47.1	0.095	-0.942	-0.672	92.1	-0.60	-30.8	0.29	10.0	18.60
G70-17	4733	-44206	0.88	0.11	85	-7.0	-115.1	-43.2	-0.083	-1.357	-0.499	123.1	-0.37	-20.5	0.44	10.0	14.99
G1-28	4814	100524	0.78	0.04	79	110.3	-20.4	-8.7	1.260	-0.471	0.218	112.5	-0.08	-4.4	0.32	14.2	24.46
G1-30	4926	64124	0.52	0.23	240	-166.9	-290.0	-28.1	-0.486	-0.888	-0.683	335.8	-0.08	-4.8	0.93	13.1	-2.50
G32-56	5035	185236	0.80	0.05	47	46.0	-44.7	-20.4	0.932	-1.021	-0.352	67.3	-0.32	-17.6	0.18	10.4	22.03
G70-24	5448	-20506	0.86	0.04	42	-76.7	-13.4	27.5	-1.530	0.082	-0.399	82.6	0.35	19.5	0.28	14.0	25.16
G1-35	5456	101912	0.72	0.10	140	115.9	-156.9	-9.8	0.902	-1.016	-0.237	195.3	-0.05	-2.9	0.64	11.2	10.81
G69-36	5615	293306	0.93	0.02	90	99.9	-47.5	-18.6	0.974	-0.721	-0.053	112.2	-0.17	-9.5	0.31	12.2	21.75
G33-31	5844	145854	0.87	0.38	109	237.5	63.4	-171.3	1.236	-0.694	0.162	299.6	-0.70	-34.9	0.94	238.6	32.84
G70-31	10056	44842	0.74	0.02	169	-136.1	-154.8	-14.8	-0.613	-0.674	-0.575	206.7	-0.07	-4.1	0.68	12.4	11.02
G70-33	10121	-40718	0.54	0.19	261	236.2	-319.1	53.4	0.988	-1.126	-0.090	400.6	0.13	7.7	0.88	16.1	-5.41
*G70-35	10154	-23800	0.80	0.07	39	-52.6	-6.3	4.2	-1.207	0.004	-0.364	53.1	0.08	4.5	0.21	13.2	25.87
G2-19	10329	12630	0.60	0.13	66	31.9	-63.1	-52.0	0.330	-1.136	-0.361	87.8	-0.74	-36.3	0.23	10.1	20.19
G34-9	10530	214242	0.66	0.02	31	29.4	-58.1	12.6	1.388	-1.312	-0.206	66.3	0.19	11.0	0.21	10.1	20.69
G33-42	10620	190936	1.00	-.10	101	62.7	-96.8	-39.6	0.618	-0.961	-0.388	121.9	-0.34	-19.0	0.39	10.4	16.82
G2-25	10804	125036	0.98	0.12	190	101.3	-246.1	89.0	0.858	-0.910	-0.122	280.6	0.33	18.5	0.93	10.7	1.89
G1-50	10807	104354	0.75	-.04	56	75.8	5.4	43.3	1.359	0.103	0.763	87.5	0.57	29.7	0.24	14.7	27.04
G1-51	10817	91748	0.55	0.01	36	41.2	27.8	23.1	1.029	0.640	0.872	54.8	0.46	24.9	0.26	16.6	29.28
G2-28	10956	4312	0.95	0.02	26	-4.6	-44.8	17.4	0.236	-1.295	-0.418	48.3	0.39	21.1	0.15	10.1	22.02
G70-48	11048	-15930	0.99	0.01	45	-3.0	-48.8	-29.8	-0.144	-1.159	-0.445	57.3	-0.61	-31.4	0.16	10.1	21.62
*-2-181	11054	-20800	0.69	0.13	42	-40.7	8.8	-6.6	-0.938	0.238	-0.244	42.2	-0.16	-9.0	0.21	14.3	27.38
G33-48	11353	92142	0.58	0.12	52	47.2	-49.8	-15.3	0.829	-1.039	-0.145	70.3	-0.22	-12.6	0.20	10.4	21.52
G34-16	11355	181530	0.60	0.07	48	58.9	-27.8	2.4	1.116	-0.705	0.213	65.2	0.04	2.1	0.16	11.2	23.72
G70-51	11607	-10742	0.85	0.09	20	22.5	-38.6	-14.7	0.973	-2.066	-0.336	47.0	-0.33	-18.2	0.12	10.1	22.64
G132-73	11812	374618	0.61	0.05	37	51.3	-14.9	1.5	1.098	-0.755	0.247	53.4	0.03	1.6	0.13	11.6	25.01
G69-65	11839	310454	0.93	0.01	25	47.5	-15.1	-16.6	1.341	-1.256	-0.144	52.5	-0.33	-18.4	0.12	11.4	24.99
G71-3	12017	2712	0.72	0.12	29	-58.7	-34.0	41.9	-1.154	-0.425	-0.635	79.7	0.62	31.7	0.23	11.8	23.10
G133-10	12146	340530	0.84	0.14	106	68.9	-101.1	-33.9	0.716	-0.878	-0.373	127.0	-0.28	-15.5	0.41	10.5	16.39
G33-56	12211	181430	0.87	0.00	29	51.1	-57.8	-9.6	1.725	-2.030	-0.279	77.7	-0.12	-7.1	0.23	10.4	20.72
G72-6	12226	272530	0.75	0.39	121	148.5	-77.7	4.6	1.003	-0.802	0.187	167.7	0.03	1.6	0.48	13.5	18.73
G72-7	12240	314312	0.76	0.09	38	-92.3	-18.0	12.3	-1.373	0.729	-0.613	94.8	0.13	7.5	0.32	14.6	24.70
G70-58	12427	-2448	0.74	0.02	29	9.3	-59.0	-19.6	0.275	-2.068	-0.569	62.9	-0.33	-18.2	0.20	10.0	20.60
G72-9	12554	312106	1.00	0.01	30	47.7	-17.0	1.2	1.280	-0.910	0.312	50.7	0.02	1.4	0.12	11.3	24.80
G34-32	12620	212806	0.97	0.10	15	20.2	-25.7	-6.7	1.308	-1.753	-0.397	33.4	-0.28	-11.6	0.06	10.1	23.93
G72-12	12917	341812	0.84	0.06	77	10.4	-97.3	-54.3	0.386	-0.988	-0.900	111.9	-0.55	-29.0	0.37	10.0	16.77
G34-36	13013	232630	0.62	0.15	49	-74.2	-16.3	-16.5	-1.058	0.122	-0.843	77.7	-0.22	-12.3	0.27	13.6	24.87
G2-46	13214	4136	0.54	0.09	26	-12.4	-49.9	18.9	0.884	-1.525	-0.464	54.8	0.37	20.2	0.18	10.2	21.51
G2-47	13237	52300	0.76	0.16	77	80.0	-77.3	3.0	0.999	-1.034	0.111	111.3	0.03	1.5	0.35	10.9	18.77
G35-1	13410	242954	0.64	0.24	206	176.7	-191.7	75.2	0.998	-0.794	0.218	271.3	0.29	16.1	0.79	12.9	7.33
G2-50	13414	41224	0.50	0.20	181	3.9	-309.2	38.3	0.343	-1.473	-0.392	311.6	0.12	7.1	0.83	10.0	-4.42
G34-39	13439	245500	0.90	-.03	14	-29.1	-10.9	-3.6	-1.225	0.047	-1.143	31.3	-0.12	-6.6	0.13	11.8	25.41
G3-9	13517	100442	0.81	0.27	113	145.9	-176.0	-62.4	1.070	-1.735	-0.204	237.0	-0.27	-15.3	0.73	11.9	8.90
G3-10	13531	173430	0.81	0.00	51	51.3	-56.6	-27.6	0.797	-1.294	-0.276	81.2	-0.36	-19.9	0.23	10.4	20.84
G72-20	13534	291900	0.85	-.05	36	37.2	-62.8	-17.8	1.129	-1.646	-0.580	75.1	-0.24	-13.7	0.23	10.2	20.22
G72-21	13646	275124	0.73	0.00	28	83.1	7.3	-3.6	1.778	-0.899	0.971	83.5	-0.04	-2.5	0.27	15.3	27.23
G72-25	13852	272536	0.73	0.01	42	40.2	-43.6	-14.6	0.852	-1.138	-0.252	61.1	-0.25	-13.8	0.16	10.3	22.14
G71-27	13922	13900	0.54	0.11	61	-100.1	-33.0	34.2	-1.043	-0.165	-0.594	110.8	0.32	18.0	0.35	14.0	23.20
G34-45	14003	222212	0.90	0.34	145	-182.3	-317.5	19.4	-0.122	-1.173	-1.089	366.6	0.05	3.0	0.86	14.0	-5.25
G3-13	14014	165318	0.92	0.45	93	-70.3	-299.0	50.0	0.500	-2.167	-1.041	311.2	0.16	9.2	0.88	10.5	-3.40
G133-35	14127	441248	0.67	0.09	81	115.2	-36.8	14.9	1.066	-0.839	0.348	121.8	0.12	7.0	0.33	13.4	22.82
G94-8	14306	200330	0.78	0.00	47	17.8	-56.5	5.7	0.638	-0.984	-0.171	59.5	0.10	5.5	0.19	10.0	20.85
G133-45	14631	433124	0.54	0.23	190	-30.8	-185.2	-165.8	0.173	-0.627	-1.028	250.5	-0.88	-41.4	0.71	10.2	7.98
G3-22	14711	53218	0.91	0.04	155	-126.3	-203.4	-13.5	-0.447	-1.085	-0.686	239.8	-0.06	-3.2	0.81	11.8	6.16
G72-39	14939	360554	0.92	0.02	52	40.0	-28.6	-52.6	0.383	-0.918	-0.764	72.0	-1.07	-46.9	0.11	10.6	23.64
*G71-40	15034	-13412	0.64	0.12	23	-42.0	-17.1	-10.3	-1.562	-0.621	-0.959	46.5	-0.23	-12.8	0.16	11.9	24.79
G133-53	15334	434012	0.92	0.02	41	-73.9	-19.5	-15.3	-0.836	0.485	-0.800	77.9	-0.20	-11.3	0.26	13.3	24.55
G272-125	15412	-142518	0.38	0.09	168	223.2	26.8	98.7	1.345	0.160	0.492	242.4	0.40	22.0	0.76	50.7	29.18
G3-28	15415	112512	0.77	0.03	86	94.7	-96.7	45.2	1.201	-1.061	0.394	142.7	0.33	18.5	0.43	11.1	16.83
G133-57	15431	415006	0.72	-.01	53	48.9	-58.2	-11.1	0.942	-1.079	-0.219	76.8	-0.15	-8.3	0.23	10.4	20.68
G72-50	15611	325818	0.77	-.05	22	-11.1	-54.0	-11.8	0.511	-1.568	-1.240	56.4	-0.21	-12.1	0.19	10.1	21.10
G3-37	20023	83742	0.52	0.16	258	15.8	-293.8	-1.2	0.238	-1.041	-0.246	294.2	0.00	-0.2	0.89	10.0	-2.88
G71-55	20118	-4630	0.47	0.21	151	-122.1	-124.6	-62.8	-0.711	-0.787	-0.585	185.4	-0.36	-19.8	0.58	12.2	14.04
G72-54	20145	251036	0.74	0.04	22	-49.6	-28.1	9.9	-0.695	-0.102	-0.895	57.9	0.17	9.9	0.19	11.6	23.69
G35-24	20210	223400	0.89	-.02	46	25.2	-111.3	-27.9	0.812	-2.229	-0.852	117.5	-0.24	-13.7	0.43	10.0	15.37
G72-58	20531	280436	0.79	0.08	57	29.5	-79.9	-49.2	0.462	-1.444	-0.821	98.4	-0.58	-30.0	0.30	10.1	18.51
G72-59	20531	280418	0.88	0.03	68	29.3	-82.9	-50.1	0.396	-1.245	-0.710	101.2	-0.57	-29.7	0.31	10.1	18.21
G134-3	20534	445142	0.63	0.11	94	140.9	-49.7	-39.8	0.920	-1.069	-0.202	154.6	-0.27	-14.9	0.42	14.3	21.53
*G72-60	20538	310924	0.56	0.19	95	173.1	-12.8	-17.3	0.949	-0.825	0.426	174.4	-0.10	-5.7	0.52	20.8	25.22
G74-5	20730	293430	0.58	0.20	43	52.9	-60.6	-43.0	0.810	-1.728	-0.697	91.2	-0.53	-28.1	0.25	10.4	20.44
G134-9	20834	453136	0.93	-.02	47	-96.3	-7.0	-23.8	-1.039	0.784	-0.870	99.4	-0.25	-13.8	0.35	15.9	25.80
G134-10	20835	454124	0.89	0.00	47	38.4	-43.4	12.3	0.882	-0.862	0.237	59.2	0.21	12.0	0.16	10.3	22.16

TABLE II. (continued).

NAME	RA	DEC	B-V	EX(.6)	D	U	V	W	DU/DR	DV/DR	DW/DR	S	TAN I	I	ECC.	RMAX	H
G4-2	20840	92318	0.74	0.19	73	22.6	-84.7	-66.8	-0.002	-1.315	-0.522	110.2	-0.76	-37.3	0.32	10.0	10.03
*G4-6	21059	114236	0.56	0.18	112	57.5	-112.7	83.0	0.844	-0.835	0.352	151.3	0.66	33.3	0.45	10.3	15.23
G74-10	21211	321000	0.79	0.20	163	224.9	-340.0	59.9	1.602	-1.917	0.224	412.0	0.15	8.4	0.83	15.6	-7.50
G94-48	21234	270736	0.69	0.00	37	32.3	-48.9	-3.3	0.866	-1.326	-0.085	58.7	-0.06	-3.2	0.17	10.2	21.61
G4-9	21345	120900	0.79	-.03	29	-6.6	-48.4	5.8	0.201	-1.411	-0.379	49.2	0.12	6.8	0.16	10.1	21.66
G94-49	21404	271112	0.66	0.16	81	-174.7	-102.7	-13.1	-0.732	-0.281	-1.232	203.1	-0.06	-3.7	0.62	15.6	16.23
G4-10	21417	212012	0.62	0.14	50	66.4	-65.1	63.7	1.611	-1.126	1.023	112.7	0.69	34.4	0.28	10.7	19.99
G73-44	21756	132636	0.79	0.11	35	53.9	-18.7	-14.2	0.825	-0.888	0.360	58.8	-0.25	-14.8	0.14	11.5	24.63
G4-16	21949	151730	0.76	0.32	139	34.7	-170.0	23.5	0.488	-1.102	-0.071	175.1	0.14	7.7	0.65	10.1	9.50
G4-17	21954	181054	0.90	-.07	37	61.0	-4.6	4.8	0.978	-0.492	0.758	61.4	0.08	4.5	0.18	12.8	26.04
G73-50	22033	151118	0.68	0.04	61	60.4	30.5	35.7	0.703	0.355	0.875	76.5	0.53	27.8	0.30	17.9	29.55
G73-51	22035	151118	0.61	0.09	53	52.2	26.3	31.3	0.702	0.355	0.875	66.3	0.54	28.2	0.27	16.7	29.13
G4-19	22047	175224	0.61	0.14	173	-117.9	-234.7	-3.9	-0.041	-1.013	-0.623	262.7	-0.01	-0.9	0.90	11.5	3.03
G73-57	22323	53312	0.78	0.09	23	19.7	-20.8	43.7	1.538	-0.674	1.043	52.3	1.53	56.8	0.04	10.2	24.42
G73-58	22454	72924	0.97	0.04	42	23.2	-37.6	-45.8	-0.047	-1.111	-0.379	63.6	-1.04	-46.0	0.11	10.1	22.74
G75-15	22516	-51506	0.74	0.03	51	59.5	-11.5	19.8	1.026	-0.242	0.616	63.8	0.33	18.1	0.16	12.2	25.35
G94-70	22520	253730	0.53	0.17	71	79.2	-54.3	-34.0	0.589	-1.083	-0.093	101.9	-0.35	-19.5	0.27	11.2	21.07
G94-71	22555	173506	0.83	0.07	58	-60.5	-8.9	-39.0	-0.801	-0.032	-0.894	72.5	-0.64	-32.5	0.23	13.4	25.61
G94-72	22616	223900	0.88	0.03	37	47.0	-26.6	-45.2	0.332	-1.252	-0.472	70.4	-0.84	-39.9	0.13	10.8	23.84
G4-26	23039	75806	0.96	0.10	78	157.6	-78.6	72.3	1.752	-1.096	1.228	190.4	0.41	22.3	0.58	14.0	18.64
G74-30	23058	400448	0.60	0.21	150	72.5	-180.4	53.9	0.889	-0.960	0.224	201.8	0.28	15.5	0.70	10.4	8.46
G74-31	23058	423412	0.66	0.02	38	51.4	-37.5	-6.3	1.238	-1.617	-0.035	63.9	-0.10	-5.7	0.16	10.7	22.75
G74-32	23112	324700	0.60	0.13	109	127.9	-140.0	43.5	1.115	-1.323	0.432	194.6	0.23	12.9	0.60	11.6	12.50
*G73-67	23158	51406	0.90	0.01	48	-148.5	-63.5	-41.1	-2.118	-1.046	-2.021	166.7	-0.25	-14.3	0.58	15.5	20.15
G74-33	23249	345200	0.69	0.07	62	23.4	-64.3	-29.9	0.421	-1.007	-0.503	74.7	-0.44	-23.6	0.23	10.0	20.07
G73-70	23321	63906	0.95	-.06	8	76.5	-1.0	45.5	0.303	-0.502	7.129	89.0	0.59	30.7	0.23	14.0	26.40
G75-28	23409	-32230	0.93	-.03	22	27.6	-17.8	7.3	1.035	-0.834	0.652	33.6	0.22	12.5	0.06	10.5	24.72
G134-40	23426	434642	0.52	0.17	106	49.2	-159.0	-46.3	0.784	-1.253	-0.544	172.8	-0.28	-15.5	0.61	10.2	10.60
*G36-28	23531	303618	0.57	0.12	28	-125.0	-41.6	-26.5	-1.665	0.225	-2.595	134.4	-0.28	-11.4	0.42	15.1	22.34
*G75-31	23545	21348	0.46	0.19	146	173.2	-143.0	49.2	0.971	-1.024	0.605	229.9	0.22	12.4	0.67	13.3	12.20
G74-38	23713	420306	0.84	0.06	45	57.5	-43.1	-22.8	0.828	-1.290	-0.343	75.4	-0.32	-17.6	0.19	10.8	22.19
G78-1	23826	470836	0.52	0.15	68	6.1	-55.0	-83.5	0.227	-0.708	-1.264	100.2	-1.51	-56.5	0.19	10.8	21.00
*G76-21	23832	93324	0.44	0.29	111	52.8	-118.5	114.5	0.903	-0.933	0.591	173.8	0.88	41.4	0.47	10.2	14.65
*G78-2	23933	484524	0.94	0.10	41	-55.1	-96.8	-46.2	0.417	-0.941	-1.523	128.6	-0.41	-22.5	0.41	10.6	16.82
*G4-37	24155	81618	0.47	0.25	191	-209.7	-125.5	-86.6	-0.723	-0.553	-0.843	259.3	-0.35	-19.5	0.72	17.7	13.95
G37-4	24320	252636	0.83	0.03	22	20.5	-21.4	-7.1	0.547	-1.165	-0.067	30.5	-0.24	-13.5	0.04	10.2	24.36
G76-30	24453	62924	0.76	0.15	59	19.1	-83.1	-72.8	-0.274	-1.547	-0.596	112.1	-0.85	-48.5	0.31	10.0	18.19
G36-33	24512	265142	0.83	0.05	19	18.3	-21.0	0.3	0.734	-1.225	0.163	27.9	0.01	0.6	0.04	10.1	24.40
G5-1	24546	222348	0.56	0.13	98	-50.6	-119.1	-104.9	-0.332	-1.132	-1.201	166.6	-0.81	-39.0	0.48	10.5	14.59
*G4-44	24916	111012	0.54	0.15	46	-27.8	-68.8	-58.0	-0.674	-1.516	-1.195	94.2	-0.78	-38.0	0.27	10.3	19.62
G37-10	24954	352606	0.79	0.03	30	80.9	-15.2	-27.7	0.896	-1.583	-0.118	86.9	-0.34	-18.6	0.23	12.9	24.98
G4-46	25242	183424	0.80	0.11	48	86.0	-63.1	-28.9	0.762	-1.699	0.171	110.5	-0.27	-15.2	0.31	11.3	20.19
G74-48	25454	381742	0.69	0.20	192	147.8	-156.4	-96.9	0.465	-1.001	-0.388	236.0	-0.45	-24.2	0.67	12.1	10.86
G75-56	25754	-60930	0.45	0.19	257	-85.0	-378.2	-66.4	-0.373	-1.469	-0.202	393.3	-0.17	-9.7	0.62	11.0	-11.32
*G75-57	25756	54724	0.83	-.06	31	89.1	-79.8	-14.9	1.411	-2.804	0.975	120.5	-0.12	-7.1	0.37	11.1	18.52
G78-12	25850	423242	0.74	0.14	60	86.2	-31.8	15.9	0.764	-0.966	0.465	93.2	0.17	9.8	0.25	12.2	23.32
G75-62	30109	-55130	0.67	0.10	31	-10.8	-65.1	30.1	0.190	-2.142	0.283	72.5	0.46	24.5	0.24	10.1	19.99
G95-4	30150	343442	0.61	0.09	49	9.4	-13.6	-62.6	-0.206	-0.492	-1.108	64.7	-3.79	-75.2	0.01	10.2	25.14
G78-14	30224	445354	0.77	0.12	50	2.7	-73.7	2.1	0.676	-1.060	-0.112	73.8	0.03	1.6	0.27	10.0	19.13
G78-17	30429	362542	0.66	0.02	27	41.0	-23.5	-18.6	0.617	-1.364	-0.348	58.8	-0.39	-21.5	0.18	10.7	24.15
*G37-26	30528	260906	0.44	0.30	42	-168.3	-132.0	-92.1	-1.245	-1.996	-3.728	232.9	-0.43	-23.3	0.66	14.3	13.30
G95-11	30656	343936	0.58	0.15	210	324.4	-103.7	66.3	0.734	-0.912	0.646	347.8	0.19	11.0	0.88	46.4	16.13
*G5-17	30713	151124	0.83	0.00	41	-51.4	-31.3	-27.1	-0.663	-0.609	-1.102	66.0	-0.45	-24.2	0.20	11.6	23.37
G5-19	30842	122618	0.60	0.20	124	-254.4	-216.6	-34.0	-0.731	-1.465	-1.319	335.8	-0.10	-5.8	0.91	19.9	4.84
G76-68	31036	33812	0.93	0.27	34	-4.7	-49.8	1.7	0.007	-1.455	-0.090	50.0	0.03	1.9	0.17	10.1	21.52
G95-16	31112	343224	0.86	0.22	125	-28.3	-197.0	43.3	0.591	-1.169	0.023	203.7	0.22	12.3	0.75	10.1	6.80
G79-18	31205	84806	0.87	-.01	22	-8.4	-60.9	10.9	0.308	-2.669	-0.088	62.4	0.18	10.1	0.22	10.1	20.41
G37-29	31206	342654	0.92	-.07	51	25.3	-68.8	-9.6	0.558	-1.302	-0.212	73.2	-0.13	-7.5	0.25	10.1	19.70
G77-35	31229	5106	0.68	0.15	72	143.3	-46.1	23.1	1.173	-0.645	1.151	152.3	0.15	8.7	0.42	14.7	21.89
G37-31	31352	305100	0.90	0.02	39	44.8	-33.5	-30.3	0.346	-1.212	-0.419	63.6	-0.54	-28.4	0.14	10.6	23.15
G77-37	31407	45024	0.62	0.13	56	-88.0	-57.9	4.3	-0.576	-0.974	-0.704	98.8	0.04	2.5	0.33	11.9	28.71
G5-27	31540	150000	0.82	0.11	15	-7.8	-15.6	-11.0	-0.370	-1.003	-0.835	20.6	-0.63	-32.2	0.06	10.6	24.94
*G37-34	31631	332536	0.85	0.07	44	-51.1	-178.3	-4.7	1.021	-3.043	-0.973	185.5	-0.03	-1.5	0.69	10.3	8.67
G79-29	31755	85118	0.68	0.07	37	26.9	-41.0	17.7	0.604	-1.121	0.578	52.1	0.36	19.8	0.13	10.1	22.40
G6-3	31912	170342	0.99	-.06	76	70.3	-79.0	-50.6	0.173	-1.216	-0.174	117.2	-0.48	-25.6	0.34	10.7	18.60
G95-31	31944	454354	0.66	-.02	59	-65.4	9.6	-52.5	-0.512	0.526	-1.003	84.4	-0.79	-38.5	0.28	15.8	27.46
G78-33	32010	434700	0.98	0.11	25	27.8	-21.9	-29.5	0.490	-1.237	-1.042	46.1	-0.83	-39.8	0.06	10.4	24.31
G37-37	32030	334806	0.48	0.19	208	-188.4	-284.7	-395.6	-0.223	-0.794	-1.537	522.5	-1.16	-49.2	0.95	14.1	-1.97
G95-35	32152	415700	0.78	-.02	57	40.4	-60.8	-9.5	0.591	-1.132	-0.138	73.6	-0.13	-7.4	0.23	10.2	20.42
*G5-35	32204	120518	0.54	0.27	109	122.3	-369.7	-49.8	0.519	-3.483	-0.017	392.6	-0.13	-7.3	0.66	11.3	-10.47
G78-37	32237	451700	0.85	-.02	69	50.7	-94.8	-11.8	0.770	-1.353	-0.178	108.2	-0.11	-6.3	0.37	10.3	17.02
*G5-36	32402	233630	0.53	0.17	140	42.2	-262.3	-54.9	0.349	-1.859	-0.417	271.3	-0.21	-11.7	0.99	10.1	0.27
G5-40	32446	205224	0.57	0.13	133	-128.2	-201.1	-68.8	-0.194	-1.307	-0.955	248.2	-0.29	-16.1	0.80	11.8	6.39
*G77-54	32552	-64206	0.62	0.13	36	60.5	-79.9	-25.6	0.401	-1.965	0.712	103.4	-0.26	-14.3	0.33	10.5	18.51
G77-56	32643	14824	0.75	0.03	86	35.2	-128.9	-8.5	0.109	-1.489	0.174	133.9	-0.06	-3.6	0.50	10.1	13.61
G6-13	32647	123800	0.81	0.11	104	-52.9	-125.2	-35.6	-0.216	-1.162	-0.546	140.5	-0.26	-14.7	0.50	10.5	13.98
G79-42	32654	102348	0.50	0.20	140	-2.8	-226.1	-71.5	-0.137	-1.628	-0.425	237.2	-0.32	-17.5	0.85	10.0	3.89
G79-43	32718	91606	0.48	0.19	218	-23.2	-242.8	-72.1	-0.134	-1.116	-0.310	254.3	-0.30	-16.5	0.91	10.1	2.22
G95-40	32721	400906	0.91	-.03	46	-19.1	-44.8	-46.8	0.072	-0.727	-1.144	67.5	-0.96	-43.9	0.16	10.3	22.02
G5-42	32822	203600	0.68	0.05	34	-21.3	-14.1	-31.4	-0.469	-0.377	-1.009	40.5	-1.23	-58.9	0.10	11.2	25.09
G78-40	32840	433006	0.70	-.03	48	44.0	-53.3	14.0	0.732	-1.210	0.329	70.5	0.20	11.5	0.20	10.3	21.17
G5-44	33121	224924	0.61	0.04	69	42.5	-73.9	-20.3	0.257	-1.167	-0.110	87.6	-0.24	-13.4	0.29	10.2	19.11
G78-41A	33133	381006	0.82	-.03	78	43.6	-33.1	-17.5	0.260	-0.643	-0.148	57.5	-0.32	-17.7	0.13	10.6	23.19
G78-41	33141	380830	0.67	0.10	81	35.5	-107.6	-21.8	0.522	-1.289	-0.293	115.4	-0.19	-10.9	0.42	10.1	15.74
G5-45	33254	115242	0.93	-.02	67	0.3	-75.7	-76.3	-0.442	-1.179	-0.834	107.5	-1.01	-45.2	0.28	10.0	18.93
G6-22	33457	193948	0.78	0.08	97	-106.2	-86.9	-59.2	-0.387	-0.746	-0.997	149.4	-0.43	-23.3	0.45	12.3	17.81
G78-44	33531	421406	0.81	-.05	46	21.0	-70.8	-27.6	0.612	-1.459	-0.632	78.8	-0.37	-28.5	0.26	10.0	19.42
*G80-15	33750	-32230	0.54	0.18	19	106.1	-63.9	-50.0	1.100	-2.591	1.627	133.6	-0.40	-22.0	0.36	12.0	20.11
G80-16	33815	-22924	0.96	0.01	12	32.8	-28.2	-22.6	0.162	-1.948	0.502	48.8	-0.52	-27.6	0.09	10.4	23.68
G79-56	33859	91412	0.73	0.28	106	-33.3	-169.4	44.8	0.144	-1.577	0.103	178.4	0.26	14.5	0.65	10.2	9.56
G78-47	34022	422700	0.56	0.05	34	56.7	-46.0	-2.0	0.883	-1.744	0.892	73.0	-0.03	-1.6	0.20	10.7	21.90
G78-49	34117	455248	0.87	0.05	18	28.1	-14.2	8.4	0.744	-1.228	0.581	32.6	0.27	14.9	0.06	10.7	25.08
G79-63	34121	94700	0.83	0.07	111	143.2	-211.9	8.3	0.502	-1.945	0.609	255.9	0.03	1.9	0.83	11.7	5.31
G79-65	34156	100124	0.66	0.04	47	1.2	-68.6	-9.5	-0.038	-1.463	-0.160	69.3	-0.14	-7.9	0.25	10.0	19.64
G38-13	34221	285348	0.74	0.20	104	-117.6	-184.3	-1.3	0.218	-1.354	-0.528	218.6	-0.01	-0.3	0.74	11.6	8.07
G7-6	34731	171942	0.64	-.06	37	-8.3	-47.2	-11.3	-0.044	-1.249	-0.401	49.2	-0.24	-13.3	0.16	10.1	21.78
G6-38	34907	223142	0.68	0.01	29	9.8	-53.9	-19.1	0.190	-1.899	-0.565	58.0	-0.35	-19.2	0.18	10.0	21.11
G7-10	35000	105812	0.78	0.20	152	81.1	-179.5	74.1	0.395	-1.186	0.573	210.4	0.38	20.6	0.78	10.5	8.55
G38-18	35017	345712	0.96	0.10	99	102.0	-93.0	-9.5	0.439	-1.155	0.066	138.4	-0.07	-3.9	0.43	11.3	17.20
G80-31	35026	5148	0.72	0.09	102	-88.8	-144.9	-58.5	-0.733	-1.439	-0.682	179.7	-0.34	-19.0	0.60	11.1	12.01

TABLE II. (continued).

NAME	RA	DEC	B-V	EX(.6)	D	U	V	W	DU/DR	DV/DR	DW/DR	S	TAN I	I	ECC.	RMAX	H
G6-40	35331	223200	0.68	0.02	32	35.6	-37.3	-23.2	0.124	-1.349	-0.297	56.5	-0.45	-24.2	0.13	10.3	22.77
G6-41	35358	243036	0.79	0.06	129	1.8	-180.9	49.6	0.378	-1.325	0.237	187.6	0.27	15.3	0.69	10.0	8.41
G8-6	40003	200618	0.74	0.24	140	68.5	-110.4	-138.8	-0.189	-0.879	-0.691	190.1	-1.07	-46.9	0.45	10.5	15.46
G81-2	40032	393612	0.56	0.13	131	176.6	-146.3	7.9	0.595	-1.415	0.196	229.5	0.03	2.0	0.68	13.4	11.87
G80-41	40157	648	0.75	-.05	40	-72.3	-23.6	-45.0	-1.266	-0.691	-1.529	88.4	-0.59	-30.6	0.26	13.0	24.14
G7-20	40247	105454	0.79	0.14	112	-167.5	-33.9	-121.6	-0.828	-0.309	-1.463	209.7	-0.71	-35.4	0.54	19.8	23.11
*G38-25	40258	324942	0.97	0.06	42	166.0	-174.7	-53.7	1.314	-4.944	-0.583	246.9	-0.22	-12.6	0.74	12.6	9.03
G39-1	40414	375642	0.84	0.03	15	30.1	-10.5	-8.5	0.411	-1.274	-0.263	33.0	-0.27	-14.9	0.07	11.1	25.45
G7-22	40544	121236	0.90	-.03	30	-1.0	-44.1	-16.2	-0.229	-1.469	-0.434	47.0	-0.37	-20.2	0.14	10.0	22.09
G81-8	40902	415154	0.64	0.16	89	23.5	-75.5	-125.2	0.177	-0.883	-1.396	148.1	-1.58	-57.7	0.28	10.0	18.95
G7-27	40953	194612	0.56	0.12	97	85.3	-73.6	51.8	0.383	-0.807	0.739	124.0	0.46	24.7	0.34	11.1	19.14
*G8-16	41136	221348	0.40	0.25	96	368.6	-217.8	-80.8	0.494	-2.694	0.407	435.7	-0.19	-10.7	0.97	55.6	4.72
G80-42	41153	25336	0.96	-.02	28	69.9	15.5	-5.9	0.742	0.847	0.926	71.8	-0.08	-4.7	0.26	15.7	28.05
G82-5	41229	-54524	0.71	0.17	76	341.9	-177.9	9.4	1.535	-1.350	2.488	385.5	0.02	1.4	0.93	40.2	8.71
G7-31	41315	74636	0.76	0.09	123	-24.7	-187.3	-54.3	-0.341	-1.510	-0.362	196.6	-0.29	-16.0	0.71	10.1	7.77
G39-5	41513	355230	0.67	0.11	34	-40.9	-39.1	-49.4	-0.870	-0.808	-1.666	75.1	-0.87	-41.1	0.19	11.0	22.59
G8-27	41655	140924	0.97	-.07	17	-25.8	-19.5	5.3	-0.149	-1.153	-0.315	32.8	0.16	9.3	0.11	11.1	24.55
G81-15	41722	454218	0.60	0.14	80	95.5	-83.9	65.3	0.614	-1.301	0.849	142.9	0.51	27.2	0.39	11.2	18.11
G82-12	41745	-35154	0.62	0.08	33	-51.8	-23.1	-10.0	-0.880	-0.916	-0.810	57.6	-0.18	-10.0	0.20	12.0	24.19
G82-18	42307	50936	0.82	0.15	110	-151.0	-225.9	-15.1	-0.656	-2.170	-0.539	272.1	-0.06	-3.2	0.88	12.5	3.91
G81-19	42346	464448	0.68	-.04	22	46.9	-10.4	-18.5	0.493	-1.185	-0.795	51.5	-0.39	-21.1	0.12	11.7	25.46
G8-36	42450	242000	0.86	0.07	38	83.5	-20.9	41.6	0.565	-0.744	1.586	95.6	0.48	25.8	0.23	12.7	24.41
G82-22	42731	-31012	0.64	0.08	53	36.2	-72.4	1.0	-0.033	-1.133	0.500	81.0	0.01	0.7	0.27	10.1	19.26
G39-18	42821	381200	0.65	0.14	111	-85.4	-144.7	-33.3	0.247	-0.999	-0.425	171.3	-0.28	-11.2	0.68	11.0	12.03
G8-40	42929	262136	0.85	0.16	63	16.6	-85.2	-6.3	0.163	-1.366	-0.074	87.0	-0.07	-4.2	0.32	10.0	17.98
G39-23	43005	335700	0.89	0.00	86	-11.6	-96.4	-18.3	0.201	-1.042	-0.269	98.8	-0.19	-10.7	0.37	10.1	16.86
G82-30	43112	51706	0.80	0.11	21	-55.7	-9.8	-1.6	-0.720	-0.820	-1.086	56.6	-0.03	-1.6	0.21	13.1	25.52
G83-18	43138	123806	0.58	0.15	75	-111.7	-84.2	-40.0	-0.486	-1.192	-0.958	145.5	-0.29	-16.0	0.46	12.5	18.08
G8-43	43233	264600	1.10	0.49	62	202.5	-80.5	-22.9	0.309	-1.685	0.360	219.1	-0.11	-6.0	0.60	17.4	18.45
G82-36	43405	32500	0.83	0.09	27	11.3	-31.6	-25.1	-0.464	-0.974	-0.456	41.9	-0.75	-36.8	0.88	10.0	23.34
G8-46	43453	195812	0.88	0.06	80	55.6	-80.7	-72.2	-0.169	-1.035	-0.626	121.7	-0.74	-36.4	0.32	10.4	18.43
G83-26	43528	124506	0.96	0.34	94	109.9	-144.1	87.6	0.391	-1.472	1.247	201.3	0.48	25.8	0.60	11.1	12.09
G83-27	43648	130136	0.83	0.13	30	-20.6	-33.9	23.7	0.098	-1.190	0.478	46.2	0.60	30.9	0.13	10.5	23.11
G81-30	43804	420142	0.60	0.10	26	147.1	-39.3	13.0	1.039	-3.034	0.733	152.8	0.09	4.9	0.43	15.4	22.57
*G8-51	43822	204830	1.08	0.10	14	8.2	-2.4	-25.5	-0.498	-0.189	-1.673	25.6	-10.59	-84.6	0.88	11.6	26.26
G82-42	43931	-42212	0.61	0.21	219	-189.6	-252.8	-139.2	-0.853	-1.156	-0.644	344.7	-0.44	-23.8	0.97	14.2	1.30
G85-11	44028	273554	0.89	-.01	23	19.4	-26.8	-18.6	0.828	-1.264	-0.633	38.0	-0.56	-29.3	0.06	10.1	23.82
G81-33	44115	430642	0.87	0.00	32	51.7	10.9	45.4	0.102	-0.172	1.464	69.7	0.86	40.7	0.20	14.2	27.59
G85-13	44137	255042	0.59	0.12	95	195.2	-60.7	36.8	0.257	-0.888	0.796	207.7	0.18	10.2	0.57	18.8	20.43
G84-9	44243	35254	0.54	0.16	187	-163.6	-188.1	25.8	-0.338	-1.135	-0.131	250.5	0.10	5.7	0.79	13.2	7.69
G96-1	44338	455354	0.80	0.03	69	116.8	-41.8	46.5	0.398	-1.879	0.662	132.2	0.38	20.6	0.34	13.3	22.40
G82-47	44405	-44142	0.89	0.04	52	-79.1	32.1	-31.8	-0.613	0.250	-1.157	90.8	-0.36	-20.8	0.40	21.8	29.71
G39-36	44451	330424	1.06	0.36	70	-9.8	-97.4	75.4	0.379	-1.295	1.007	123.6	0.77	37.6	0.37	10.1	16.76
G84-12	44611	52736	0.96	-.01	63	-8.5	-62.2	26.3	-0.052	-1.805	0.379	68.1	0.42	22.7	0.23	10.1	20.28
G85-17	44653	222436	0.66	0.14	85	-1.9	-58.7	-83.7	-0.211	-0.697	-0.937	102.3	-1.43	-54.9	0.21	10.8	20.63
G39-38	44802	324836	0.85	0.01	42	-10.4	-37.0	-43.9	0.007	-0.836	-1.079	58.3	-1.14	-48.8	0.12	10.2	22.80
G81-38	44803	454524	0.52	0.10	28	63.2	-70.5	-11.5	1.076	-2.945	-0.434	95.4	-0.12	-6.9	0.90	10.6	19.45
G85-21	44832	191648	0.59	0.17	126	-65.1	-149.3	34.6	0.015	-1.194	0.126	166.5	0.21	12.0	0.60	10.6	11.57
G84-16	45047	-40236	0.67	0.18	331	-246.9	-452.0	137.5	-0.463	-1.482	0.253	533.1	0.27	14.9	0.75	27.8	-18.70
G83-40	45134	71730	0.90	0.03	26	36.8	-45.9	-7.8	-0.157	-1.438	0.345	59.3	-0.13	-7.6	0.17	10.2	21.91
G83-41	45134	71748	0.84	-.04	26	36.1	-45.7	-7.5	-0.157	-1.438	0.345	58.7	-0.13	-7.3	0.16	10.2	21.93
G97-5	45219	51806	0.58	0.24	213	30.7	-197.6	117.6	0.040	-0.902	0.597	232.0	0.59	30.5	0.75	10.0	6.74
G84-22	45317	-14224	0.66	0.12	124	-159.3	-93.1	-33.9	-0.675	-0.976	-0.594	187.6	-0.18	-10.4	0.57	14.9	17.19
G83-46	45332	145042	0.90	0.51	86	137.6	-220.1	-66.1	-0.282	-2.381	-0.182	267.9	-0.25	-14.3	0.85	11.5	4.49
G84-23	45333	25136	0.83	-.08	36	-5.6	-56.3	-12.3	-0.505	-1.462	-0.181	57.9	-0.22	-12.3	0.20	10.1	20.87
*G39-43	45440	341142	0.73	0.05	30	51.2	-62.9	45.4	0.565	-2.301	1.620	92.9	0.56	29.2	0.25	10.4	20.21
G96-14	45638	391724	1.00	0.22	101	-18.8	-166.2	84.1	0.399	-1.501	0.813	187.2	0.50	26.7	0.64	10.1	9.88
G84-28	45805	-1354	0.00	0.00	0	88.6	-31.6	-42.9	-0.137	-1.235	0.627	103.4	-0.46	-24.5	0.25	12.3	23.34
G96-16	45832	445812	0.86	-.02	58	11.7	-56.0	-68.2	0.343	-0.918	-1.170	89.0	-1.19	-58.0	0.19	10.0	20.98
G85-37	45834	243406	0.69	0.07	30	31.2	-44.1	-19.5	-0.033	-1.507	-0.451	57.4	-0.36	-19.8	0.15	10.2	22.09
G96-17	45835	422618	0.85	0.13	52	-29.9	-14.9	-77.0	0.042	-0.107	-1.475	83.9	-2.30	-66.5	0.13	11.5	25.01
*G84-29	45838	40224	0.36	0.27	147	126.0	-205.4	-24.2	-0.192	-1.103	0.288	242.2	-0.10	-5.7	0.88	11.2	5.96
G83-50	45920	140854	0.72	0.05	32	-40.6	-53.8	-14.2	-0.426	-1.783	-0.695	68.9	-0.21	-11.9	0.23	10.7	21.12
G84-30	50016	50718	0.90	0.00	72	-76.6	-54.0	-26.6	-0.485	-0.904	-0.603	97.4	-0.28	-15.8	0.31	11.9	21.10
G96-19	50127	431448	0.61	0.11	70	-9.5	-46.7	-73.6	0.193	-0.570	-1.044	87.7	-1.54	-57.1	0.16	10.1	21.83
*G96-20	50159	401124	0.42	0.19	117	141.3	-102.5	117.4	0.284	-1.106	1.011	210.4	0.67	33.9	0.52	12.6	16.25
G97-19	50351	142300	0.80	0.03	22	19.9	-43.1	3.1	-0.115	-1.030	0.428	47.6	0.07	3.7	0.13	10.0	22.19
G86-26	50653	273454	0.92	0.08	32	23.8	-30.2	14.0	0.122	-0.979	0.516	40.9	0.36	20.0	0.08	10.1	23.48
*G84-37	50716	52942	0.52	0.19	83	-7.5	-74.2	82.8	0.883	-0.941	0.934	111.4	1.11	48.0	0.28	10.1	19.08
G85-45	50740	250500	0.59	0.04	52	-64.8	-42.5	-38.5	-0.122	-0.794	-0.910	86.5	-0.50	-26.4	0.26	11.7	22.25
G97-25	50907	42048	0.57	0.02	29	-5.7	-30.5	15.0	-0.138	-1.068	0.495	34.5	0.48	25.8	0.09	10.2	23.45
G85-51	50939	235012	0.88	-.07	77	74.2	-93.8	29.9	0.079	-1.215	0.526	123.3	0.25	14.0	0.39	10.6	17.12
G96-24	50943	455742	0.97	0.14	56	48.2	-31.5	-71.0	0.333	-0.732	-1.307	91.4	-1.23	-51.0	0.14	10.7	23.35
G84-39	51006	41548	0.79	0.09	74	77.3	-93.6	30.7	0.008	-0.946	0.802	125.2	0.25	14.2	0.40	10.7	17.14
G85-58	51236	213936	0.80	0.07	28	-45.5	-31.1	-6.5	-0.131	-1.172	-0.485	55.5	-0.12	-6.7	0.19	11.4	23.39
G84-44	51423	-1448	0.46	0.26	207	-115.8	-302.1	19.9	-0.549	-1.464	0.892	324.1	0.06	3.5	0.88	11.4	-3.71
G99-2	51738	-24236	0.79	0.19	179	-56.2	-190.6	101.5	-0.262	-1.089	0.545	223.1	0.51	27.1	0.73	10.4	7.44
G96-35	51901	475206	0.59	0.13	61	63.1	12.8	-66.8	0.170	-0.078	-1.199	92.8	-1.04	-46.1	0.23	15.8	27.78
*G98-3	52212	322206	0.60	0.15	73	-10.1	-93.8	18.6	0.124	-1.261	0.248	96.2	0.20	11.2	0.36	10.1	17.12
G96-38	52221	443512	0.84	0.07	135	42.5	-144.2	-146.0	0.388	-1.048	-1.074	209.6	-0.97	-44.2	0.56	10.1	12.08
G86-40	52317	344218	0.58	0.27	157	-120.1	-218.0	8.4	0.158	-1.274	0.049	249.0	0.03	1.9	0.85	11.6	4.70
G85-71	52433	184824	0.92	-.01	42	-45.0	-49.0	-24.6	-0.252	-1.257	-0.715	70.9	-0.37	-20.3	0.23	10.9	21.60
G97-43	52608	44518	0.74	0.01	50	77.8	36.0	32.5	0.692	1.034	0.927	91.7	0.38	20.8	0.37	20.2	30.10
G86-43	52637	325508	0.86	0.12	100	-47.7	-227.7	135.4	0.121	-1.230	0.747	269.2	0.58	30.2	0.86	10.3	3.73
*G97-45	52822	154430	0.64	0.05	49	35.5	-75.2	-63.9	-0.417	-1.344	-1.105	104.9	-0.77	-37.5	0.28	10.1	18.98
G97-46	52858	161118	0.76	0.13	155	-108.9	-195.0	-49.4	-0.279	-1.326	-0.390	228.7	-0.22	-12.5	0.77	11.3	7.00
G99-16	52910	406	0.70	0.07	33	-39.0	-65.3	-6.4	-0.986	-2.063	-0.263	76.3	-0.08	-4.8	0.27	10.5	19.97
G100-17	53009	200012	0.90	0.06	28	-9.0	-27.4	-33.1	-0.254	-0.983	-1.191	43.9	-1.15	-48.9	0.08	10.3	23.76
G100-27	53404	204224	0.66	0.10	26	-31.0	-41.2	-36.3	-0.331	-1.672	-1.485	63.1	-0.70	-35.1	0.17	10.6	22.38
*G102-20	53721	120912	0.65	0.21	69	22.7	-72.0	66.2	-0.050	-0.951	1.027	100.4	0.88	41.2	0.26	10.0	19.30
G99-22	53721	60212	0.82	-.08	42	-46.4	-39.2	-11.7	-0.499	-1.142	-0.425	61.9	-0.19	-10.9	0.20	11.1	22.58
-5-1355	53730	-50400	0.64	0.09	51	50.8	36.0	28.9	0.779	0.915	0.707	74.8	0.42	22.7	0.33	19.0	30.10
G98-28	53733	291042	0.92	0.08	117	-19.2	-132.6	64.2	0.023	-1.131	0.547	148.6	0.48	25.6	0.51	10.1	13.24
G96-48	53815	381812	0.54	0.17	233	108.1	-288.5	47.2	0.176	-1.281	0.181	311.7	0.15	8.7	0.92	10.8	-2.35
*G99-26	54008	23948	0.89	-.01	29	16.8	-92.7	-18.5	-1.089	-2.507	-0.191	96.0	-0.20	-11.1	0.35	10.0	17.23
G99-30	54106	33354	0.67	0.20	262	64.1	-352.4	-73.3	-0.452	-1.066	-0.102	365.6	-0.20	-11.6	0.68	10.3	-8.74
*G99-31	54212	91342	0.56	0.26	166	-178.3	-429.5	-164.7	-0.985	-2.614	-1.009	493.3	-0.35	-19.5	0.62	16.0	-16.45
G96-51	54236	371618	0.82	-.04	21	-23.1	-71.3	10.3	0.353	-3.211	0.602	75.7	0.14	7.8	0.28	10.2	19.37
G102-27	54249	144018	0.65	0.08	53	27.7	-64.5	-16.5	-0.255	-1.049	-0.208	72.1	-0.24	-13.2	0.23	10.1	20.05
G100-43	54729	232706	0.69	0.10	40	-51.9	-19.6	-48.4	-0.097	-0.601	-1.251	73.6	-0.87	-41.1	0.20	12.2	24.54

TABLE II. (continued).

NAME	RA	DEC	B-V	EX(.6)	D	U	V	W	DU/DR	DV/DR	DW/DR	S	TAN I	I	ECC.	RMAX	H
G99-40	55025	-33000	0.56	0.09	71	28.1	-84.5	65.1	-0.167	-0.874	1.086	110.3	0.73	36.2	0.32	10.1	10.85
G102-42	55409	154424	0.64	0.10	35	-28.1	-39.7	-7.7	-0.302	-1.248	-0.261	49.2	-0.16	-9.0	0.16	10.6	22.53
G99-48	55627	41036	0.70	0.32	106	-86.9	-115.5	90.6	-0.398	-1.269	0.777	170.6	0.63	32.1	0.51	11.2	14.95
G98-34	55707	312554	0.93	-.08	46	62.4	-71.7	-3.8	0.027	-1.572	-0.175	95.1	-0.04	-2.3	0.30	10.5	19.33
G101-14	55730	462706	0.69	0.16	117	76.6	-84.2	-91.3	0.367	-0.789	-0.840	145.9	-0.80	-38.7	0.36	10.8	10.08
G99-50	55749	-33900	0.60	0.09	103	-30.4	-96.8	-79.6	-0.622	-0.748	-0.685	129.0	-0.78	-38.1	0.38	10.2	16.82
G100-52	55926	272418	0.68	-.02	66	7.4	-74.2	-8.8	-0.857	-1.114	-0.141	75.1	-0.12	-6.7	0.27	10.0	19.08
G102-44	55954	130448	0.71	0.10	97	-51.3	-95.0	64.0	-0.245	-1.059	0.636	125.5	0.59	30.7	0.40	10.6	17.00
*G100-54	60016	192212	0.60	0.19	54	-220.2	-183.1	74.7	-0.695	-4.005	1.301	296.0	0.26	14.6	0.83	16.9	8.19
G99-54	60228	62718	0.76	0.07	80	27.0	-111.2	10.2	-0.406	-1.092	0.229	114.9	0.09	5.1	0.43	10.0	15.38
*G98-42	60249	263348	0.89	0.01	42	-93.7	-37.2	-76.4	0.001	-1.054	-1.713	126.5	-0.76	-37.2	0.33	13.3	22.78
*G102-47	60315	71936	0.64	0.22	73	53.9	-131.3	-23.9	-0.528	-1.308	-0.169	143.9	-0.17	-9.6	0.51	10.2	13.37
G102-48	60509	81348	0.89	0.07	30	-33.9	-34.5	-18.1	-0.581	-1.356	-0.661	51.6	-0.37	-20.5	0.16	10.8	23.05
G100-60	60526	222648	0.74	0.08	132	-56.6	-134.8	74.9	-0.165	-1.059	0.573	164.3	0.51	27.1	0.54	10.5	13.02
G98-47	60638	340854	0.79	0.06	29	34.8	-34.5	-10.2	0.102	-1.224	-0.488	50.1	-0.21	-11.8	0.12	10.3	23.05
G105-13	60645	190618	0.94	0.05	44	-39.0	-30.4	-33.8	-0.169	-0.835	-0.770	59.9	-0.68	-34.4	0.17	11.1	23.46
G102-51	60705	175648	0.67	0.09	37	6.1	-55.4	10.9	-0.301	-1.395	0.300	56.8	0.20	11.1	0.19	10.0	20.96
G98-51	60832	325130	0.00	0.00	0	-46.0	-0.5	-5.5	0.104	-0.984	-0.784	46.3	-0.12	-6.8	0.20	13.5	26.45
G104-25	60906	221154	0.97	0.02	52	-23.1	-64.1	-10.9	-0.191	-1.272	-0.203	69.0	-0.16	-9.1	0.25	10.2	20.09
G102-57	60918	64800	0.63	0.04	23	-55.0	-17.8	8.3	-0.602	-1.509	0.169	58.4	0.14	8.2	0.21	12.5	24.72
G101-25	60935	385536	0.82	-.09	115	-35.6	-160.0	-1.7	0.129	-1.345	0.862	163.9	-0.01	-0.6	0.62	10.2	10.50
G98-53	61032	332612	0.51	0.14	176	156.2	-242.0	-84.6	0.099	-1.388	-0.584	300.2	-0.29	-16.4	0.93	12.0	2.30
G101-26	61034	385130	0.99	-.03	56	2.2	-73.6	-36.9	0.241	-1.293	-0.624	82.4	-0.50	-26.6	0.27	10.0	19.14
G106-34	61145	51118	0.88	0.08	23	53.5	-58.7	-22.1	-0.622	-1.235	-0.632	82.4	-0.28	-15.5	0.24	10.5	20.63
*G98-58	61236	374436	0.59	0.23	42	249.7	-51.1	21.0	0.220	-1.674	-0.496	255.7	0.08	4.7	0.71	28.2	21.39
G101-30	61257	470506	0.77	0.08	42	55.8	-89.8	-27.7	0.738	-2.276	-0.810	109.3	-0.26	-14.7	0.36	10.3	17.52
G101-31	61311	444342	0.79	0.08	38	-3.1	-36.8	-80.1	0.619	-0.834	-1.944	88.2	-2.17	-65.2	0.11	10.1	22.82
G103-27	61336	295812	0.62	0.16	151	-7.9	-146.4	-115.4	0.043	-0.974	-0.754	186.6	-0.79	-38.2	0.56	10.0	11.86
*G101-33	61534	383318	0.75	0.11	69	140.0	-99.7	16.6	0.164	-1.609	-0.114	172.7	0.10	5.5	0.51	12.6	16.53
G103-31	61815	335924	0.58	0.13	102	153.2	-123.2	-34.5	0.105	-1.224	-0.564	199.6	-0.18	-10.0	0.59	12.7	14.18
G106-46	62234	4048	0.57	0.13	61	-25.8	-59.4	-44.3	-0.577	-0.886	-0.709	78.5	-0.68	-34.4	0.23	10.3	20.56
G104-38	62442	242118	0.81	0.02	46	20.8	-69.5	-16.2	-0.171	-1.417	-0.418	74.3	-0.22	-12.6	0.25	10.0	19.55
*G101-41	62525	363048	0.60	0.13	23	4.8	-5.1	-38.5	0.345	-0.217	-1.644	39.1	-5.50	-79.7	0.06	11.2	25.99
G103-34	62559	270242	0.87	-.03	32	-48.9	-36.5	-71.9	0.120	-1.324	-2.030	94.3	-1.18	-49.7	0.21	11.3	22.85
G105-38	62609	174654	0.60	0.08	32	-13.7	-10.9	-36.7	-0.049	-0.438	-1.123	40.7	-2.10	-64.5	0.08	11.1	25.41
G104-43	62732	191918	0.56	0.10	56	-90.8	-36.2	40.6	-0.293	-0.963	0.826	105.8	0.42	22.6	0.32	13.2	22.88
G106-53	62852	-13154	0.86	0.06	53	57.7	-50.5	-120.9	-0.286	-0.093	-2.134	143.2	-1.58	-57.6	0.22	10.7	21.45
G106-55	62918	4118	0.68	0.12	52	69.0	-17.3	-77.9	0.104	0.376	-1.398	105.5	-1.10	-47.6	0.19	12.2	24.77
G105-44	62940	70606	0.72	0.12	154	-133.3	-141.4	-27.3	-0.498	-1.086	-0.184	196.2	-0.14	-8.0	0.64	12.5	12.36
G103-42	63121	372754	0.93	-.02	62	44.8	4.8	-79.3	0.316	0.058	-1.373	91.2	-1.76	-60.4	0.16	13.1	26.98
G103-44	63322	375348	0.75	0.00	59	88.1	-51.7	-32.0	0.252	-0.939	-0.842	107.0	-0.31	-17.4	0.29	11.6	21.33
G105-47	63343	140236	0.93	0.07	34	-50.0	-28.0	-31.9	-0.359	-1.202	-0.875	65.6	-0.56	-29.1	0.20	11.7	23.70
G101-47	63436	485048	0.70	0.09	71	96.8	-76.6	37.7	0.262	-1.339	0.163	129.1	0.31	17.0	0.37	11.4	18.84
G103-48	63655	300454	0.85	-.02	94	-52.4	-110.9	62.2	-0.239	-1.206	0.723	137.5	0.51	26.9	0.45	10.5	15.41
G103-50	63659	283000	0.86	0.37	89	-202.9	-123.2	19.9	-0.279	-1.599	0.589	238.2	0.08	4.8	0.70	17.1	14.18
G103-52	63934	310130	0.62	0.26	199	-65.6	-304.1	-130.3	0.013	-1.553	-0.583	337.3	-0.42	-22.7	0.86	10.5	-3.91
G103-53	64041	253448	0.68	0.13	73	0.2	-103.8	-45.1	-0.115	-1.403	-0.638	113.2	-0.43	-23.5	0.40	10.0	16.12
G87-2	64201	353524	0.67	0.06	48	49.3	-56.3	8.8	0.019	-1.173	-0.073	75.3	0.12	6.7	0.22	10.4	20.87
G87-3	64250	323630	0.95	0.04	25	-19.7	38.7	-58.8	0.551	1.480	-2.037	73.1	-1.35	-53.6	0.31	10.9	30.37
G103-58	64309	355548	0.61	0.12	84	21.7	-54.3	-83.0	0.260	-0.646	-0.988	101.5	-1.42	-54.8	0.19	10.0	21.07
G87-13	65136	353500	0.48	0.15	185	198.6	-224.2	27.6	0.027	-1.198	-0.152	300.8	0.09	5.3	0.89	13.7	4.08
G88-1	65532	190400	0.94	0.07	57	-16.4	-48.7	42.2	-0.380	-0.826	0.724	66.5	0.82	39.4	0.18	10.2	21.63
*G108-43	65604	-2424	0.57	0.12	61	-189.6	-116.5	3.3	-1.870	-2.750	0.090	222.6	0.01	0.8	0.67	16.2	14.85
G87-19	65923	313836	0.87	0.09	52	145.9	-88.9	-7.4	0.129	-1.466	-0.913	171.0	-0.04	-2.5	0.50	13.1	17.61
*G87-20	65940	381312	0.64	0.15	55	79.8	-64.5	-4.2	0.191	-1.196	-0.498	102.7	-0.04	-2.3	0.30	11.1	20.05
G88-5	70312	184254	0.72	0.09	73	-96.7	-38.8	41.9	-0.426	-0.818	0.766	112.3	0.40	21.9	0.34	13.4	22.62
G87-24	70455	295506	0.92	0.11	20	24.8	-24.6	-19.6	0.239	-1.097	-1.279	40.1	-0.56	-29.3	0.06	10.2	24.04
G88-8	70614	153018	0.62	0.04	39	38.3	-54.3	-42.5	-0.106	-0.974	-1.310	78.9	-0.64	-32.6	0.20	10.2	21.07
G87-27	70646	372136	0.81	0.06	52	-42.9	-63.8	-36.0	0.122	-1.230	-0.358	84.9	-0.47	-25.1	0.27	10.6	20.12
G88-9	70709	212006	0.87	0.04	10	-1.3	-20.6	-16.3	-0.167	-2.044	-1.641	26.3	-0.79	-38.3	0.04	10.2	24.44
G88-11	70739	203136	0.69	0.04	52	-52.1	-61.4	5.6	-0.457	-1.343	0.241	80.7	0.07	4.0	0.28	10.9	20.36
G88-13	71024	173118	0.80	0.07	64	-9.6	-55.7	-57.2	-0.106	-0.885	-0.883	80.4	-1.01	-45.3	0.20	10.1	20.93
G88-14	71051	250600	0.80	0.01	31	-29.0	18.0	-77.4	0.641	0.233	-2.039	84.6	-2.27	-66.2	0.22	15.1	28.30
G88-16	71216	160112	0.94	-.10	0	100.9	-39.1	23.7	-0.557	-1.011	0.706	110.8	0.22	12.4	0.30	12.6	22.59
G88-20	71522	272042	0.62	0.12	33	-41.0	-28.7	6.7	-0.355	-1.039	0.488	50.5	0.13	7.6	0.17	11.3	23.63
G87-35	71735	292630	0.76	0.11	101	38.0	-133.6	33.7	-0.235	-1.227	0.123	142.9	0.24	13.6	0.52	10.1	13.14
G89-13	71943	90006	0.91	-.02	41	-89.0	-27.3	-11.2	-0.777	-1.421	0.033	93.8	-0.12	-6.9	0.31	13.7	23.77
*G89-14	71948	85512	0.47	0.22	125	-112.6	-148.7	-1.5	-0.709	-1.294	0.030	186.5	-0.01	-0.5	0.63	11.7	11.63
G88-23	72022	190700	0.49	0.28	228	-257.7	-221.1	-135.8	-0.327	-1.248	-0.362	365.7	-0.40	-21.8	0.92	20.2	4.39
G89-16	72059	130406	0.94	-.08	26	14.0	-66.9	-6.3	-0.766	-1.970	-0.573	68.6	-0.09	-5.3	0.24	10.0	19.81
*G88-27	72407	191212	0.44	0.22	162	24.5	-185.2	-97.1	-0.151	-1.037	-0.693	210.5	-0.52	-27.5	0.70	10.0	7.98
G89-20	72528	93618	0.76	-.05	48	-37.7	-40.3	-46.8	-0.362	-1.068	-0.868	72.4	-0.85	-40.3	0.19	10.8	22.47
G88-29	72537	194530	0.77	0.05	45	22.1	-73.9	17.4	-0.476	-1.309	0.078	79.1	0.23	12.7	0.27	10.0	19.11
G90-1	72549	320548	0.93	0.08	16	-17.0	9.7	11.0	-0.324	0.517	0.979	22.5	0.56	29.3	0.16	13.5	27.47
*G90-3	72637	325830	0.48	0.21	123	28.7	-150.1	-36.1	0.024	-1.198	-0.378	157.0	-0.24	-13.3	0.58	10.0	11.49
G87-40	72714	292912	0.78	0.00	52	13.7	-52.4	-30.5	0.006	-0.976	-0.654	62.2	-0.56	-29.4	0.17	10.0	21.26
G90-4	72717	272236	0.64	0.14	174	-61.8	-189.0	-31.5	-0.189	-1.121	-0.119	201.3	-0.16	-9.0	0.73	10.5	7.60
*G88-31	72734	190418	0.51	0.17	50	56.4	-128.9	-7.9	-0.499	-1.991	-0.684	140.9	-0.06	-3.2	0.51	10.2	13.61
*G88-32	72739	241142	0.36	0.30	225	-308.1	-216.4	-22.8	-0.410	-1.218	0.240	377.2	-0.06	-3.5	0.95	31.0	4.86
G88-34	72846	200430	0.89	-.02	50	-36.0	-44.1	10.4	-0.439	-0.978	0.302	57.9	0.18	10.4	0.19	10.7	22.09
G87-45	72947	311336	0.64	0.22	122	-8.0	-179.1	-6.8	-0.168	-1.454	-0.897	179.4	-0.04	-2.2	0.68	10.0	8.59
G88-38	73013	171148	0.77	0.00	120	-80.6	-109.1	74.7	-0.590	-0.943	0.649	154.9	0.55	28.8	0.48	11.1	15.59
*G88-40	73143	170048	0.51	0.16	62	-51.5	-67.0	-40.7	-0.356	-1.274	-0.500	93.8	-0.48	-25.7	0.30	10.8	19.80
*G88-41	73148	250406	0.64	0.08	26	-132.3	-18.8	-45.4	-0.488	-1.905	-0.006	141.1	-0.34	-18.8	0.45	17.7	24.62
G87-48	73503	364900	0.86	0.13	51	54.0	-213.7	-12.8	0.119	-4.146	-0.683	220.8	-0.06	-3.3	0.81	10.2	5.13
G89-33	73512	55812	0.62	0.12	96	-17.4	-141.1	83.1	-0.857	-1.029	0.680	164.7	0.58	30.3	0.54	10.1	12.39
G89-34	73523	54206	0.61	0.08	40	139.3	-96.8	-10.3	0.159	-0.244	-1.166	169.9	-0.06	-3.5	0.50	12.6	16.82
G89-35	73600	60606	0.98	0.05	37	45.0	-16.4	-32.5	0.377	0.101	-1.114	57.9	-0.68	-34.2	0.11	11.2	24.86
*G112-36	73718	-12418	0.82	0.19	33	19.6	-78.8	10.6	-0.927	-1.117	-0.029	81.9	0.13	7.4	0.29	10.0	10.62
G89-38	73735	121418	0.91	-.04	52	51.2	19.2	-48.1	0.628	0.552	-1.041	72.8	-0.88	-41.3	0.23	15.4	28.42
G112-44	74111	330	0.48	0.25	136	-130.5	-62.2	-171.6	-0.426	-0.890	-1.121	224.4	-1.19	-49.9	0.46	14.3	20.28
*G112-43	74111	318	0.44	0.20	136	-125.0	-66.6	-170.1	-0.426	-0.890	-1.121	221.3	-1.20	-50.2	0.45	13.8	19.84
*G90-25	75022	304524	0.62	0.30	24	-249.4	-182.3	-87.8	-1.895	-9.114	0.538	321.2	-0.28	-15.9	0.86	20.1	8.27
G91-20	75304	234936	0.63	0.03	29	13.1	-22.0	-25.8	0.246	-0.691	-0.987	36.3	-1.01	-45.2	0.03	10.0	24.30
G90-32	75335	303224	0.70	0.08	216	-162.6	-219.4	-45.9	-0.234	-1.113	0.051	276.9	-0.17	-9.5	0.87	13.0	4.56
G40-1	75601	184336	0.84	0.32	267	124.6	-404.9	-33.6	-0.290	-1.195	-0.474	425.0	-0.08	-4.5	0.56	11.6	-13.99
G50-13	75605	101600	0.81	0.07	24	11.1	-28.9	52.5	-0.900	-0.374	1.621	60.9	1.70	59.5	0.06	10.0	23.61
G40-2	75638	205918	0.85	0.06	18	-41.4	-40.1	-12.6	-0.998	-2.722	-0.077	59.0	-0.22	-12.3	0.19	10.9	22.49
G91-23	75649	130718	0.77	-.03	36	48.2	-11.9	-28.3	0.547	0.102	-1.131	57.1	-0.57	-29.7	0.12	11.6	25.31
G90-35	75713	321548	0.86	-.05	76	21.3	-87.7	-22.6	0.048	-1.116	-0.421	93.0	-0.25	-14.1	0.33	10.0	17.73

TABLE II. (continued).

NAME	RA	DEC	B-V	EX(.6)	D	U	V	W	DU/DR	DV/DR	DW/DR	S	TAN I	I	ECC.	RMAX	H
G90-36	75723	290900	0.58	0.24	249	204.0	-598.2	-84.6	-0.069	-2.207	-0.800	637.7	-0.13	-7.6	0.86	102.6	-33.32
G90-37	75754	325424	0.52	0.23	235	-72.8	-230.7	148.8	-0.444	-0.962	0.561	284.0	0.62	31.6	0.88	10.6	3.43
G90-38	75936	361036	0.73	0.17	99	46.3	-120.4	-1.9	0.044	-1.180	-0.257	129.0	-0.01	-0.8	0.47	10.2	14.46
G40-5	80146	153036	0.85	0.03	28	32.7	-39.6	-19.1	0.115	-0.883	-1.183	54.8	-0.37	-20.4	0.13	10.2	22.54
G40-8	80555	244636	0.68	0.13	57	-54.3	-84.8	-48.7	-0.278	-1.702	-0.489	111.9	-0.48	-25.8	0.36	10.7	18.02
G51-1	80724	330348	0.84	0.18	139	80.2	-251.9	44.7	-0.188	-1.694	-0.126	268.1	0.17	9.6	0.95	10.4	1.31
G50-23	81025	91600	0.86	0.12	159	-125.2	-223.5	-3.3	-0.875	-1.347	-0.064	256.2	-0.01	-0.7	0.87	11.7	4.15
G40-14	81313	195124	0.38	0.31	231	-209.4	-338.5	-36.0	-0.670	-1.568	-0.024	399.7	-0.09	-5.2	0.83	15.9	-7.35
G51-7	81655	345200	0.96	0.29	132	53.4	-253.7	19.1	-0.117	-1.855	-0.189	260.0	0.07	4.2	0.96	10.2	1.13
G40-20	82034	251900	0.96	0.02	47	6.2	-58.2	-18.8	-0.064	-1.173	-0.522	61.5	-0.32	-17.8	0.20	10.0	20.68
*G51-10	82203	324648	1.00	0.20	36	-76.7	-99.2	-67.3	-0.168	-3.100	-0.576	142.3	-0.54	-28.2	0.44	11.1	16.58
G52-19	83157	93248	0.80	-.06	48	-69.7	-40.6	24.9	-1.193	-1.035	0.683	84.4	0.31	17.2	0.27	12.0	22.44
G51-20	83428	314342	0.76	0.07	148	32.8	-197.5	-93.8	0.192	-1.328	-0.655	221.1	-0.47	-25.1	0.75	10.0	6.75
G9-13	83707	114230	0.82	0.01	21	-21.6	-42.2	-36.3	-0.605	-2.299	-1.444	59.7	-0.77	-37.4	0.16	10.4	22.28
G9-14	83749	134406	0.80	0.03	67	56.1	-18.5	-115.2	0.930	-0.336	-1.655	129.5	-1.95	-62.9	0.15	11.6	24.65
*G46-5	84746	74900	0.74	0.22	100	18.8	-386.6	144.2	-1.803	-2.197	-0.051	413.0	0.37	20.4	0.55	10.0	-12.16
G9-27	84858	190442	0.61	0.25	175	183.0	-218.0	-44.3	0.251	-0.824	-0.877	288.1	-0.16	-8.8	0.87	13.0	4.70
G9-29	84919	202006	0.93	0.04	59	-54.8	-40.6	23.4	-0.777	-0.757	0.505	71.5	0.35	19.1	0.23	11.4	22.44
G41-4	85020	92242	0.69	-.01	49	-36.6	-54.5	-7.4	-0.759	-1.104	-0.161	66.1	-0.11	-6.4	0.23	10.6	21.05
G41-5	85033	93648	0.77	0.04	113	210.9	-58.1	-98.3	1.126	0.074	-1.374	236.7	-0.41	-22.4	0.61	20.1	20.69
G47-10	85053	272318	1.03	0.23	90	-35.9	-152.7	32.2	-0.655	-1.612	0.150	168.1	0.21	11.6	0.59	10.2	11.23
*G9-36	85503	244812	0.57	0.24	179	-187.8	-176.3	66.7	-0.866	-1.059	0.526	266.1	0.26	14.5	0.78	14.6	8.87
*G114-26	85639	-34936	0.48	0.25	84	-215.7	-211.3	23.5	-2.851	-2.145	0.053	302.9	0.08	4.5	0.88	16.1	5.37
G47-19	85651	302612	0.91	0.04	43	-59.3	-58.2	18.6	-1.020	-1.448	0.741	85.1	0.22	12.6	0.28	11.1	20.68
G9-42	85754	213912	0.82	-.03	40	-42.0	-70.0	27.5	-1.244	-1.656	0.520	86.1	0.34	18.6	0.29	10.5	19.50
G9-47	90352	204236	0.79	0.08	20	122.7	-80.3	87.4	0.289	-0.975	-0.885	170.7	0.60	30.8	0.43	12.3	18.47
G48-1	91353	74406	0.98	0.08	77	-51.1	-101.8	-15.2	-0.803	-1.190	-0.335	114.9	-0.13	-7.6	0.42	10.5	16.32
G47-35	91757	323618	0.80	0.11	67	114.1	-89.8	24.3	0.553	-1.074	-0.795	147.2	0.17	9.5	0.44	11.7	17.52
G41-34	92006	112906	0.77	-.02	65	82.0	33.0	-45.5	1.228	0.537	-0.736	99.4	-0.51	-27.2	0.36	19.8	29.80
G48-13	92151	55936	0.70	0.16	212	111.2	-154.5	-175.3	0.400	-0.597	-0.960	258.8	-0.92	-42.6	0.63	11.1	11.05
G161-24	92240	-124436	0.92	0.20	34	-91.1	-99.8	51.2	-3.454	-1.289	0.620	144.5	0.38	20.8	0.46	11.5	16.52
*G41-41	92635	85124	0.38	0.28	243	-156.1	-418.4	184.5	-1.230	-1.149	0.098	483.2	0.41	22.4	0.60	14.1	-15.34
G49-19	93556	283806	0.55	0.10	133	-18.9	-230.2	45.7	-0.493	-1.606	-0.066	235.5	0.20	11.2	0.87	10.1	3.48
*G48-29	93808	11430	0.39	0.28	170	-303.8	-260.8	-147.8	-1.619	-1.768	-0.649	426.8	-0.37	-20.3	0.99	28.7	0.42
G48-31	93830	114718	0.66	-.11	73	-55.6	-74.0	10.6	-0.864	-0.919	0.015	93.2	0.11	6.5	0.33	10.8	19.10
G49-21	93927	215742	0.94	0.08	38	85.6	-96.9	42.4	0.456	-1.541	-1.082	136.1	0.33	18.2	0.42	10.9	16.81
*G43-3	94612	135918	0.36	0.27	75	-219.8	-210.5	-13.6	-2.724	-2.986	0.097	304.6	-0.04	-2.6	0.88	16.4	5.45
G48-39	94709	112030	0.60	0.14	28	55.4	-49.3	19.0	0.776	-0.580	-0.977	76.6	0.26	14.4	0.21	10.6	21.57
G43-5	94713	65048	0.63	0.32	153	-96.9	-251.5	7.6	-0.948	-1.270	-0.395	269.6	0.03	1.6	0.95	11.0	1.35
G43-7	94736	52306	0.80	0.07	127	-174.0	-72.9	13.6	-1.264	-0.708	0.259	189.1	0.07	4.1	0.58	17.0	19.21
G43-14	95258	161954	0.59	0.20	329	-340.2	-207.8	55.3	-0.956	-0.694	0.279	402.5	0.14	7.9	0.96	48.8	5.72
G43-15	95347	174448	0.87	-.05	70	-109.4	-43.9	-15.2	-1.173	-0.921	0.338	118.9	-0.13	-7.3	0.38	13.9	22.11
G54-7	95625	274548	0.57	-.02	46	49.8	-31.2	-48.2	1.110	-0.698	-1.008	76.0	-0.82	-39.4	0.14	10.8	23.38
G42-30	95628	150136	0.89	0.12	121	30.2	-154.3	-67.0	0.113	-1.155	-0.756	170.9	-0.43	-23.1	0.59	10.0	11.07
G42-34	100027	200512	0.85	0.14	65	8.9	-109.8	-8.8	-0.248	-1.510	-0.527	110.2	-0.08	-4.6	0.42	10.0	15.52
G162-16	100129	5000	0.57	0.05	100	143.4	9.4	-3.6	1.258	0.389	-0.344	143.8	-0.03	-1.4	0.46	20.9	27.44
G43-26	100243	121524	0.53	0.22	333	25.3	-481.6	34.6	-0.296	-1.063	-0.496	483.5	0.07	4.1	0.16	10.1	-21.66
G53-24	100442	3242	0.94	-.02	115	-70.0	-113.3	-81.0	-0.584	-1.027	-0.660	155.9	-0.61	-31.3	0.48	10.8	15.17
G162-21	100505	-61142	0.50	0.11	40	69.7	-19.4	-27.7	1.600	-0.152	-0.974	77.5	-0.38	-21.0	0.19	12.1	24.56
G43-30	100724	182606	0.81	-.05	30	-13.9	-31.3	-19.1	-0.302	-1.167	-0.374	39.2	-0.56	-29.1	0.11	10.3	23.37
G49-38	100746	215618	0.81	0.04	120	118.6	-150.4	20.7	0.460	-0.918	-0.661	192.7	0.11	6.2	0.63	11.3	11.46
*G54-17	100902	240006	0.63	0.06	44	108.6	-20.7	20.5	1.554	0.040	-0.973	112.4	0.19	10.5	0.31	14.1	24.43
*G43-33	100936	173254	0.54	0.14	38	37.7	-69.5	17.2	0.260	-1.226	-0.764	80.9	0.22	12.3	0.26	10.2	19.55
G53-30	100956	-2318	0.67	0.04	94	-102.4	-109.0	36.2	-1.309	-0.741	-0.053	153.9	0.24	13.6	0.51	11.8	15.60
G43-34	101031	95100	0.90	0.06	47	-57.5	-99.7	-71.8	-0.978	-2.419	-1.087	135.7	-0.62	-32.0	0.42	10.7	16.53
G44-6	101132	32418	0.62	0.17	26	-55.6	-18.9	-19.7	-1.812	-1.257	-0.125	61.9	-0.34	-18.5	0.21	12.4	24.61
G54-21	101408	260654	0.59	0.05	34	-37.7	-40.5	-6.2	-0.896	-1.296	0.161	55.7	-0.11	-6.4	0.19	10.8	22.45
G43-44	101930	113400	0.75	-.15	41	-35.9	-46.6	-28.0	-0.737	-1.300	-0.412	65.1	-0.48	-25.5	0.20	10.7	21.84
G162-51	102205	-51554	0.57	0.12	86	46.1	-85.2	-78.4	0.479	-0.834	-1.061	124.6	-0.81	-39.0	0.33	10.2	17.98
G55-16	102411	-61548	0.93	0.00	45	-58.4	-109.5	-54.3	-1.447	-1.992	-1.617	135.5	-0.44	-23.6	0.45	10.6	15.55
G43-52	102533	65918	0.92	-.02	27	25.6	23.1	34.8	0.657	1.304	0.614	48.4	0.99	44.6	0.21	15.3	28.81
G55-22	102542	-62030	0.79	-.04	28	26.1	-54.2	-28.5	0.719	-1.285	-1.625	66.6	-0.47	-25.3	0.19	10.1	21.08
G44-25	103245	74706	0.92	0.19	129	-273.7	-291.9	19.0	-2.316	-1.952	-0.327	400.6	0.05	2.7	0.96	22.3	-2.69
G44-28	103330	160806	0.60	0.12	57	-63.4	-41.8	-26.9	-0.907	-0.942	-0.026	80.6	-0.35	-19.5	0.25	11.7	22.32
G54-33	103358	215154	0.79	0.03	36	48.7	-37.8	12.9	0.853	-0.690	-0.660	63.0	0.21	11.8	0.16	10.6	22.72
*G44-30	103743	112724	0.64	0.19	121	-18.0	-221.2	45.9	-0.518	-1.322	-0.527	226.6	0.21	11.7	0.83	10.1	4.30
G58-12	104025	203648	0.61	0.12	110	-92.6	-120.8	-8.1	-0.823	-1.113	-0.035	152.4	-0.05	-3.0	0.53	11.3	14.42
G58-15	104357	225918	0.61	0.28	232	-229.9	-245.4	28.9	-0.995	-1.055	0.116	337.5	0.09	4.9	0.96	17.0	1.96
*G58-23	104712	204530	0.60	0.16	78	55.3	-70.0	-48.7	0.713	-0.901	-0.611	101.6	-0.55	-28.6	0.28	10.4	19.50
G58-25	104848	203254	0.46	0.24	46	39.5	-131.9	9.9	0.362	-2.443	-0.999	138.0	0.07	4.1	0.51	10.1	13.31
G45-9	104859	92136	0.74	-.06	97	-77.7	-82.2	-51.9	-0.727	-0.973	-0.315	124.4	-0.46	-24.6	0.39	11.3	18.28
G44-44	105000	51606	0.64	0.06	38	47.0	-28.9	-21.9	1.179	-0.632	-0.770	59.4	-0.40	-21.6	0.13	10.8	23.61
G58-28	105306	204106	0.52	0.11	124	-24.7	-157.9	-69.8	-0.134	-1.330	-0.396	174.4	-0.44	-23.6	0.61	10.1	10.71
G45-18	105338	21942	0.88	-.02	72	-24.1	-101.6	-1.4	-0.482	-1.000	-0.593	104.4	-0.01	-0.8	0.40	10.2	16.34
G58-30	105429	220430	0.62	0.04	38	15.4	-49.9	-12.1	0.329	-1.252	-0.515	53.6	-0.23	-13.0	0.16	10.0	21.51
G56-4	105656	181612	0.98	0.01	26	19.5	-39.4	-3.5	0.557	-1.309	-0.688	44.1	-0.08	-4.6	0.12	10.0	22.56
G56-8	105805	154324	0.86	-.02	47	68.9	-43.5	15.0	1.158	-0.534	-0.610	82.9	0.18	10.4	0.22	11.1	22.15
G58-39	110048	182436	0.66	0.11	119	-115.9	-109.1	35.1	-1.054	-0.829	0.055	163.0	0.22	12.4	0.53	12.2	15.59
G45-30	110145	60354	0.63	0.04	42	56.8	-18.8	-8.4	1.283	-0.276	-0.482	60.4	-0.14	-8.0	0.15	11.6	24.62
G58-41	110235	252824	0.56	0.11	33	48.0	-30.0	-19.8	1.404	-0.879	-0.732	68.0	-0.35	-19.3	0.14	10.8	23.50
G58-44	110544	225648	0.71	0.02	69	89.1	-65.1	9.7	1.046	-0.752	-0.566	110.8	0.09	5.0	0.32	11.3	19.99
G163-54	110706	24336	0.78	0.01	24	34.2	-12.2	-5.3	1.376	-0.333	-0.485	36.7	-0.15	-8.3	0.08	11.1	25.28
*G10-4	110826	64148	0.72	0.36	79	111.8	-260.9	-100.6	1.268	-2.913	-1.951	301.1	-0.35	-19.5	0.98	10.9	0.41
*G119-64	111004	360024	0.42	0.24	111	-208.6	-231.1	-130.6	-1.209	-2.135	0.433	337.6	-0.42	-22.8	0.92	15.4	3.39
G10-12	111640	55718	0.80	0.09	39	61.9	-94.7	87.3	1.092	-0.795	-0.639	142.9	0.77	37.7	0.38	10.4	17.03
G45-48	111755	54636	0.76	0.08	68	82.9	14.1	24.8	1.165	0.395	0.033	87.7	0.29	16.4	0.29	16.3	27.91
G56-30	111858	182830	0.52	0.19	147	-28.2	-229.1	-37.7	-0.236	-1.503	-0.427	233.9	-0.16	-9.3	0.86	10.1	3.59
G56-34	111944	144312	0.96	0.02	57	119.4	-54.2	-18.0	1.995	-0.779	-0.757	132.4	-0.14	-7.8	0.37	12.9	21.08
*G56-36	112039	201018	0.48	0.16	111	87.4	-228.4	13.8	0.575	-1.823	-0.682	244.9	0.06	3.2	0.87	10.5	3.66
G56-39	112337	210742	0.68	0.17	171	113.5	-180.5	-0.7	0.561	-0.949	-0.400	213.2	0.00	-0.2	0.72	11.0	8.45
G56-40	112351	104154	0.67	0.04	46	73.8	-32.8	-4.3	1.531	-0.523	-0.510	80.9	-0.05	-3.0	0.21	11.6	23.22
G10-26	112625	12212	0.85	-.05	62	53.4	-42.9	-11.4	0.840	-0.542	-0.417	69.4	-0.17	-9.4	0.18	10.7	22.21
G57-7	113000	111054	0.60	0.10	96	48.6	-136.0	-32.5	0.462	-1.291	-0.629	148.0	-0.22	-12.7	0.53	10.2	12.90
G57-11	113628	62012	0.60	0.08	24	27.5	-33.6	3.0	1.084	-1.027	-0.613	43.5	0.07	4.0	0.10	10.2	23.14
G57-19	114522	151030	0.86	0.44	90	110.0	-21.8	-47.1	1.255	-0.328	-0.261	121.6	-0.42	-22.8	0.31	14.1	24.32
G10-54	114714	62542	0.60	0.23	223	-185.0	-288.3	-67.1	-0.839	-1.183	-0.531	349.1	-0.20	-11.1	0.94	14.0	-2.33
G10-55	114735	51118	0.78	0.08	40	21.6	-66.0	12.6	0.514	-1.188	-0.608	70.6	0.18	10.3	0.24	10.0	19.90
G10-56	114749	-5824	0.79	0.01	48	76.6	-42.7	-5.7	1.606	-0.718	-0.393	87.9	-0.06	-3.7	0.24	11.4	22.23
G57-27	114934	190212	0.86	0.01	28	-20.9	-35.2	-9.5	-0.729	-1.285	-0.223	42.0	-0.23	-13.1	0.13	10.4	22.98
G12-28	115859	34748	0.97	0.05	72	-8.7	-99.8	-26.8	-0.120	-1.235	-0.639	102.9	-0.27	-15.1	0.38	10.1	16.60

TABLE II. (continued).

NAME	RA	DEC	B-V	EX(.6)	D	U	V	W	DU/DR	DV/DR	DW/DR	S	TAN I	I	ECC.	RMAX	H
G12-2A	115059	34748	0.79	0.05	64	-7.7	-87.8	-24.2	-0.120	-1.235	-0.639	91.4	-0.27	-15.4	0.33	10.1	17.72
G12-9	115312	144954	0.92	0.04	111	115.0	-77.7	-75.4	1.065	-0.804	-0.347	157.9	-0.54	-28.5	0.41	12.0	18.73
G12-11	115417	133936	0.70	0.07	70	61.1	-103.5	-13.5	0.849	-1.370	-0.517	120.9	-0.11	-6.4	0.42	10.4	16.15
*G13-1	115629	-42948	0.58	0.17	52	-47.6	-13.5	-39.5	-0.951	-0.482	-0.430	63.3	-0.88	-38.6	0.18	12.4	25.15
G12-13	115741	53036	0.76	0.03	32	30.0	-40.7	-8.1	0.943	-1.145	-0.522	51.2	-0.16	-9.1	0.13	10.2	22.43
*G11-36	120132	33748	0.60	0.17	55	-98.7	-127.4	-53.7	-1.639	-2.221	-1.171	165.4	-0.34	-19.0	0.55	11.2	13.76
*G11-37	120241	-11354	0.75	0.07	28	68.7	-25.3	7.4	2.493	-0.668	-0.137	73.6	0.10	5.8	0.19	11.7	23.97
G12-16	120327	145548	0.84	0.10	53	-89.6	-22.0	-43.9	-1.653	-0.624	-0.099	102.2	-0.48	-25.4	0.31	14.1	24.30
*G13-9	120442	-52712	0.40	0.28	131	54.6	-200.3	-50.9	0.478	-1.270	-0.775	213.8	-0.25	-13.8	0.76	10.2	6.47
G12-17	120456	131854	0.97	-.03	42	52.2	-66.8	9.4	1.223	-1.374	-0.466	85.3	0.11	6.3	0.27	10.4	19.82
G13-12	120545	1024	0.97	0.07	63	68.7	-47.8	-19.0	1.092	-0.756	-0.305	85.8	-0.23	-12.8	0.23	11.0	21.72
G59-1	120623	220400	0.63	0.11	65	110.4	-47.6	-32.6	1.719	-0.766	-0.299	124.6	-0.27	-15.2	0.33	12.7	21.74
G11-43	120738	43530	0.97	0.00	33	-19.3	-36.9	-37.7	-0.616	-1.341	-0.654	56.2	-0.91	-42.2	0.14	10.4	22.81
*G11-44	120822	4100	0.42	0.25	204	-173.7	-398.0	-120.8	-0.808	-1.732	-1.005	458.7	-0.28	-15.5	0.67	14.6	-13.30
G12-20	120829	122518	0.81	0.09	143	239.8	-74.6	22.6	1.675	-0.424	-0.148	252.2	0.09	5.1	0.69	22.6	19.04
*G12-21	120929	133248	0.45	0.21	121	-19.0	-270.0	29.0	-0.168	-1.984	-0.590	272.2	0.11	6.1	0.98	10.1	-0.58
G11-45	120958	-24848	0.71	0.03	24	76.8	-8.4	25.7	3.263	0.241	0.636	81.0	0.33	18.5	0.23	14.1	26.46
G12-22	121024	101912	0.79	-.04	29	-48.7	-23.5	-21.4	-1.687	-0.942	-0.363	58.2	-0.40	-21.6	0.19	11.8	24.15
G12-24	121040	110624	0.69	0.07	24	-31.2	-43.6	-47.4	-1.313	-2.223	-0.765	71.6	-0.88	-41.5	0.18	10.6	22.14
G59-5	121056	233236	0.57	0.10	75	102.5	-19.4	-43.1	1.404	-0.313	-0.176	112.9	-0.41	-22.4	0.29	13.8	24.56
G11-46	121059	74900	0.84	0.02	121	-118.0	-99.1	-30.6	-0.970	-0.781	-0.350	157.1	-0.20	-11.2	0.51	12.5	16.59
G13-21	121131	51630	0.79	0.00	39	30.1	-44.5	-0.1	0.800	-0.981	-0.371	53.7	0.00	-0.1	0.15	10.1	22.05
G13-29	121646	24324	0.90	0.03	86	-3.2	-123.4	-13.2	0.813	-1.235	-0.578	124.1	-0.11	-6.1	0.47	10.0	14.16
*G59-18	122100	171054	0.72	0.19	60	56.5	-67.0	14.8	0.940	-1.016	-0.220	88.9	0.17	9.6	0.27	10.5	19.80
*G13-35	122302	13406	0.42	0.26	103	-122.4	-239.2	37.8	-0.979	-1.693	-0.958	271.3	0.14	8.0	0.91	11.6	2.58
G13-38	122426	15054	0.70	0.16	77	-95.8	-142.6	94.3	-0.949	-0.995	-0.615	196.0	0.55	28.8	0.60	11.3	12.24
G60-6	122529	74354	0.94	0.03	77	96.3	15.9	-11.9	1.219	0.094	0.160	98.3	-0.12	-7.0	0.34	17.5	28.89
*G13-43	122710	-30306	0.69	0.12	43	4.7	-118.4	-69.4	0.889	-2.800	-1.530	137.3	-0.59	-30.4	0.45	10.0	14.66
G59-22	123013	265342	0.64	0.22	284	339.3	-268.3	87.2	1.171	-0.925	-0.110	441.3	0.28	11.4	1.00	33.9	-0.33
*G59-24	123155	153324	0.42	0.29	282	325.6	-315.9	-125.2	1.142	-1.174	-0.193	470.6	-0.28	-15.4	0.94	30.3	-5.09
G59-25	123229	232530	0.59	0.04	59	-53.5	-50.9	-47.0	-0.894	-0.930	-0.071	87.5	-0.64	-32.5	0.25	11.1	21.41
*G59-27	123412	274506	0.40	0.29	190	41.9	-260.2	-117.5	0.250	-1.384	-0.048	288.6	-0.45	-24.0	0.98	10.1	0.48
G59-29	123538	222242	0.99	-.04	76	36.4	-111.4	8.7	0.479	-1.439	-0.147	117.5	0.07	4.2	0.43	10.1	15.36
G13-50A	123609	-50306	1.00	0.07	35	-53.2	2.8	15.1	-1.348	0.414	-0.156	55.4	0.28	15.8	0.23	14.2	26.78
G13-50	123609	-50306	0.84	-.04	44	-66.0	5.3	15.9	-1.348	0.414	-0.156	68.1	0.24	13.5	0.27	15.3	27.03
B402558	123624	393510	0.04	0.00	141	-1.6	-145.8	-124.3	0.143	-0.876	0.117	191.6	-0.85	-40.4	0.56	10.0	11.92
*G60-26	123728	125512	0.65	0.20	59	-54.9	-100.7	86.3	-0.751	-1.257	-0.380	143.5	0.75	37.0	0.42	10.6	16.43
G59-32	123737	210512	0.77	-.10	60	-101.9	-53.0	-30.1	-1.705	-0.924	-0.145	118.7	-0.26	-14.7	0.37	13.0	21.20
G13-54	124026	-34624	0.66	0.09	29	9.3	-52.9	19.9	0.653	-1.217	-0.455	57.3	0.37	20.3	0.18	10.0	21.21
G59-36	124033	213354	0.92	-.01	77	38.5	-83.7	-35.3	0.490	-1.124	-0.104	98.7	-0.38	-21.0	0.32	10.1	18.13
G61-11	124223	134548	0.66	0.01	61	57.6	-50.2	-22.3	0.915	-0.882	-0.095	79.6	-0.29	-16.3	0.22	10.7	21.48
G60-31	124251	43806	0.60	0.11	71	-49.5	-47.0	-64.6	-0.788	-0.826	-0.465	94.0	-0.95	-43.4	0.23	11.1	21.80
G61-14	124405	242512	0.53	0.01	31	-6.0	-39.6	-3.4	-0.192	-1.280	-0.072	40.2	-0.08	-4.9	0.12	10.1	22.54
G59-38	124424	224536	0.60	0.07	79	90.4	-53.1	-24.8	1.136	-0.695	-0.022	107.7	-0.24	-13.3	0.30	11.6	21.19
*G14-5	124712	12818	0.68	0.13	29	-35.6	-72.1	-39.2	-1.231	-2.488	-1.343	89.5	-0.49	-26.0	0.29	10.4	19.29
G60-46	125233	80412	0.66	0.20	137	-45.3	-151.1	-84.7	-0.374	-1.163	-0.408	179.0	-0.54	-28.2	0.59	10.3	11.39
G60-47	125244	80612	0.80	0.04	58	-67.2	-16.6	-5.1	-1.117	-0.228	-0.294	69.4	-0.07	-4.2	0.24	13.2	24.84
*G60-48	125312	124954	0.49	0.26	172	82.3	-207.9	-44.5	0.480	-1.671	-0.272	302.7	-0.15	-8.5	0.91	10.4	-2.29
G61-23	125501	185642	0.70	0.11	62	79.1	-11.3	-28.5	1.220	-0.244	0.097	84.8	-0.36	-19.6	0.22	13.1	25.37
G61-24	125504	185748	0.66	0.08	50	64.5	-8.4	-29.8	1.220	-0.244	0.097	71.5	-0.46	-24.6	0.18	12.6	25.66
*G14-22	125844	-81018	0.71	0.00	52	84.0	-49.8	-26.2	1.428	-1.205	-0.071	101.1	-0.27	-15.0	0.27	11.5	21.52
G14-23	125853	-91112	0.54	0.13	85	78.8	47.8	93.6	1.028	0.696	0.875	131.4	1.02	45.4	0.43	23.5	31.28
G14-26	130036	-55112	0.57	0.04	97	125.8	17.2	43.0	1.247	0.113	0.567	134.1	0.34	18.7	0.43	20.4	28.22
G61-28	130232	163954	1.00	0.02	124	141.5	-113.3	43.5	1.184	-0.878	0.068	186.4	0.24	13.5	0.55	12.4	15.17
G60-62	130244	31400	0.98	-.01	73	60.1	-66.2	-0.8	0.836	-0.892	-0.053	89.4	-0.01	-0.5	0.28	10.5	19.88
G61-30	130406	111848	0.60	0.04	52	50.0	-46.3	-18.2	0.889	-0.960	-0.007	70.5	-0.27	-15.0	0.19	10.5	21.87
*G60-66	130541	40236	0.68	0.06	67	77.0	-44.5	-51.8	0.920	-0.908	-0.012	102.9	-0.58	-30.2	0.24	11.4	22.85
*G14-32	130551	-70236	0.94	0.28	16	-6.8	-32.1	70.2	1.284	0.004	0.577	77.5	2.14	64.9	0.09	10.2	23.29
G14-33	130614	-34224	0.66	0.21	106	126.2	-60.3	-90.0	0.877	-0.926	-0.071	166.3	-0.64	-32.8	0.40	13.0	20.47
G60-67	130619	52854	0.65	0.02	22	-40.6	-54.3	-12.4	-1.674	-2.294	-1.153	68.9	-0.18	-10.4	0.24	10.7	21.07
G63-5	130853	95318	0.62	0.12	46	127.9	-23.3	54.8	2.916	-0.387	0.637	141.1	0.42	22.9	0.37	15.2	24.17
*G63-9	130954	174654	0.53	0.13	30	65.3	-53.6	54.8	2.438	-1.641	0.251	100.7	0.65	33.0	0.24	10.8	21.14
G62-23	131308	91654	0.66	0.03	44	54.8	-59.3	-12.6	1.165	-1.411	0.012	81.7	-0.16	-8.9	0.24	10.5	20.57
G61-45	131315	120930	0.88	0.02	39	30.7	3.1	58.4	1.072	0.281	0.302	66.1	1.89	62.1	0.12	12.5	26.81
G14-41	131332	-30542	0.72	0.07	75	87.9	23.1	27.3	1.089	0.225	0.559	94.9	0.30	16.7	0.34	18.2	28.81
G63-18	131422	171700	0.87	-.01	12	-39.2	9.1	-4.0	-3.226	0.776	-0.532	40.4	-0.18	-5.7	0.21	14.3	27.41
*G14-45	131624	-24830	1.00	0.21	55	74.2	-165.4	111.6	2.207	-2.190	0.053	212.9	0.62	31.6	0.65	10.4	9.96
G62-33	131813	42336	0.96	0.03	23	66.8	-7.1	-12.1	2.482	-0.643	0.682	68.3	-0.18	-10.2	0.19	12.9	25.79
G63-26	132206	204306	0.46	0.19	313	-138.5	-365.6	18.4	-0.415	-1.165	-0.098	391.4	0.05	2.7	0.70	12.4	-10.06
G14-54	132544	-3430	0.66	0.08	24	-29.3	-16.9	-28.8	-1.363	-0.815	-0.886	44.4	-0.85	-40.4	0.12	11.4	24.81
*G62-44	132907	-20354	0.78	0.14	16	86.1	-2.1	-27.4	3.897	-1.267	1.403	98.4	-0.32	-17.6	0.26	14.4	26.29
*G63-44	133536	192418	0.68	0.16	37	-42.0	-26.9	-54.7	-1.407	-0.733	-0.338	74.0	-1.10	-47.6	0.17	11.4	23.81
*G64-12	133729	1254	0.38	0.30	270	-4.3	-402.6	395.4	0.684	-1.057	0.813	564.3	0.98	44.5	0.49	10.8	-13.76
*G63-46	133732	125042	0.58	0.20	58	-66.1	-38.7	-55.9	-1.293	-0.713	-0.482	94.8	-0.73	-36.1	0.26	11.9	22.63
G62-63	133944	83830	0.40	0.12	29	34.9	-46.6	-10.2	1.021	-1.680	0.129	59.1	-0.18	-9.9	0.17	10.2	21.84
G63-51	134110	143700	0.63	0.00	25	28.7	-25.4	4.4	1.113	-1.023	0.286	38.6	0.11	6.5	0.07	10.3	23.96
G62-67	134201	-25330	0.55	0.30	301	-322.1	-277.3	-90.5	-0.838	-0.776	-0.725	434.5	-0.21	-12.0	0.99	35.2	-1.23
G64-23	134346	-1230	0.93	-.05	42	72.9	-45.3	-15.0	1.376	-1.281	0.339	87.1	-0.17	-9.9	0.24	11.2	21.97
LFT1036	134430	63600	0.64	0.03	18	44.1	-26.9	-25.3	1.682	-1.803	0.403	57.5	-0.49	-26.1	0.12	10.7	23.81
G65-13	135142	102948	0.73	0.02	48	-69.3	-12.3	4.1	-1.206	-0.201	-0.504	70.5	0.06	3.3	0.25	13.6	25.27
G65-16	135322	124118	0.62	0.10	44	-47.8	-64.5	19.6	-0.776	-1.421	-0.373	82.6	0.24	13.7	0.28	10.7	20.05
G65-17	135449	71336	0.88	-.03	61	70.2	-62.0	-51.2	0.692	-1.150	0.163	106.7	-0.55	-28.7	0.28	10.8	20.30
G64-34	135716	-50824	1.01	0.40	75	65.9	-65.2	52.9	1.059	-0.776	0.429	106.7	0.57	29.7	0.28	10.7	19.98
*G65-22	135916	91018	0.75	0.28	100	-281.5	-240.3	-124.7	-2.727	-2.385	-1.442	398.6	-0.34	-18.6	0.96	23.7	2.47
*G64-37	135953	-52424	0.36	0.25	276	-211.3	-420.8	-183.6	-0.608	-1.445	-0.900	505.4	-0.39	-21.3	0.70	18.7	-15.58
G64-46	140405	-51648	0.87	0.03	26	56.3	-22.9	-23.5	1.241	-1.313	0.432	65.2	-0.39	-21.1	0.15	11.3	24.21
G65-29	140826	70706	0.92	0.04	122	44.6	-156.1	-51.7	0.167	-1.316	-0.039	170.4	-0.32	-17.7	0.68	10.1	10.89
G65-33	140933	72018	1.04	0.40	109	362.0	-286.1	-77.6	2.430	-2.777	1.011	467.9	-0.17	-9.5	0.99	47.1	-2.11
G64-54	141010	-30500	0.74	0.08	17	-17.0	-33.0	18.4	0.011	-1.546	-0.400	41.4	0.50	26.4	0.12	10.4	23.20
G65-43	141547	125830	0.88	0.11	61	-41.5	-77.2	-29.6	-0.752	-1.262	-0.329	92.5	-0.34	-18.7	0.32	10.5	18.78
G65-45	141847	91206	0.97	[illegible].09	74	-72.5	-48.1	-39.3	-0.976	-0.650	-0.537	95.5	-0.45	-24.3	0.29	11.9	21.69
G65-47	142042	12824	0.63	0.10	15	-14.8	-12.7	-40.7	-1.862	-1.844	-1.380	45.1	-2.09	-64.4	0.88	11.1	25.23
G65-51	142335	133936	0.73	0.01	32	18.9	-41.8	11.4	0.592	-1.307	0.352	47.3	0.25	14.0	0.13	10.0	22.32
G65-52	142548	43636	0.60	0.22	187	59.8	-278.1	-70.9	0.113	-1.514	-0.052	293.2	-0.25	-14.0	0.95	10.2	-1.31
G66-8	143238	43436	0.94	0.16	189	-40.5	-394.1	-29.0	-0.163	-2.081	-0.231	397.2	-0.07	-4.2	0.53	10.3	-12.91
G66-9	143249	122636	0.51	0.33	197	30.8	-299.0	-5.2	0.071	-1.508	0.132	300.6	-0.02	-1.0	0.87	10.0	-3.40
G66-11	143333	95800	0.98	0.02	14	-12.2	-5.4	-24.6	-1.419	-0.356	-0.814	28.0	-1.84	-61.5	0.89	11.6	25.96
G66-16	143458	111506	0.82	-.05	103	146.7	-72.3	14.0	1.122	-0.674	0.670	164.1	0.89	4.9	0.46	13.6	19.27
G66-15	143458	111436	0.65	0.05	74	116.6	-53.0	-9.6	1.122	-0.674	0.670	128.4	-0.08	-4.3	0.36	12.8	21.20
G66-18	143539	-3748	0.86	0.09	207	408.5	-353.7	187.2	1.794	-1.741	1.138	571.9	0.35	19.1	1.00	1161.8	-8.87

TABLE II. (continued).

NAME	RA	DEC	B-V	EX(.6)	D	U	V	W	DU/DR	DV/DR	DW/DR	S	TAN I	I	ECC.	RMAX	H
*G66-22	144051	60224	0.70	0.17	73	266.5	-195.4	2.8	2.532	-2.690	1.691	330.5	0.01	0.5	0.87	19.3	6.96
G66-24	144445	25442	0.90	0.07	17	5.6	-20.4	14.1	0.638	-1.179	0.425	25.4	0.67	33.7	0.03	10.0	24.46
G66-26	144529	41000	0.99	-.04	75	11.2	-88.6	-16.9	0.002	-1.186	-0.025	90.9	-0.19	-10.7	0.33	10.0	17.64
*G66-30	144735	10254	0.40	0.22	237	204.8	-294.1	-2.8	0.563	-1.266	0.365	358.4	-0.01	-0.4	0.92	14.0	-2.91
G66-33	144907	75654	0.63	0.08	70	111.8	19.2	11.3	1.171	0.306	0.785	114.8	0.10	5.7	0.39	19.4	28.42
G66-35	144957	1906	0.62	0.08	49	-29.6	-52.4	-35.7	-0.679	-1.075	-0.638	70.0	-0.59	-30.7	0.21	10.4	21.26
G66-38	145007	71000	0.53	0.23	341	-233.4	-323.9	-97.2	-0.612	-0.954	-0.389	410.9	-0.24	-13.7	0.88	17.7	-5.89
*G151-10	145227	-85330	0.72	0.14	49	44.1	-69.2	-73.8	-0.121	-1.652	-0.529	110.4	-0.90	-42.0	0.27	10.2	19.58
G66-43	145351	90454	0.92	0.01	49	63.4	-49.5	-22.2	0.630	-0.927	0.512	83.4	-0.28	-15.4	0.23	10.8	21.55
G66-44	145423	84748	0.83	0.05	30	62.1	-11.0	0.8	1.400	-0.285	0.995	63.1	0.01	0.7	0.17	12.3	25.40
G66-47	145751	111324	0.90	-.01	55	93.9	-58.1	16.6	1.260	-0.968	0.970	111.7	0.15	8.5	0.32	11.6	20.69
G66-49	145809	84806	0.69	0.05	22	-17.1	-30.7	0.0	-0.581	-1.422	-0.275	35.1	0.00	0.0	0.11	10.4	23.43
G66-51	145819	21936	0.71	0.17	77	114.9	-93.1	-67.5	0.453	-1.216	0.370	162.6	-0.46	-24.5	0.45	11.7	17.19
G66-55	150035	85306	0.80	0.13	100	-147.4	-175.8	-65.7	-1.371	-1.774	-0.799	238.6	-0.29	-16.0	0.74	12.7	8.92
G66-59	150124	105612	0.65	0.29	220	-180.9	-183.4	-101.4	-0.828	-0.833	-0.453	276.8	-0.39	-21.5	0.79	14.2	8.16
G66-60	150225	102554	0.82	0.22	74	73.0	-110.3	84.2	1.097	-1.512	0.981	156.8	0.64	32.5	0.45	10.5	15.47
G15-6	150230	41648	0.70	0.12	61	113.3	-50.1	19.0	1.249	-0.790	1.055	125.3	0.15	8.7	0.35	12.7	21.49
G66-63	150433	120112	0.90	0.03	61	73.4	-67.9	-8.7	0.674	-0.982	0.629	100.4	-0.09	-5.0	0.30	10.8	19.71
*G66-65	150522	90418	0.56	0.15	41	81.5	-82.1	-0.3	1.162	-1.857	1.103	115.7	0.00	-0.1	0.36	10.9	18.29
G15-7	150617	-33524	0.72	0.16	74	76.5	-93.6	-51.3	0.221	-1.331	0.112	131.3	-0.42	-23.0	0.40	10.7	17.14
G15-10	150708	-43330	0.65	0.31	122	-205.4	-189.1	-94.6	-1.125	-1.497	-1.314	294.8	-0.34	-18.7	0.83	15.6	7.59
G15-13	151005	61324	0.75	0.31	125	-225.1	-481.5	155.6	-0.669	-3.996	-0.134	553.8	0.29	16.3	0.70	27.6	-21.65
G15-14	151013	-5836	0.79	0.05	44	41.3	-75.2	-52.6	-0.100	-1.727	-0.128	100.6	-0.61	-31.5	0.29	10.2	18.98
G15-17	151752	2542	0.80	0.08	40	-27.1	-18.8	-44.3	-0.905	-0.462	-0.878	55.2	-1.34	-53.3	0.12	11.2	24.62
G15-20	152011	13612	0.99	-.07	24	20.1	-62.5	-18.2	-0.037	-2.544	0.140	68.1	-0.28	-15.5	0.22	10.0	20.25
*G15-23	152704	61924	0.70	0.25	83	-4.2	-191.3	-61.7	-0.593	-2.199	-0.150	201.0	-0.32	-17.9	0.72	10.0	7.37
*G15-24	152817	83400	0.57	0.21	150	152.3	-254.2	71.9	0.639	-1.601	0.910	304.9	0.24	13.6	0.96	11.8	1.08
G16-8	154308	-20618	0.73	0.27	107	75.0	-136.8	51.8	0.446	-1.257	0.689	164.4	0.33	18.4	0.55	10.5	12.82
G16-9	154324	51148	0.00	0.00	0	-18.6	4.2	17.8	0.795	-0.405	0.928	26.1	0.93	43.0	0.14	12.8	26.92
*G16-13	154834	83430	0.59	0.16	82	32.3	-123.5	5.7	0.011	-1.383	0.454	127.8	0.04	2.6	0.48	10.1	14.15
G16-15	155152	-40806	0.96	0.04	89	165.7	-81.7	56.0	0.894	-0.838	1.330	193.0	0.30	16.9	0.52	14.4	18.33
G16-20	155547	21148	0.62	0.22	95	-165.5	-104.3	98.8	-0.365	-1.387	-0.090	219.2	0.51	26.8	0.60	14.9	16.07
G16-25	155854	53212	0.58	0.25	333	-97.0	-629.2	131.2	-0.242	-1.904	0.351	650.0	0.21	11.6	0.79	80.5	-36.42
G16-28	160106	24524	0.72	0.24	136	-34.0	-164.3	33.0	-0.157	-1.230	0.169	171.0	0.20	11.1	0.63	10.2	10.07
G16-31	160624	15918	0.85	0.07	55	-114.9	-87.8	62.3	-0.519	-1.973	-0.061	157.5	0.43	23.3	0.47	12.6	17.72
G16-32	160643	63106	1.00	-.02	7	-9.9	-17.2	-20.2	-2.428	-2.125	-2.034	28.3	-1.02	-45.5	0.06	10.6	24.78
G16-34	160945	53730	0.94	0.08	101	-103.2	-335.5	-11.8	-1.104	-3.295	-0.050	351.2	-0.03	-1.9	0.77	11.2	-7.05
G16-35	161025	65142	0.66	0.17	275	-19.7	-494.1	-36.6	-0.441	-1.667	0.174	495.8	-0.07	-4.2	0.13	10.4	-22.91
G17-10	161713	30818	0.90	0.15	78	-0.5	-92.5	-8.7	-0.269	-1.107	0.080	92.9	-0.09	-5.4	0.35	10.0	17.25
G17-12	161924	71742	0.79	0.08	54	0.5	-81.1	24.2	-0.124	-1.449	0.554	84.6	0.30	16.6	0.30	10.0	18.39
G17-14	162346	21748	0.96	0.07	45	-141.4	-50.3	-20.1	-1.521	-1.603	-1.542	151.4	-0.13	-7.6	0.47	15.7	21.47
*G17-16	162514	-5730	0.72	0.15	51	148.7	-107.6	-40.8	0.190	-1.449	0.878	188.0	-0.22	-12.5	0.54	12.8	15.74
G17-19	162606	32206	0.77	-.01	43	-76.5	-78.1	-39.4	-1.422	-1.931	-1.160	116.2	-0.36	-19.8	0.38	11.4	18.69
*G17-21	162801	41806	0.53	0.17	27	-44.5	-185.8	-61.4	-3.106	-6.368	-1.266	200.7	-0.32	-17.8	0.71	10.3	7.92
G17-22	163022	32112	0.88	0.06	29	52.7	-72.4	-6.2	0.011	-1.884	0.981	89.8	-0.07	-4.0	0.29	10.4	19.26
*G17-25	163204	-40706	0.75	0.28	41	94.0	-155.5	-121.2	-1.211	-3.070	-1.075	218.4	-0.67	-33.7	0.62	10.7	10.95
G17-29	163513	830	0.76	-.05	35	33.0	-59.8	-12.2	-0.208	-1.372	0.327	69.4	-0.18	-10.1	0.22	10.1	20.52
*G17-30	163542	-22024	0.62	0.15	38	25.6	-66.2	-21.0	-0.360	-1.486	0.014	74.0	-0.30	-16.5	0.24	10.1	19.88
G17-31	163722	53630	0.88	0.00	30	-67.3	-9.9	-6.9	-1.024	-0.821	-1.040	68.4	-0.10	-5.8	0.25	13.7	25.51
G17-35	164234	61054	0.87	0.09	10	2.3	-17.8	-1.1	-0.435	-1.493	0.322	18.0	-0.06	-3.5	0.03	10.2	24.72
*G19-4	165027	418	0.77	0.08	13	-71.5	-79.6	8.9	-2.727	-7.044	-0.746	107.4	0.08	4.8	0.37	11.2	18.54
G19-11	170200	34836	0.96	-.07	94	69.4	-151.2	17.5	-0.183	-1.206	0.663	167.3	0.11	6.0	0.59	10.4	11.38
L15049	170239	460942	0.47	0.10	49	-55.0	10.3	19.9	-0.953	-0.306	-0.010	59.4	0.36	19.6	0.26	15.3	27.53
*L15157	172027	245536	0.54	0.18	21	-34.0	16.6	4.2	-0.707	-0.202	-0.574	38.1	0.11	6.3	0.23	15.1	28.16
G19-25	172322	-24142	0.78	0.38	81	-27.2	-138.6	-40.6	-0.708	-1.573	-0.374	147.0	-0.29	-16.0	0.54	10.2	12.64
G19-26	172344	33200	0.97	0.07	138	37.7	-307.3	0.8	-0.690	-1.754	0.407	309.6	0.00	0.1	0.84	10.1	-4.23
L15182	172449	310600	0.71	0.15	54	58.4	-93.8	43.9	0.414	-0.797	1.497	118.9	0.40	21.7	0.38	10.4	17.12
*L15181	172451	310706	0.61	0.18	37	50.7	-79.3	19.1	0.414	-0.797	1.497	96.0	0.20	11.5	0.31	10.3	18.57
*G19-27	172849	-23006	0.67	0.16	28	-11.2	-27.1	27.2	-0.134	-1.073	0.888	40.0	0.93	42.8	0.09	10.3	23.79
*G20-8	173716	22630	0.45	0.30	104	365.6	-236.4	71.1	0.288	-0.645	1.790	441.1	0.16	9.3	0.98	50.7	2.86
*L15244	173756	371312	0.57	0.18	39	-156.2	-74.7	68.4	-3.595	-2.694	1.254	186.2	0.40	21.6	0.54	15.4	19.03
L15268	174429	100812	0.54	0.14	50	-65.0	-22.6	-7.2	-0.742	-0.840	-0.376	69.2	-0.10	-6.0	0.24	12.6	24.24
*G20-15	174443	-84530	0.60	0.25	88	-129.3	-45.4	-156.2	-0.687	-0.789	-1.934	207.8	-1.14	-48.7	0.44	15.1	21.96
G20-19	175129	30400	0.70	0.27	216	-258.5	-212.4	107.9	-0.626	-1.301	0.335	351.5	0.32	17.9	0.91	20.5	5.26
*G183-11	175235	201654	0.44	0.22	101	29.6	-308.7	-53.1	-1.283	-1.449	0.350	314.6	-0.17	-9.7	0.83	10.0	-4.37
L15336	180200	302300	0.51	0.09	27	-30.6	-17.2	-4.5	-1.121	-0.653	-0.174	35.4	-0.13	-7.3	0.13	11.4	24.78
G20-23	180350	20300	0.65	0.11	136	-47.8	-239.0	-4.4	-0.828	-1.487	0.074	243.8	-0.02	-1.0	0.90	10.3	2.60
*G20-24	180526	15212	0.46	0.16	197	-153.3	-224.1	69.6	-0.627	-1.223	0.321	280.3	0.26	14.4	0.88	12.6	4.09
L15369	180724	30700	0.46	0.04	21	5.9	-22.8	-13.8	-0.482	-0.625	-0.487	27.3	-0.59	-30.4	0.04	10.0	24.22
G21-6	181108	-83906	1.06	0.40	51	71.1	-135.2	-49.7	-0.763	-1.825	-0.799	160.6	-0.33	-18.0	0.54	10.4	12.98
L15462	182730	91000	0.54	0.06	63	-68.6	-32.1	6.4	-0.673	-0.843	0.018	76.0	0.08	4.8	0.25	12.3	23.29
*G141-19	183059	130718	0.64	0.26	79	-145.2	-5.0	-16.5	-0.932	-0.899	-0.425	146.2	-0.11	-6.5	0.58	21.1	26.00
*L15478	183242	342200	0.50	0.19	32	48.0	-8.3	-25.5	1.016	0.685	-0.450	55.0	-0.52	-27.6	0.13	11.9	25.67
G21-19	183437	-5600	0.63	0.22	154	-15.4	-266.2	21.3	-0.775	-1.331	0.176	267.5	0.08	4.6	1.00	10.1	-0.12
G21-20	183515	-65030	0.84	-.01	29	23.4	-71.6	-2.4	-0.807	-1.704	-0.087	75.4	-0.03	-1.8	0.26	10.0	19.34
*G21-22	183636	430	0.54	0.18	130	-213.5	-236.0	-27.0	-1.272	-2.044	-0.229	319.4	-0.08	-4.8	0.93	15.7	2.90
L15529	184330	203000	0.47	0.04	10	-27.3	10.3	-1.8	-1.209	-0.837	-0.626	29.2	-0.06	-3.5	0.18	13.9	27.53
G21-25	184538	-50842	0.76	0.28	51	-18.8	-16.1	-70.4	-0.178	-0.417	-1.375	74.6	-2.84	-70.6	0.09	11.0	24.89
L15548	184942	383354	0.53	0.17	26	18.5	5.0	-37.8	0.536	0.633	-1.314	42.4	-1.97	-63.1	0.11	12.5	27.00
*G22-6	185145	-43948	0.59	0.18	51	-69.5	-83.5	-10.9	-1.012	-1.831	-0.193	109.2	-0.10	-5.7	0.38	11.1	18.15
G22-7	185313	-54824	0.78	0.00	22	46.9	-72.0	5.3	-0.890	-1.648	0.024	86.1	0.06	3.5	0.28	10.3	19.30
G22-8	185342	-42906	0.96	0.46	93	17.8	-159.7	-29.3	-0.673	-1.227	-0.368	163.3	-0.18	-10.3	0.61	10.0	10.53
G22-9	185342	-42836	0.72	0.12	67	-106.5	-47.4	-28.5	-0.673	-1.227	-0.368	120.0	-0.24	-13.7	0.38	13.5	21.76
G22-19	191014	63830	0.68	0.24	191	-322.7	-129.4	54.0	-1.080	-1.214	0.306	351.8	0.16	8.8	0.91	52.2	13.56
*G22-20	191048	-4036	0.51	0.16	70	-52.2	-188.4	35.5	-1.538	-2.138	0.420	198.7	0.18	10.3	0.72	10.4	7.66
L15637	191247	102912	0.52	0.20	70	37.8	-88.5	79.3	-0.367	-0.356	1.124	124.7	0.82	39.5	0.34	10.1	17.65
L15649	191524	465400	0.47	0.07	22	34.5	-32.3	3.5	1.241	0.089	0.599	47.4	0.07	4.2	0.11	10.3	23.27
G22-24	191751	-43600	0.91	0.08	60	-61.9	-102.1	-69.4	-0.917	-1.774	-1.136	138.1	-0.58	-30.2	0.43	10.7	16.29
*L15675	192324	244900	0.52	0.12	18	-44.3	-32.8	-12.5	-2.634	-1.535	-0.667	56.5	-0.23	-12.8	0.19	11.3	23.22
*G23-1	192555	135354	0.78	0.14	34	19.2	17.7	-37.0	0.605	0.476	-1.086	45.3	-1.42	-54.8	0.18	14.3	28.27
G92-6	192712	5518	0.58	0.17	187	-202.4	-152.8	91.9	-0.871	-0.984	0.529	269.7	0.36	19.9	0.75	16.1	11.22
L15699	192906	360300	0.73	0.17	64	-141.7	-63.7	-79.2	-2.328	-0.687	-1.189	174.4	-0.51	-27.0	0.49	15.0	20.13
G23-3	193028	71800	0.69	0.10	52	-30.6	-62.9	-57.0	-0.810	-0.993	-1.129	90.2	-0.81	-39.2	0.25	10.4	20.21
L15703	193035	482900	0.46	0.02	82	132.6	-31.7	18.1	1.529	0.158	0.357	137.5	0.13	7.6	0.38	14.9	23.33
L15705	193042	500400	0.65	0.12	30	35.8	-25.3	27.9	1.097	-0.141	1.112	52.0	0.64	32.5	0.09	10.5	23.97
G23-4	193142	123148	0.81	0.08	32	-32.9	-31.9	-10.9	-1.066	-0.953	-0.344	47.1	-0.24	-13.4	0.15	10.9	23.31
G23-6	193233	111848	0.68	0.09	28	54.5	-35.2	-27.4	0.509	0.343	-1.140	70.4	-0.42	-22.9	0.17	10.8	22.98
*G92-11	193311	-2048	0.65	0.09	47	-26.9	-69.4	-9.4	-0.893	-1.227	-0.270	75.0	-0.13	-7.2	0.27	10.3	19.56
*G23-7	193312	13712	0.96	0.40	22	43.9	-75.3	1.9	-0.811	-1.104	-0.492	87.2	0.02	1.2	0.29	10.2	18.97
*G92-14	193327	-100	0.69	0.06	24	-7.5	-42.7	-14.4	-0.884	-1.331	-0.729	45.7	-0.33	-18.4	0.14	10.1	22.23

TABLE II. (continued).

NAME	RA	DEC	B-V	EX(.6)	D	U	V	W	DU/DR	DV/DR	DW/DR	S	TAN I	I	ECC.	RMAX	H
G92-15	193347	43918	0.66	0.12	50	-83.0	9.7	-40.5	-0.595	-0.776	-0.615	92.9	-0.48	-25.9	0.34	17.1	27.47
L15729	193506	500600	0.38	0.10	15	17.6	-18.0	4.9	1.027	-0.022	0.622	25.6	0.19	11.0	0.03	10.2	24.70
G92-16	193519	41154	0.70	0.09	74	-77.2	-59.1	-23.1	-0.037	-0.984	-0.272	99.9	-0.24	-13.4	0.33	11.7	20.59
G92-19	193638	-24330	0.66	0.14	80	99.0	-81.4	-77.1	0.156	-0.229	-1.244	149.6	-0.60	-31.8	0.39	11.4	18.36
G92-23	194002	80200	0.75	0.13	36	43.7	9.9	-13.6	0.809	0.695	-0.455	46.8	-0.30	-16.9	0.18	13.8	27.49
L15756	194100	242900	0.58	0.15	20	-11.7	-17.1	-19.1	-0.813	-0.450	-0.950	28.2	-0.92	-42.7	0.07	10.7	24.79
L15789	194736	412800	0.51	0.13	34	-19.8	-1.7	-24.2	-0.583	-0.045	-0.713	31.3	-1.22	-50.6	0.12	12.2	26.33
G23-12	194826	34912	0.93	0.06	37	79.1	-79.8	-23.9	0.106	-0.235	-1.198	114.8	-0.21	-11.7	0.35	10.8	18.52
G23-14	194922	52912	0.74	0.30	60	-67.5	-41.1	4.4	-0.922	-0.888	0.129	79.2	0.06	3.2	0.26	11.9	22.39
G23-15	195143	14854	0.89	-.01	32	-26.3	-28.6	-20.5	-0.707	-0.994	-0.604	43.9	-0.53	-27.8	0.13	10.8	23.64
G23-16	195154	14848	0.90	0.00	33	-25.9	-31.6	-20.6	-0.724	-1.013	-0.607	45.8	-0.50	-26.8	0.13	10.7	23.34
G23-17	195233	35554	0.98	-.03	35	-80.5	-2.3	11.6	-1.243	-1.086	0.648	81.4	0.14	8.2	0.30	15.3	26.27
G92-39	195340	41018	0.72	0.06	54	-74.1	-15.6	6.8	-0.859	-0.791	0.281	76.0	0.09	5.1	0.27	13.6	24.94
L15834	195448	292400	0.45	0.10	56	-49.2	-29.2	-2.6	-0.928	-0.407	-0.045	57.3	-0.05	-2.6	0.19	11.6	23.58
*G23-20	195810	91306	0.64	0.21	134	28.6	-296.6	98.5	-1.017	-0.778	0.376	313.8	0.33	18.3	0.88	10.0	-3.16
G23-23	200033	140724	0.86	0.06	88	-128.7	-46.0	2.9	-1.214	-0.865	0.098	136.7	0.02	1.2	0.44	15.0	21.90
G92-49	200045	-30548	1.02	0.51	42	79.1	-93.3	-16.1	-0.066	-0.663	-1.161	123.4	-0.13	-7.5	0.40	10.7	17.17
*G24-3	200315	35424	0.46	0.23	129	27.9	-247.7	74.2	-0.882	-0.810	0.171	260.1	0.30	16.6	0.93	10.0	1.73
L15895	200454	530100	0.43	0.03	25	40.9	-44.3	-15.3	1.556	0.114	-0.238	62.2	-0.25	-14.2	0.17	10.3	22.07
G24-11	201219	34842	0.91	0.14	99	138.8	-41.3	-62.4	0.716	0.303	-0.925	157.7	-0.43	-23.3	0.41	14.6	22.37
*G24-13	201756	55242	0.62	0.21	72	-115.5	-2.9	-98.5	-0.742	-1.031	-0.974	151.8	-0.85	-40.4	0.41	10.1	26.21
*G24-15	202347	91730	0.47	0.23	48	77.9	-270.5	-10.0	-1.393	-1.656	-1.653	281.7	-0.04	-2.0	0.98	10.4	-0.55
-16-5613	202717	-162412	0.63	0.11	78	-60.0	-48.4	82.1	-0.906	-0.546	0.966	112.6	1.07	46.8	0.26	11.4	21.66
G24-17	202740	42424	0.87	0.15	89	-92.9	-242.1	29.7	-1.910	-1.724	-0.134	261.0	0.11	6.5	0.92	10.9	2.29
G24-21	203243	55724	0.96	0.00	29	40.9	-53.4	-41.7	0.409	-0.599	-2.011	79.1	-0.62	-31.8	0.20	10.3	21.16
G24-25	203742	2242	0.60	0.28	83	198.6	-249.8	37.2	0.075	-0.555	-1.035	321.3	0.12	6.6	0.96	13.6	1.52
G25-5	204649	14424	0.68	0.09	76	-65.4	-98.0	9.3	-1.114	-0.997	-0.058	118.2	0.08	4.5	0.42	10.8	16.70
G25-7	204838	65036	0.90	-.02	52	20.9	-95.1	-47.0	-0.268	-0.902	-1.379	108.1	-0.48	-25.8	0.36	10.0	16.99
L16139	205800	400400	0.55	0.10	21	35.7	-26.3	-3.2	1.511	0.181	-0.249	44.5	-0.07	-4.1	0.09	10.5	23.87
G25-13	210048	65312	0.98	-.02	53	40.6	-68.5	-44.4	0.260	-0.538	-1.264	91.2	-0.56	-29.1	0.26	10.2	19.65
G25-15	210137	24800	0.53	0.13	30	-52.0	-36.1	10.9	-1.775	-1.149	0.329	64.2	0.17	9.8	0.21	11.4	22.89
G25-17	210328	75112	0.84	0.30	135	-85.5	-181.1	45.4	-1.052	-0.688	-0.027	205.4	0.23	12.8	0.71	10.9	8.39
*L16213	210942	173200	0.58	0.25	27	-66.0	-93.5	-43.5	-3.007	-2.160	-2.137	122.4	-0.38	-20.8	0.41	10.9	17.15
G25-22	211223	104818	0.55	0.30	202	-172.2	-327.2	-91.5	-1.167	-1.042	-0.761	380.9	-0.25	-13.9	0.83	13.5	-6.22
*G25-24	211406	-13036	0.50	0.27	187	28.5	-126.8	-302.2	0.340	-0.903	-1.430	329.0	-2.33	-66.7	0.49	10.0	13.82
G26-1	212408	-83648	0.49	0.20	180	-32.8	-165.9	-149.2	-0.120	-0.982	-0.760	225.5	-0.88	-41.4	0.64	10.2	9.91
*G25-29	212413	51342	0.58	0.16	42	33.5	-99.9	-3.5	-0.128	-0.875	-1.137	105.4	-0.03	-1.9	0.38	10.1	16.51
G25-31	212458	72648	0.58	0.11	126	-173.4	-24.0	-25.0	-1.144	-0.600	0.069	176.8	-0.14	-8.1	0.57	21.9	24.10
G26-3	212458	14754	0.97	0.00	82	98.1	21.9	-14.2	1.054	0.469	-0.333	101.5	-0.14	-8.0	0.36	18.7	20.69
G126-2	212642	115806	1.10	0.35	39	78.6	-263.0	53.6	-0.561	-1.246	-1.737	279.7	0.20	11.0	0.99	10.4	0.20
G26-8	212910	-20854	0.86	0.08	61	88.2	-74.7	-8.1	0.736	-0.318	-0.968	115.9	-0.07	-4.0	0.35	11.2	19.03
G26-11	212956	4742	0.60	0.09	43	-81.9	-37.3	3.6	-1.779	-1.046	0.234	90.1	0.04	2.3	0.30	12.7	22.77
G126-8	213041	235412	0.86	0.12	25	47.5	-48.3	-3.3	1.381	0.040	-0.866	67.8	-0.05	-2.8	0.19	10.4	21.67
G26-12	213102	1018	0.44	0.28	281	376.4	-177.8	-89.2	0.926	-0.050	-0.820	425.7	-0.21	-12.1	0.96	79.6	8.72
G126-10	213234	104154	0.45	0.21	260	-220.9	-183.1	68.4	-0.987	-0.412	0.084	295.0	0.24	13.4	0.83	17.0	8.19
G126-12	213405	182430	0.69	0.07	39	67.3	-59.0	13.6	1.164	0.175	-0.450	90.5	0.15	8.6	0.26	10.8	20.60
G126-14	213459	150336	0.59	0.12	152	-118.6	-104.7	-115.8	-0.775	-0.703	-0.754	196.1	-0.73	-36.2	0.52	12.4	16.03
G26-20	213529	-110718	0.60	0.13	52	59.5	36.2	-27.9	1.192	0.652	-0.478	75.0	-0.48	-21.8	0.33	19.1	30.12
G126-17	213611	184836	0.72	0.00	96	58.2	-54.6	-89.8	0.529	-0.328	-1.049	120.1	-1.13	-48.4	0.23	10.6	21.04
*G126-19	213719	230212	0.77	0.18	41	55.8	-73.5	68.8	0.777	0.501	0.743	115.1	0.75	36.7	0.30	10.4	19.15
G93-27	213724	60918	0.87	0.13	99	117.7	-26.2	-56.3	1.044	0.003	-0.765	133.1	-0.47	-25.0	0.34	14.3	23.88
G93-28	213752	-21436	0.66	0.08	41	40.0	-47.1	-14.3	0.517	-0.533	-0.946	63.4	-0.23	-13.0	0.17	10.3	21.79
G26-22	213832	-74224	0.68	0.13	161	-198.6	-94.6	-72.2	-0.928	-0.920	-0.058	231.5	-0.33	-18.2	0.65	18.1	17.04
G126-36	214559	194442	0.61	0.24	66	-69.0	-108.8	3.1	-1.333	-0.593	-0.470	128.9	0.02	1.4	0.46	10.8	15.62
G26-34	214905	3654	0.83	0.02	32	49.0	-39.9	-13.4	1.042	-0.447	-1.164	64.6	-0.21	-12.0	0.17	10.6	22.51
G93-47	214939	72430	0.63	0.09	121	139.6	-19.5	-57.1	1.065	0.030	-0.616	152.1	-0.41	-22.1	0.41	16.5	24.55
G18-5	215139	44430	0.62	0.11	59	82.7	-49.3	-21.5	1.075	-0.195	-0.896	98.7	-0.22	-12.6	0.27	11.5	21.57
G26-38	215612	3418	0.79	0.01	77	-65.5	-69.0	-11.0	-0.917	-0.782	-0.254	95.8	-0.12	-6.6	0.33	11.2	19.60
G18-10	215636	25730	0.74	0.00	38	49.2	-8.1	-11.5	1.139	0.085	-0.572	51.2	-0.23	-13.0	0.13	12.0	25.69
G18-12	215742	80754	0.77	0.05	100	-79.1	-121.0	36.8	-1.066	-0.552	-0.139	149.2	0.25	14.3	0.51	11.0	14.40
G26-42	215751	12654	0.51	0.27	272	-196.6	-303.8	-41.5	-0.866	-0.860	-0.397	364.2	-0.11	-6.5	0.90	14.7	-3.88
G18-14	215826	94206	0.98	0.20	41	-55.1	-50.3	-72.4	-1.209	-1.577	-1.508	104.0	-0.97	-44.1	0.25	11.2	21.47
G27-8	220039	-12748	0.51	0.26	163	88.6	-148.6	-102.5	0.413	-0.651	-0.853	195.3	-0.62	-31.7	0.57	10.7	12.44
G126-52	220151	191836	0.38	0.27	233	-152.8	-384.9	-113.4	-0.859	-0.735	-0.990	429.4	-0.27	-15.3	0.67	13.2	-11.99
G18-21	220207	110800	0.58	0.31	273	-169.8	-404.4	6.0	-0.893	-0.697	-0.541	438.6	0.01	0.8	0.65	14.5	-13.94
G18-24	220232	82342	0.58	0.30	165	182.9	-181.1	-97.7	0.871	-0.493	-1.065	275.3	-0.38	-20.8	0.77	13.3	8.39
G18-27	220258	53042	0.86	0.00	77	-98.0	-48.5	-5.0	-1.275	-0.626	-0.068	109.5	-0.05	-2.6	0.36	13.0	21.65
*G18-28	220314	120818	0.65	0.16	55	32.6	-222.0	28.6	-0.343	-1.157	-1.494	226.2	0.13	7.3	0.83	10.0	4.38
G18-29	220357	54054	0.75	0.06	87	-49.4	-72.0	-55.9	-0.574	-0.813	-0.654	103.7	-0.64	-32.6	0.31	10.7	19.38
G18-30	220359	13630	0.52	0.01	38	86.0	-2.2	22.7	1.833	0.762	-0.203	89.0	0.26	14.8	0.26	14.4	26.28
G127-2	220524	242306	0.87	0.09	95	82.9	-116.6	-47.3	0.744	-0.326	-0.920	150.7	-0.33	-18.3	0.48	10.7	14.84
G126-56	220651	112706	0.68	0.15	145	162.5	-30.8	-28.0	1.036	0.052	-0.385	167.7	-0.17	-9.6	0.47	17.4	23.42
G126-59	220802	183300	0.61	0.11	28	50.7	-81.8	9.9	1.278	-0.388	-1.125	96.7	0.10	5.9	0.32	10.3	18.32
G126-60	220812	223306	0.94	0.07	31	-74.6	-12.9	62.1	-2.536	0.411	1.582	97.9	0.82	39.4	0.27	13.9	25.21
G18-35	220908	55642	0.58	0.12	46	58.3	-9.2	-16.9	1.183	0.007	-0.546	61.4	-0.29	-16.0	0.16	12.3	25.58
G126-63	220912	174812	0.54	0.23	224	302.5	-196.9	-124.0	1.222	-0.285	-0.911	381.6	-0.34	-19.0	0.91	25.0	6.81
G27-21	221329	-72006	0.68	0.02	49	-17.5	-94.2	-31.3	-0.522	-1.690	-0.957	100.8	-0.33	-18.1	0.36	10.1	17.88
G127-12	221335	244048	0.67	0.07	49	-56.0	8.1	16.8	-1.132	0.066	0.391	59.0	0.30	16.5	0.25	15.0	27.31
*G18-39	221606	81142	0.46	0.20	131	140.4	-271.3	0.6	0.621	-0.737	-1.122	305.5	0.00	0.1	0.98	11.5	-0.63
G27-22	221630	-73348	0.61	0.02	62	72.3	-97.3	5.5	0.649	-0.844	-0.930	121.3	0.05	2.6	0.40	10.6	16.77
G18-40	221721	51036	0.52	0.28	251	446.5	-167.4	-75.9	1.573	-0.135	-0.798	482.9	-0.16	-9.0	1.04	-73.3	9.76
G18-44	221918	114318	0.97	0.04	78	-93.5	-53.5	39.5	-1.320	-0.230	0.156	114.7	0.37	20.1	0.35	12.6	21.15
G127-26	222128	240830	0.55	0.08	144	-137.9	-84.7	-35.4	-0.984	-0.294	-0.398	165.7	-0.22	-12.3	0.51	13.8	18.03
G27-28	222401	42118	0.82	0.09	46	69.3	-22.6	8.8	1.289	0.096	-0.389	73.4	0.12	6.9	0.19	11.9	24.24
G27-29	222520	-53206	0.81	0.23	80	-91.3	-88.2	0.7	-1.222	-0.969	-0.173	126.9	0.01	0.3	0.43	11.7	17.68
G127-33	222540	244100	0.93	0.13	43	51.7	-55.6	-4.9	1.133	-0.264	-0.651	76.1	-0.06	-3.7	0.23	10.5	20.94
G127-34	222556	275124	0.71	0.16	96	105.0	-28.2	-41.0	1.091	-0.189	-0.476	116.2	-0.38	-20.7	0.30	13.4	23.68
*G18-54	222903	15424	0.48	0.20	142	-30.6	-299.5	29.4	-0.596	-1.150	-0.838	302.5	0.10	5.6	0.87	10.1	-3.45
G27-33	223011	-61242	0.77	0.22	98	-122.1	-28.5	40.7	-1.271	-0.248	0.354	131.8	0.32	18.0	0.41	15.8	23.65
G18-55	223020	100900	0.83	0.14	36	-58.0	5.2	-14.9	-1.492	-0.353	0.010	60.1	-0.26	-14.4	0.25	14.8	27.02
G18-58	223238	113736	0.86	-.05	35	-85.7	-35.5	10.4	-2.539	-0.583	-0.062	93.3	0.11	6.4	0.31	13.0	22.95
G18-60	223305	50706	0.70	0.05	34	41.1	-40.3	-46.5	1.179	-1.095	-1.458	74.8	-0.81	-38.9	0.15	10.4	22.47
S114-256	223514	-2630	0.71	0.04	70	69.9	-26.7	-16.2	0.917	-0.185	-0.469	76.6	-0.22	-12.2	0.19	11.7	23.83
G67-7	223553	93600	0.85	-.01	81	-97.0	-20.3	8.1	-1.194	-0.260	0.011	99.1	0.00	0.1	0.34	14.7	24.47
G67-8	223602	101712	0.76	0.06	52	-123.3	-112.7	-9.6	-2.548	-1.337	-0.907	167.3	-0.06	-3.3	0.55	12.5	15.23
G127-43	223622	251836	0.83	0.04	58	65.1	-29.9	-18.1	1.115	-0.229	-0.466	73.9	-0.25	-14.2	0.18	11.4	23.51
G67-9	223706	110530	0.82	0.11	64	78.2	-47.1	-0.9	1.113	-0.189	-0.479	91.3	-0.01	-0.6	0.25	11.3	21.79
G127-44	223814	164306	0.83	0.03	114	-118.4	-32.7	-54.3	-1.025	-0.402	-0.393	134.3	-0.44	-23.8	0.48	15.2	23.23
G67-11	223832	184024	0.92	0.04	58	89.9	-3.1	5.2	1.535	0.118	-0.028	90.1	0.06	3.3	0.27	14.5	26.19
G127-48	224039	181312	0.60	0.04	56	-58.1	-28.1	-15.8	-1.051	-0.351	-0.373	66.3	-0.23	-13.1	0.22	12.0	23.69

TABLE II. (continued).

NAME	RA	DEC	B-V	EX(.6)	D	U	V	W	DU/DR	DV/DR	DW/DR	S	TAN I	I	ECC.	RMAX	H
G27-42	224045	-63936	0.97	-.01	20	-20.6	-28.5	11.3	-1.288	-0.949	-0.161	36.9	0.32	17.8	0.11	10.6	23.65
*G27-44	224118	33712	0.49	0.13	34	62.2	7.5	42.5	1.684	0.963	0.437	75.7	0.68	34.2	0.21	14.2	27.25
*G27-45	224220	-23654	0.66	0.30	96	220.2	-193.0	-200.6	2.265	-1.943	-2.178	354.9	-0.69	-34.4	0.83	15.2	7.20
G28-15	224308	-15924	0.79	0.17	98	93.6	-9.9	-54.7	1.077	-0.201	-0.488	108.9	-0.58	-30.2	0.27	14.1	25.51
G67-17	224309	185936	0.74	0.07	38	-28.0	29.9	-81.7	-0.634	-0.780	-1.072	91.4	-1.99	-63.4	0.28	17.2	29.49
G128-2	224441	293518	0.71	0.40	84	140.0	-304.1	11.4	1.825	-0.711	-1.268	335.0	0.03	2.0	0.87	11.5	-3.91
G127-55	224455	173254	0.69	0.08	29	-40.8	-0.6	-2.3	-1.401	-0.115	-0.011	40.9	-0.06	-3.2	0.18	13.2	26.44
G28-16	224506	60936	0.81	0.16	102	86.8	-79.9	-56.5	0.804	-0.587	-0.756	130.8	-0.48	-25.6	0.36	11.0	18.51
*G28-17	224813	13618	0.68	0.14	49	-32.3	-74.6	-60.5	-0.639	-1.586	-1.159	101.3	-0.74	-36.7	0.30	10.3	19.04
G28-18	224852	-23342	0.97	0.07	91	13.9	-132.1	-70.3	0.095	-1.304	-0.975	150.3	-0.53	-27.9	0.51	10.0	13.29
G67-27	224856	134206	0.83	0.06	24	52.6	-1.4	-4.6	2.183	0.021	-0.256	52.8	-0.09	-5.0	0.16	12.8	26.36
G128-11	225104	272930	0.82	0.42	65	107.1	-308.7	19.8	1.861	-1.022	-1.700	327.4	0.06	3.5	0.85	10.8	-4.37
G67-31	225159	125048	0.82	0.12	62	-14.1	-30.3	-74.1	-0.193	-0.812	-0.914	81.3	-2.22	-65.7	0.10	10.4	23.47
G67-35	225343	104800	0.74	0.11	47	68.4	-35.8	-2.5	1.394	-0.287	-0.495	77.2	-0.03	-1.9	0.20	11.3	22.92
G67-36	225355	171112	1.00	0.04	26	10.7	-27.9	-22.8	0.399	-0.809	-1.078	37.6	-0.76	-37.3	0.06	10.0	23.71
G67-38	225649	115536	0.58	0.08	47	44.2	-134.0	28.4	0.762	-0.952	-1.125	143.9	0.20	11.4	0.52	10.1	13.10
G67-40	225915	113306	0.75	0.13	78	80.2	-78.9	-41.0	0.999	-0.685	-0.830	119.7	-0.36	-20.0	0.35	10.9	18.61
G28-31	230124	-24842	0.52	0.28	268	-197.5	-267.1	55.3	-0.842	-0.672	-0.271	336.8	0.17	9.5	0.99	14.6	-0.21
G28-34	230312	-22642	1.00	0.36	115	248.4	-255.4	-142.1	2.059	-1.890	-1.720	383.6	-0.40	-21.7	0.98	16.8	8.96
G128-31	230313	283924	0.72	0.15	61	-69.9	-23.9	-31.8	-1.125	-0.209	-0.621	80.4	-0.43	-23.3	0.25	12.8	24.11
G28-35	230336	42500	0.67	0.12	51	52.3	-11.9	-29.5	1.044	-0.346	-0.445	61.2	-0.55	-28.8	0.14	11.8	25.31
G28-37	230359	-2800	0.86	-.02	45	-43.5	-13.4	52.7	-1.111	0.264	0.400	69.6	1.16	49.2	0.17	12.2	25.16
G128-32	230419	324530	0.87	0.15	49	-32.6	-37.7	-38.9	-0.603	-0.367	-0.982	63.2	-0.78	-38.0	0.17	10.7	22.73
G29-3	230445	122518	0.99	-.01	53	83.3	-74.0	-21.0	1.543	-0.803	-0.946	113.4	-0.19	-10.7	0.34	11.0	19.10
G28-40	230535	85306	0.72	0.13	114	119.3	-102.2	0.6	1.002	-0.417	-0.491	157.1	0.00	0.2	0.48	11.7	16.28
G128-36	230623	264454	0.90	0.07	115	-72.8	-153.8	-109.3	-0.564	-0.718	-1.318	202.2	-0.64	-32.7	0.62	10.7	11.12
G28-42	230649	64454	0.62	0.25	181	275.9	-243.6	34.2	1.434	-0.575	-0.668	369.6	0.89	5.3	0.96	19.7	2.14
*G28-43	230700	2718	0.70	0.26	51	-195.1	-269.5	-26.5	-4.112	-3.992	-2.271	333.8	0.00	-4.6	0.99	14.5	-0.45
*G67-49	230815	183818	0.60	0.07	50	-72.8	-19.4	6.2	-1.443	-0.051	-0.139	75.6	0.00	4.7	0.26	13.3	24.56
G28-45	230817	830	0.85	0.03	35	-33.2	-20.3	-34.3	-0.875	-0.911	-0.522	51.9	-0.88	-41.4	0.14	11.3	24.47
G128-38	230939	263930	1.00	0.06	33	10.3	-23.8	-27.0	0.329	-0.584	-0.901	37.4	-1.04	-46.2	0.04	10.0	24.12
G28-48	231027	13154	0.88	0.29	62	-62.5	-15.8	-35.0	-0.963	-0.498	-0.243	73.4	-0.54	-28.5	0.23	13.0	24.92
G68-3	231049	204824	0.80	0.14	46	-8.6	-107.5	3.1	-0.073	-0.789	-1.075	107.9	0.03	1.6	0.41	10.0	15.75
G128-42	231351	302342	0.89	0.03	21	32.2	-7.1	-5.8	1.524	-0.394	-0.243	33.5	-0.18	-10.0	0.08	11.4	25.79
G128-43	231441	312718	0.84	0.03	105	-145.0	-48.0	25.4	-1.262	0.186	-0.091	154.8	0.17	9.4	0.48	16.2	21.70
G29-20	231528	84812	0.75	0.23	34	57.6	-162.1	92.2	1.550	-1.196	-1.161	195.2	0.54	28.2	0.63	10.2	10.29
G128-45	231533	311530	0.75	0.07	145	144.8	-51.1	-78.3	0.982	-0.442	-0.493	172.4	-0.51	-27.8	0.43	14.5	21.39
G29-21	231621	50800	0.83	0.06	22	40.5	-28.5	-13.4	1.815	-1.010	-0.960	51.3	-0.27	-15.1	0.11	10.6	23.65
*G29-23	231706	30554	0.43	0.25	127	146.5	-272.1	88.9	1.017	-0.966	-0.832	321.6	0.29	16.0	0.98	11.7	-0.71
*G128-48	231729	283542	0.78	0.05	37	100.4	-87.3	-37.6	2.876	-1.412	-1.569	138.3	-0.28	-15.8	0.41	11.3	17.77
G68-10	231927	162130	0.61	0.10	55	86.5	-64.7	-26.1	1.597	-0.808	-0.796	111.1	-0.24	-13.6	0.32	11.3	20.03
G29-25	231946	115306	0.67	0.20	89	96.9	-103.8	26.5	1.103	-0.445	-0.419	143.9	0.19	10.6	0.45	11.1	16.20
G29-26	231949	-4112	0.84	0.01	31	9.4	-36.8	-24.4	0.299	-1.167	-0.816	45.1	-0.64	-32.7	0.10	10.0	22.82
G68-12	232019	215136	0.82	0.01	54	35.2	-71.1	-10.3	0.742	-0.618	-0.707	80.0	-0.13	-7.4	0.27	10.1	19.39
G128-58	232301	294954	0.57	0.22	199	206.2	-201.2	10.1	1.161	-0.407	-0.293	288.3	0.04	2.0	0.84	14.3	6.38
G128-64	232352	325454	0.74	0.05	56	-61.0	-41.0	-13.0	-0.936	-0.072	-0.569	74.6	-0.18	-10.0	0.25	11.6	22.40
G128-67	232745	312554	0.93	0.14	19	3.4	-32.9	-6.7	0.441	-0.627	-0.952	33.7	-0.20	-11.5	0.09	10.0	23.21
G68-28	233051	152512	0.92	0.16	77	96.6	-59.2	-22.9	1.275	-0.590	-0.464	115.6	-0.20	-11.4	0.32	11.7	20.58
*G190-34	233207	334536	0.80	0.04	38	56.8	-36.5	16.2	1.653	-0.383	0.133	69.4	0.24	13.5	0.17	10.9	22.85
G68-29	233231	250730	0.81	0.08	82	35.4	-180.1	-22.1	0.697	-0.945	-1.143	184.9	-0.12	-6.9	0.68	10.1	8.49
G29-48	233249	15642	0.72	0.09	32	35.3	27.3	28.0	1.097	0.998	0.661	52.7	0.63	32.1	0.25	16.3	29.23
G128-83	233257	305318	0.85	0.05	21	-36.4	-13.3	-7.0	-1.569	0.003	-0.699	39.4	-0.18	-10.2	0.15	11.9	25.17
*G68-30	233312	201818	0.56	0.14	61	-69.7	-24.6	-3.7	-1.086	-0.078	-0.328	74.0	-0.05	-2.9	0.25	12.8	24.04
G29-50	233316	1818	0.90	0.15	49	-75.2	-14.8	9.4	-1.544	-0.152	-0.037	77.2	0.12	7.0	0.27	13.8	25.02
G30-2	233323	81354	1.02	0.38	92	-21.5	-86.7	-103.8	-0.242	-1.103	-0.937	136.9	-1.16	-49.3	0.34	10.2	17.83
G68-31	233333	180948	0.71	0.04	26	82.7	-39.9	5.8	3.290	-0.852	-0.376	92.0	0.06	3.6	0.25	11.7	22.51
G128-84	233357	324542	0.91	0.06	50	58.2	-46.9	-5.7	1.276	-0.527	-0.333	75.0	-0.08	-4.4	0.21	10.7	21.81
*S115-147	233924	-1554	0.73	0.03	42	34.9	-29.7	-7.7	0.829	-0.585	-0.377	46.5	-0.17	-9.5	0.18	10.4	23.53
G130-7	234228	300336	0.65	0.29	114	33.3	-185.7	-46.4	0.551	-0.741	-0.949	194.3	-0.25	-13.8	0.78	10.0	7.93
*G130-8	234236	291706	0.85	0.05	26	116.3	8.0	-56.5	3.897	-1.698	-0.915	129.5	-0.48	-25.9	0.37	17.9	27.30
G130-10	234338	345812	0.78	0.05	42	-3.9	-72.3	-27.1	0.249	-0.678	-1.174	77.3	-0.37	-20.5	0.27	10.0	19.27
G31-3	234518	-53118	0.61	0.08	44	-52.5	-26.7	15.3	-1.213	-0.365	-0.134	60.9	0.26	14.6	0.20	11.8	23.83
G29-65	234518	35354	0.62	0.02	36	47.6	-41.9	0.1	1.347	-0.816	-0.495	63.4	0.00	0.1	0.17	10.5	22.31
G29-71	234727	82648	0.53	0.32	135	157.2	-204.9	60.2	1.271	-0.783	-0.476	265.2	0.23	13.1	0.82	12.1	6.01
G29-72	234731	23548	0.75	0.01	35	78.1	-16.5	14.2	2.253	-0.194	-0.016	81.1	0.18	10.1	0.22	12.7	24.85
G30-24	234807	170354	0.88	0.01	71	92.7	28.1	11.0	1.243	0.120	0.420	97.5	0.11	6.5	0.37	19.5	29.31
G130-18	234914	310906	0.76	0.07	134	127.1	-82.1	-57.7	0.958	-0.585	-0.447	161.9	-0.30	-20.9	0.44	12.4	18.29
G31-12	235006	-61618	1.08	0.15	26	43.2	-40.0	17.7	1.630	-0.975	-0.504	61.5	0.30	16.7	0.15	10.4	22.50
G30-27	235131	171618	0.96	0.02	48	51.4	-20.0	9.5	1.113	-0.245	0.034	56.0	0.17	9.8	0.13	11.3	24.50
G129-42	235230	200624	0.80	0.12	32	30.9	-38.4	12.4	1.155	-0.513	-0.219	50.8	0.25	14.1	0.13	10.2	22.66
G31-16	235259	31336	0.77	0.03	23	-32.5	-8.6	-23.3	-1.452	-0.671	-0.557	40.9	-0.69	-34.7	0.14	12.1	25.64
G30-31	235519	82018	1.16	0.36	50	19.6	-73.5	-102.6	0.301	-1.937	-1.442	127.7	-1.35	-53.4	0.27	10.0	19.15
G30-34	235613	85754	0.67	0.09	53	69.9	-36.2	-68.7	1.221	-1.148	-0.697	104.5	-0.87	-41.1	0.21	11.4	22.88
G130-29	235616	332754	0.64	0.03	35	14.9	-59.9	-11.8	0.778	-0.779	-0.863	62.8	-0.19	-10.8	0.21	10.0	20.51
G130-32	235731	335442	0.65	0.09	40	-55.2	-5.8	14.9	-1.147	0.459	0.035	57.5	0.27	15.0	0.22	13.4	25.92
G129-52	235732	194536	0.74	-.01	68	-89.9	2.5	-41.2	-1.353	-0.062	-0.514	98.9	-0.46	-24.6	0.34	16.6	26.75
G30-36	235815	164248	0.94	0.00	29	-31.4	-37.3	-14.3	-0.933	-0.764	-1.019	50.8	-0.29	-16.3	0.16	10.7	22.77
G130-36	235922	254354	0.94	0.30	59	-178.5	-109.5	-67.7	-2.603	-0.650	-2.059	220.1	-0.32	-17.9	0.64	15.6	15.55

TABLE III. Kinematic data for 247 stars from the literature not contained in Table II.

NAME	RA	DEC	V	B-V	U-B	EX.e	RADVEL G	U	V	W	S	TAN I	I	ECC.	RMAX	H	SOURCE
G 30- 52	0 9.9	14 17	8.59	.81	.27	.25	9.1	33	-21	-21	44.4	-0.54	-28.2	0.08	10.6	24.40	S3
G 30- 56	0 13.8	16 22	9.74	.56	.04	.04	-1.3	97	-81	-38	132.0	-0.30	-16.7	0.38	11.3	18.40	S3
G130- 65	0 20.0	23 38	11.62	.43 -	.25	.25	-272.6	-148	-370	-63	403.5	-0.16	-9.0	0.70	12.8	-10.50	S3
HD3222	0 32.6	-63 57	8.56	.84	.52	.00	1.6	48	-73	21	89.9	0.24	13.5	0.29	10.3	19.20	E2
-9 122	0 36.0	-8 35	9.27	.45 -	.16	.19	-41.9	-107	-196	-32	225.6	-0.14	-8.2	0.77	11.3	6.90	S2
-52 78	0 38.5	-51 39	11.27	.49 -	.26	.28	91.0	28	-188	-29	192.3	-0.15	-8.7	0.71	10.0	7.70	C E2
+71 31	0 40.3	71 54	10.27	.36 -	.16	.22	-116.0 B	187	-267	49	329.6	0.15	8.5	0.99	13.1	-0.20	E SY
G 70- 4	0 40.8	-1 10	9.25	.67	.18	.03	-43.7	-86	-37	12	94.4	0.13	7.3	0.31	12.9	22.80	S3
-8 128	0 41.4	-7 48	9.40	.59	.02	.10	-112.1	-75	-62	87	130.5	0.89	41.8	0.33	11.6	20.30	S2
HD4308	0 42.5	-65 54	6.55	.65	.10	.08	98.4	-52	-116	-26	129.8	-0.20	-11.6	0.47	10.5	14.90	E2
G 70- 14	0 46.1	-1 39	10.92	.56 -	.06	.15	9.1	131	-116	-25	176.8	-0.14	-8.1	0.54	12.0	14.90	S3
G 32- 53	0 48.6	18 31	8.76	.76	.24	.15	-83.0	-69	-54	34	94.0	0.39	21.2	0.29	11.6	21.10	S3
G 33- 30	0 58.5	16 6	10.66	.54 -	.17	.25	-80.1	80	-184	15	201.2	0.07	4.3	0.71	10.5	8.10	S3
GC 1360	1 4.9	54 41	5.16	.70	.10	.17	-97.2 A	41	-155	-34	163.9	-0.21	-12.0	0.60	10.1	11.00	E SY
+29 366	1 7.1	29 39	8.74	.58 -	.10	.20	28.1	75	-148	-90	188.8	-0.54	-28.5	0.59	10.4	11.70	E2
-11 220	1 7.7	-10 39	9.21	.57 -	.02	.12	43.8	74	-48	-38	96.0	-0.43	-23.3	0.24	11.2	21.70	S2
-17 219	1 11.7	-16 42	10.06	.72	.02	.42	81.4	34	-40	-81	96.5	-1.54	-57.1	0.14	10.2	22.50	S2
-1 306	1 11.9	-1 22	9.10	.56 -	.09	.17	19.2	198	-202	64	290.0	0.23	12.7	0.83	13.8	6.30	E2
GC 1586	1 16.5	-9 12	8.90	.58 -	.02	.12	-4.4 B	-116	-59	-40	136.2	-0.31	-17.1	0.42	13.6	20.60	E SY
G 2- 38	1 24.3	11 45	11.38	.51 -	.21	.27	-166.5	-217	-220	-42	311.9	-0.14	-7.7	0.90	16.1	4.50	S3
CD-31 622	1 30.0	-30 56	10.77	.63 -	.12	.28	-160.0	-59	-12	169	179.4	2.81	70.4	0.22	13.1	25.30	E2
CD-61 282	1 34.4	-61 19	10.10	.53 -	.16	.23	223.0	-226	-229	-47	325.2	-0.15	-8.3	0.92	16.8	3.60	E2
GC 2029	1 37.9	66 40	7.66	.68	.21	.02	16.0 B	93	-50	-16	106.8	-0.15	-8.6	0.29	11.8	21.50	E SY
HD10607	1 39.7	-67 55	8.33	.56 -	.10	.18	-0.2	0	-125	99	159.5	0.79	38.4	0.48	10.0	14.00	E2
+72 94	1 43.0	73 13	10.20	.38 -	.21	.29	-265.7	-316	-111	35	336.8	0.10	6.0	0.90	53.3	15.40	S2
HD11397	1 49.3	-16 33	8.95	.69	.10	.15	38.5	-23	-116	-49	128.0	-0.41	-22.5	0.45	10.1	14.90	E2
+68 138	1 54.7	68 47	9.31	.53 -	.03	.09	2.7	103	-83	23	134.3	0.17	9.9	0.40	11.5	18.20	S2
HD13445	2 8.4	-51 4	6.12	.82	.45	.06	52.4 B	110	-80	-23	137.9	-0.17	-9.6	0.41	11.8	18.50	E SY
GC 2694	2 12.1	-1 26	9.09	.57 -	.07	.17	19.2 B	187	-188	59	271.7	0.22	12.5	0.79	13.4	7.70	E SY
-17 484	2 29.1	-17 12	10.42	.47 -	.17	.18	234.0 C	259	-209	-145	363.0	-0.44	-23.5	0.89	18.2	5.60	E SY
-13 482	2 31.8	-12 36	9.75	.45 -	.22	.22	63.0 C	11	-81	-61	102.0	-0.75	-36.7	0.30	10.0	18.40	E SY
HD16784	2 38.5	-30 21	8.02	.57 -	.06	.16	34.0 B	91	-70	14	115.7	0.12	7.0	0.34	11.3	19.50	E SY
G 4- 36	2 40.6	13 13	11.49	.48 -	.22	.26	216.6	300	-228	-94	388.4	-0.25	-14.0	0.95	23.6	3.70	S3
HD 17288	2 42.8	-60 16	9.85	.57 -	.11	.22	9.0	57	-66	49	100.0	0.56	29.3	0.27	10.5	19.90	E2
GC 3848	3 0.0	61 31	6.60	.62	.17	-.02	-6.8 B	63	-78	-26	103.6	-0.26	-14.5	0.32	10.5	18.70	E SY
G 36- 50	3 0.8	29 24	12.04	.64 -	.11	.36	-141.2	-32	-298	-1	297.7	0.00	-0.2	0.88	10.1	-3.10	S3
LTT 1566	3 16.0	-7 19	11.22	.46 -	.25	.25	154.0	63	-231	-95	257.6	-0.40	-21.6	0.87	10.2	3.40	C
HD20794	3 17.9	-43 16	4.26	.71	.21	.06	86.8 A	82	-95	-26	128.2	-0.21	-11.7	0.41	10.8	17.00	E SY
W 1919	3 26.4	66 35	9.90	.65 -	.10	.30	-159.0 B	166	-407	-67	444.6	-0.15	-8.7	0.81	13.3	-14.20	E SY
G 5- 46	3 33.3	16 19	7.64	.58 -	.02	.12	-23.8	-45	-2	-29	53.6	-0.64	-32.8	0.19	13.3	26.30	S3
HD24049	3 45.9	-56 12	9.49	.62 -	.01	.16	9.8	107	-123	103	192.8	0.63	32.3	0.53	11.2	14.20	E2
HD24339	3 49.3	-26 5	9.46	.56 -	.08	.16	82.2	187	-97	64	220.2	0.30	16.9	0.59	15.3	16.80	E2
G 80- 28	3 49.4	-3 58	9.96	.52 -	.15	.21	133.4	145	-97	-16	175.2	-0.09	-5.2	0.51	12.8	16.80	S3
GC 4690	3 51.0	52 17	7.92	.68	.11	.12	155.9 B	145	61	-8	157.5	-0.05	-2.9	0.65	41.0	32.60	E SY
GC 4849	3 59.9	35 9	8.52	.88	.36	.43	-30.0 B	35	-184	21	188.5	0.11	6.4	0.70	10.1	8.10	E SY
HD25704	4 0.6	-57 21	8.10	.55	(1.57)	(.16)	52.0 B	165	-74	-30	183.3	-0.17	-9.4	0.51	14.7	19.10	E SY
- 16 793	4 6.9	-16 32	8.14	.34 -	.05	.11	81.9 B	103	9	-21	105.5	-0.20	-11.5	0.34	17.0	27.40	E SY
40 ERI A	4 13.0	-7 44	4.42	.81	.45	.02	-42.4 A	-97	-12	-41	106.0	-0.42	-22.8	0.34	15.4	25.30	E SY
HD 29907	4 38.0	-65 32	9.85	.63 -	.13	.27	68.0	308	-131	8	334.8	0.02	1.4	0.85	31.9	13.40	C E2
HD30229	4 40.9	-65 24	9.41	.67 -	.09	.30	300.0	-26	-235	-184	299.6	-0.78	-37.9	0.88	10.1	3.00	E2
W 2853	4 48.4	0 29	10.12	.54	.03	.03	103.2 B	103	-52	-2	115.4	-0.02	-1.0	0.32	12.2	21.30	E SY
+0 916	4 57.8	0 56	9.10	.57	.04	.06	106.0 C	98	-39	-24	108.2	-0.23	-12.8	0.29	12.4	22.60	E SY
GC 6249	5 4.3	55 22	9.33	.63 -	.01	.19	-121.4 B	-80	-110	-82	158.8	-0.60	-31.1	0.48	11.1	15.50	E SY
HD 34328	5 12.2	-59 42	9.40	.49 -	.26	.27	239.0 D	191	-342	75	398.8	0.19	10.8	0.79	13.6	-7.70	E SY
-48 1741	5 17.0	-48 55	10.68	.54	(1.50)	(.27)	320.0 B	-52	-335	-109	356.1	-0.32	-17.8	0.75	10.3	-7.00	E SY
G 86- 39	5 19.9	33 9	11.54	.84	.33	.34	217.6	250	-290	-10	383.0	-0.03	-1.5	0.95	17.0	-2.50	S3
-29 2277	5 26.9	-29 56	11.66	.48 -	.24	.25	522.0	189	-520	-145	565.7	-0.27	-14.9	0.51	20.7	-25.50	E SY
+59 886	5 28.6	59 7	9.89	.75	.33	.01	32.7	74	-55	-26	95.8	-0.28	-15.7	0.26	11.0	21.00	S2
G 99- 21	5 36.8	3 56	10.36	.64	.04	.14	134.2	85	-176	16	196.1	0.08	4.7	0.69	10.5	8.90	S3
-52 1324	5 43.2	-52 49	9.53	.49 -	.17	.19	322.0	11	-320	-42	322.9	-0.13	-7.5	0.79	10.0	-5.50	E2
-70 340	5 45.1	-70 11	8.09	.76	(1.83)	(.08)	14.2 B	154	-24	-36	160.0	-0.23	-13.0	0.45	17.3	24.10	E SY
ROSS 797	5 51.7	-14 24	11.47	.52 -	.17	.24C	12.0	-218	-223	-46	315.2	-0.15	-8.4	0.91	16.2	4.20	C E2
LTT2437	5 59.4	-12 30		.8		.28E	215.0	189	-239	248	392.9	0.81	39.1	0.93	13.2	2.60	E2
HD41667	6 3.2	-32 59	8.54	1.01	.56	.22E	302.0	290	-214	7	360.5	0.02	1.1	0.92	22.2	5.10	E2
G 98- 56	6 11.5	37 54	11.36	.63 -	.03	.21	26.4	60	-153	-118	202.3	-0.72	-35.7	0.60	10.3	11.20	S3
HD43587	6 14.6	5 7	5.70	.60	.10	.02	12.8	20	17	-13	29.3	-0.50	-26.3	0.18	14.2	28.20	E2
G101- 34	6 16.6	38 22	10.76	.74	.06	.34	219.7	222	-81	45	240.6	0.19	10.8	0.65	19.5	18.40	S3
-6 1598	6 30.2	-6 27	8.62	.56 -	.08	.16	7.5	-2	-26	51	57.3	1.96	62.9	0.06	10.1	23.90	S2
G105- 50	6 34.9	12 7	11.17	.70	.18	.07	108.0	66	-139	-63	166.3	-0.41	-22.3	0.55	10.3	12.60	S3
W 4400	6 42.5	58 41	10.33	.43 -	.19	.20	189.0 C	329	-234	-20	404.2	-0.05	-2.8	0.97	30.6	3.10	E SY
LTT 7629	6 53.0	-33 41	9.05	.46	(1.56)	(.10)	71.0 B	-2	-48	-122	131.1	-2.54	-68.5	0.16	10.0	21.70	E SY
HD51929	6 55.0	-58 54	7.43	.58 -	.03	.13	70.3	159	-72	15	175.2	0.09	4.9	0.49	14.4	19.30	E2
HD54046	7 5.2	15 37	7.80	.56	.00	.08	-12.5	-22	-50	-52	75.4	-0.95	-43.6	0.19	10.3	21.50	E2
HD54100	7 5.4	15 36	7.68	.53 -	.06	.12	-12.5	-22	-50	-52	75.4	-0.95	-43.6	0.19	10.3	21.50	E2
-57 1139	7 5.6	-57 25	9.55	.49 -	.17	.19	252.5	299	-248	-30	389.6	-0.08	-4.4	0.97	23.2	1.70	E2
HD54563	7 7.2	21 20	6.42	.88	.49	.15	-16.5	-20	-81	-82	117.0	-0.98	-44.5	0.31	10.2	18.40	E2
G 88- 10	7 7.4	24 26	11.87	.44 -	.24	.24	88.8	58	-299	-119	327.0	-0.39	-21.3	0.87	10.2	-3.40	S3
HD55720	7 10.2	-49 21	7.51	.70	.07	.18	86.9 B	86	-78	4	116.2	0.03	2.0	0.36	11.0	18.70	E SY
GC 9720	7 15.9	65 32	8.96	.62	.12	.03	36.4 B	93	-68	-14	116.1	-0.12	-6.9	0.34	11.4	19.70	E SY
G 87- 47	7 32.3	38 4	10.34	.66	.05	.15	-89.5	-125	3	60	138.7	0.48	25.6	0.45	20.0	26.80	S3
ROSS 390	7 32.4	-10 16	11.08	.67 -	.06	.30	89.0 C	-180	-280	78	341.9	0.23	13.2	0.96	13.7	-1.50	CE2SY
-45 3283	7 32.9	-45 11	10.52	.62 -	.02	.18	317.4	240	-261	-90	365.8	-0.25	-14.2	0.99	16.1	0.40	E2
HD63077	7 43.7	-34 4	5.37	.60 -	.06	.19	102.0 A	159	-53	42	172.8	0.25	14.1	0.47	15.4	21.20	E SY
GC 10821	7 57.4	29 22	7.00	.70	.18	.07	12.5 B	11	-97	-33	103.0	-0.34	-18.7	0.37	10.0	16.80	E SY
+80 245	8 3.0	80 1	10.07	.50 -	.17	.19	1.2	68	-138	92	179.3	0.60	30.9	0.55	10.4	12.70	S2
W 5494	8 15.5	54 15	9.69	.48 -	.19	.20	61.0 B	124	-235	28	267.2	0.11	6.0	0.90	11.1	3.00	E SY
WOLF 315	8 32.2	41 56	8.78	.92	.71	-.03	58.4 B	75	-81	-1	110.4	-0.01	-0.5	0.35	10.7	18.40	E SY
HD74000	8 38.5	-16 9	9.71	.42 -	.26	.26	206.0 B	-184	-327	63	380.5	0.17	9.5	0.84	14.1	-6.20	E SY
G115-22	8 40.9	36 26	10.97	.58 -	.12	.23	-5.0 C	-9	-231	-31	233.2	-0.13	-7.6	0.87	10.0	3.40	E SY
G 9- 16	8 41.6	24 59	9.32	.31 -	.16	.26	49.3 V	38	-235	-82	251.8	-0.34	-19.0	0.88	10.1	3.00	S2

TABLE III. (continued).

NAME	RA	DEC	V	B-V	U-B	EX.6	RADVEL	G	U	V	W	S	TAN I	I	ECC.	RMAX	H	SOURCE
-12 2669	8 44.4	-13 11	10.27	.30	- .15	.32	33.0	C	128	-120	-392	429.5	-2.23	-65.9	0.55	11.8	14.50	E SY
-4 2468	8 47.9	-5 21	9.18	.72	(1.78)	.09	35.0	C	-15	-96	-67	118.0	-0.69	-34.6	0.37	10.1	16.90	E SY
G 9- 31	8 49.9	22 45	10.83	.60	- .04	.18	50.8		59	-155	-73	181.2	-0.44	-23.8	0.60	10.2	11.00	S3
G114-25	8 56.6	-6 12	11.78	.56	(1.52)	(.26)	126.0	D	-197	-309	0	366.5	0.00	0.0	0.89	14.7	-4.40	E2SY
GC 12504	9 0.2	33 5	7.03	.50	- .04	.06	70.5	B	118	-10	-28	121.7	-0.24	-13.3	0.35	15.7	25.50	E SY
W 5951	9 2.1	39 0	11.59	.49	- .24	.28	-51.0	C	-47	-412	-54	418.2	-0.13	-7.4	0.47	10.4	-14.70	E SY
G 46- 31	9 14.5	3 14	10.85	.54	- .13	.20	220.7		12	-281	70	289.8	0.25	14.0	0.94	10.0	-1.60	S3
-80 328	9 25.8	-80 21	10.10	.59	(1.55)	.27C	-110.0	B	265	-118	320	431.9	1.10	47.8	0.77	22.8	14.70	CESY
-45 5210	9 29.1	-45 45	11.08	.60	- .08	.21	47.0		131	-110	-104	200.2	-0.61	-31.3	0.52	12.0	15.50	E2
+65 737	9 45.9	65 33	9.70	.67	.10	.12	-33.1		85	-89	-73	143.1	-0.59	-30.7	0.39	10.9	17.60	S2
W 6296	9 46.4	44 32	10.92	.42	- .20	.21	-90.0	C	-65	-163	-51	182.7	-0.29	-16.2	0.64	10.6	10.20	E SY
-51 4288	9 50.9	-52 15	10.06	.43	- .23	.23	194.0		-264	-137	178	346.6	0.60	30.9	0.82	24.8	12.80	E2
+55 1362	10 1.4	54 35	8.98	.70	.02	.32	-40.0		-41	-11	-16	45.4	-0.38	-20.7	0.17	12.3	25.40	S2
-43 6810	10 6.0	-43 56	9.80	.57	- .02	.12	156.8		-113	-168	-107	229.0	-0.53	-27.9	0.69	11.6	9.70	E2
LTT 3717	10 7.5	-32 22	9.73	.62	.09	.06	34.0	B	110	-4	79	135.5	0.72	35.7	0.33	15.8	26.10	E SY
-51 4628	10 15.2	-52 14	10.01	.43	- .23	.23	194.0	B	-264	-137	178	346.6	0.60	30.9	0.82	24.8	12.80	E SY
-16 3030	10 18.9	-16 48	9.33	.79	(1.85)	.09	45.0	C	100	-43	-12	109.5	-0.11	-6.3	0.30	12.4	22.20	E SY
+20 2594	10 20.9	20 15	9.93	.48	- .14	.15	97.0		113	-258	0	281.7	0.00	0.0	0.97	10.9	0.70	E2
G 53- 41	10 24.8	1 40	11.04	.48	- .14	.15	87.3		18	-259	-104	279.7	-0.40	-21.8	0.98	10.0	0.60	S3
HD91121	10 28.5	-20 57	8.75	.60		.19E	105.7		-74	-208	-127	254.7	-0.58	-29.9	0.80	10.6	5.70	E2
G162- 68	10 32.2	-9 51	10.54	.68	.06	.17	53.3		109	-17	33	115.1	0.30	16.7	0.31	14.4	24.80	S3
ROSS 626	10 44.7	28 41	10.24	.49	- .20	.22	74.0	C	-175	-359	91	409.6	0.23	12.8	0.76	14.0	-9.40	E SY
W 6728	10 47.4	56 43	12.57	.60	- .13	.30	-128.0	D	-246	-294	105	397.5	0.27	15.3	0.94	18.6	-2.90	E SY
HD94518	10 51.9	-30 53	8.36	.60	- .04	.16	92.5		-27	-116	-33	123.6	-0.28	-15.5	0.45	10.2	14.90	E2
-44 7094	11 6.1	-44 34	9.47	.38	- .08	.12	-62.0		158	-100	21	188.2	0.11	6.4	0.54	13.4	16.50	E2
-22 3101	11 12.3	-23 22	9.05	.58	(1.58)	(.18)	87.9	B	60	-95	26	115.3	0.23	13.0	0.38	10.4	17.00	E SY
GC 15489	11 13.3	2 22	9.22	.42	- .13	.13	55.4	B	-80	2	81	113.9	1.01	45.3	0.31	15.8	26.70	E SY
-38 7127	11 23.4	-38 26	8.96	.47	- .21	.21	223.0	B	-3	-201	113	230.6	0.56	29.3	0.76	10.0	6.40	E SY
LTT 13102	11 23.4	50 39	10.09	.83	.40	.11	-80.2	B	53	-28	-109	124.4	-1.82	-61.2	0.15	11.0	23.70	E SY
-14 3322	11 23.6	-15 26	10.45	.58	- .11	.21	11.4		96	37	65	121.7	0.63	32.3	0.42	21.9	30.20	S2
LTT 13142	11 29.2	76 55	11.53	.65	- .07	.33	-108.0	C	-130	-280	194	364.6	0.63	32.1	0.95	11.8	-1.50	E SY
HD 101063	11 35.2	-28 35	9.47	.76	.09	.30	187.0		3	-173	85	192.8	0.49	26.2	0.66	10.0	9.20	E2
W 7117	11 42.1	25 50	10.37	.47	- .15	.16	193.0	C	316	-189	99	381.3	0.27	15.0	0.91	28.8	7.60	E SY
GC 16123	11 42.9	47 57	8.05	.61	.05	.09	24.4	B	80	-81	13	114.6	0.11	6.5	0.36	10.9	18.40	E SY
W 7131	11 44.0	51 10	9.92	.55	- .16	.26	61.0	D	231	-276	40	362.1	0.11	6.3	0.97	15.5	-1.10	E SY
GC 16253	11 50.1	38 5	6.49	.75	.15	.25	-98.3	B	-267	-150	-17	306.7	-0.06	-3.2	0.84	24.4	11.50	E SY
-21 3420	11 53.0	-22 6	10.18	.52	- .14	.20	13.9		27	-95	-82	128.4	-0.83	-39.7	0.36	10.0	17.00	S2
-20 3540	11 54.1	-21 8	10.06	.53	- .10	.16	168.0		89	-210	50	233.5	0.22	12.4	0.80	10.5	5.50	E2
-41 6879	11 56.1	-41 38	8.91	.81	(1.85)	(.12)	160.6	B	34	-202	-8	205.0	-0.04	-2.2	0.76	10.0	6.30	E SY
HD105004	12 2.9	-26 18	10.37	.55		.16E	121.0		69	-238	-74	258.6	-0.30	-16.6	0.90	10.3	2.70	E2
GC 16626	12 8.0	65 56	8.68	.56	- .02	.10	69.0	C	89	-7	48	101.4	0.54	28.3	0.26	14.1	25.80	E SY
HD106516	12 12.6	-10 1	6.12	.45	- .14	.14	6.4	B	-66	-116	-98	165.6	-0.73	-36.3	0.48	10.7	14.90	E2SY
GC 16854	12 19.1	62 2	8.20	.61	.03	.11	-82.0	C	0	-100	-56	114.6	-0.56	-29.2	0.38	10.0	16.50	E SY
GC 16874	12 20.1	73 31	8.00	.73	.26	.04	-97.5	A	42	-78	-100	133.6	-1.13	-48.5	0.30	10.2	18.70	E SY
W 7634	12 40.2	73 14	9.30	.60	- .08	.22	-45.2	B	92	-120	-16	152.1	-0.11	-6.0	0.50	10.8	14.50	E
LTT 4859	12 40.9	-44 24	9.87	.47	- .16	.17	220.0	B	-23	-234	62	243.2	0.26	14.8	0.88	10.1	3.10	E SY
GC 17484	12 50.6	-18 14	8.38	.53	- .11	.17	144.4	B	-174	-149	-18	229.8	-0.08	-4.5	0.71	14.3	11.60	E SY
-7 3509	12 53.0	-8 27	9.86	.72	.20	.09	-14.8		7	-40	-39	56.3	-0.96	-43.8	0.12	10.0	22.50	S2
GC 17670	12 58.8	-27 6	8.04	.55	(1.58)	(.15)	227.6	B	-43	-226	-88	246.3	-0.38	-20.9	0.85	10.2	3.90	E SY
-13 3834	13 7.7	-13 45	10.68	.60	- .06	.18	125.0		-33	-289	4	290.9	0.01	0.8	0.91	10.2	-2.40	E2
GC 17853	13 8.7	67 46	8.88	.92	.67	.00	-12.0	C	77	-70	3	104.1	0.03	1.7	0.32	10.9	19.50	E SY
G 61- 38	13 9.4	18 39	9.89	.64	.03	.15	44.4		-96	-51	26	111.8	0.24	13.5	0.35	12.8	21.40	S3
+71 646	13 13.2	70 33	10.13	.75	.17	.25	-97.6		247	-432	101	507.8	0.20	11.5	0.72	21.5	-16.70	S2
G 62- 30	13 17.4	7 7	9.78	.64	.02	.15	79.4		36	-83	76	118.2	0.84	40.0	0.32	10.1	18.20	S3
W 7923	13 17.7	64 26	13.28	.59	- .10	.22	252.0	D	302	-270	390	562.3	0.96	43.9	0.99	23.6	-0.50	E SY
-38 8457	13 19.0	-39 4	8.79	.47	(1.47)	(.24)	142.0	A	76	-205	104	242.1	0.48	25.4	0.78	10.4	6.00	E SY
W 7951	13 21.1	74 27	11.66	.48	- .24	.25	-34.0	D	329	-193	-7	381.5	-0.02	-1.1	0.93	32.7	7.20	E SY
G 62- 52	13 33.5	1 28	10.89	.67	.01	.22	-45.5		-54	-75	-97	134.0	-1.05	-46.4	0.33	10.8	19.00	S3
+77 521	13 44.1	77 29	9.45	.66	.08	.12	-87.2		-8	-90	-37	97.6	-0.41	-22.3	0.34	10.1	17.50	S2
HD120559	13 48.4	-57 11	8.00	.66	- .02	.23	13.4		69	-86	-77	134.5	-0.70	-34.9	0.36	10.6	17.90	E2
HD121004	13 50.9	-46 18	9.04	.61	- .06	.22	243.8	A	-20	-289	113	311.0	0.39	21.3	0.91	10.1	-2.40	E2SY
+34 2476	13 57.0	34 7	10.04	.40	- .22	.24	-167.0	B	-209	-198	-152	325.6	-0.53	-27.8	0.85	15.8	6.70	E SY
HD 122196	13 58.1	-37 48	8.72	.48	- .18	.24	-22.8		182	-151	21	237.4	0.09	5.1	0.70	13.6	11.40	E2
-60 5215	14 6.5	-61 16	9.68	.78	(1.80)	(.18)	40.7	B	70	-118	-100	169.8	-0.73	-36.1	0.48	10.5	14.70	E SY
W 8296	14 7.8	-13 41	10.68	.60	- .10	.24	123.5	B	-36	-274	8	278.5	0.03	1.7	0.96	10.2	-0.90	E SY
-2 3811	14 12.7	-3 13	9.24	.57	.03	.07	28.8		-57	-12	-7	58.7	-0.12	-6.9	0.22	13.0	25.30	S2
HD126512	14 23.2	20 50	7.27	.54	- .04	.19E	-53.4		-141	-125	-93	210.1	-0.49	-26.3	0.61	13.0	14.00	E2
HD 126681	14 24.6	-18 11	9.31	.59	- .12	.25	-48.0		-3	-165	-173	239.1	-1.05	-46.4	0.63	10.0	10.00	E2
+26 2606	14 46.8	25 56	9.74	.42	- .22	.22	31.5	B	-115	-111	18	160.8	0.11	6.4	0.53	12.2	15.40	E2SY
GC 20090	14 53.8	53 52	7.76	.79	.33	.09	-14.9	B	95	-50	16	108.5	0.15	8.5	0.30	11.9	21.50	E SY
HD132475	14 57.0	-21 48	8.58	.56	- .16	.24	174.0	B	-56	-177	80	202.2	0.43	23.3	0.69	10.4	8.80	E2SY
W 8758	15 5.7	32 37	11.12	.68	.12	.11	-63.0	C	-152	-240	-10	284.3	-0.04	-2.0	0.92	12.5	2.50	E SY
HD134439	15 7.5	-16 8	9.08	.78	.13	.33	306.8	A	-257	-400	-8	475.5	-0.02	-1.0	0.80	24.0	-13.50	E SY
HD134440	15 7.6	-16 11	9.45	.85	.30	.33	306.5		-257	-400	-8	475.5	-0.02	-1.0	0.80	24.0	-13.50	E2
ADS9544AB	15 11.3	-1 10	6.60	.77	.33	.05	-69.6	B	90	-108	-18	141.7	-0.13	-7.3	0.46	10.9	15.70	E SY
GC 20635	15 18.4	-48 8	5.64	.65	.06	.12	-70.0	A	132	-62	44	152.3	0.30	16.8	0.41	13.2	20.30	E SY
GC 21124	15 40.4	-10 46	7.24	.49	- .23	.25	-171.1	B	190	-107	-38	221.3	-0.17	-9.9	0.62	15.1	15.80	E SY
GC 21372	15 52.6	5 13	8.62	.38	- .08	.12	-64.8	B	100	-94	39	142.7	0.28	15.9	0.43	11.2	17.10	E SY
GC 21461	15 56.5	27 53	8.03	.77	.30	.08	-69.8	B	95	-71	10	119.0	0.08	4.8	0.35	11.4	19.40	E SY
GC 21522	15 58.8	-44 32	10.02	.62	(1.68)	(.08)	-53.5	B	85	-62	-28	108.9	-0.27	-14.9	0.31	11.3	20.30	E SY
+42 2667	16 1.6	42 24	9.84	.45	- .22	.22	-154.0	B	-95	-227	-53	251.7	-0.22	-12.2	0.87	11.0	3.80	E SY
GC 21674	16 5.1	66 55	9.88	.56	- .04	.12	-73.0	C	96	-91	-32	136.1	-0.24	-13.6	0.41	11.2	17.40	E SY
HD145417	16 9.8	-57 24	7.54	.84	.24	(.40)	9.6		58	-104	-32	123.3	-0.27	-15.0	0.42	10.3	16.10	E2
-39 10388	16 14.8	-39 38	9.70	.52	(1.62)	(.06)	-28.9	B	30	-69	-178	193.2	-2.37	-67.1	0.26	10.1	19.60	E SY
HD146296	16 15.9	-71 10	9.77	.60	- .06	.18	41.0		73	-149	7	166.1	0.04	2.4	0.59	10.4	11.60	E2
W 9401	16 17.7	22 46	11.51	.70	.08	.20	167.0	D	-273	-86	78	296.7	0.27	15.2	0.81	34.5	17.90	E SY
W 9483	16 26.8	44 48	11.29	.68	- .08	.42	-301.0	C	-254	-400	-109	486.2	-0.23	-13.0	0.80	23.4	-13.50	E SY
BPM24495	16 52.3	-57 46	11.65	.47	- .23	.24	-136.0		303	-258	-20	398.5	-0.05	-2.9	0.99	23.8	0.70	SF
GC 22886	16 56.3	-57 13	7.02	.56	(1.66)	(.05)	98.7	B	-65	-83	-21	107.5	-0.20	-11.3	0.37	11.0	18.20	E SY
GC 22890	16 56.5	68 6	8.69	.65	.08	.11	-15.8	B	85	-32	-7	91.1	-0.08	-4.4	0.24	12.1	23.30	E SY

TABLE III. (continued).

NAME	RA	DEC	V	B-V	U-B	EX.6	RADVEL	G	U	V	W	S	TAN I	I	ECC.	RMAX	H	SOURCE
HD154276	17 1.6	17 17	9.12	.65	.10	.08	-55.0		6	-116	18	117.5	0.15	8.8	0.44	10.0	14.90	E2
GC 23366	17 15.7	-75 18	8.99	.60	(1.65)	(.12)	58.9	B	-14	-107	52	119.8	0.48	25.7	0.41	10.1	15.80	E SY
GC 23438	17 18.6	1 29	8.96	.58	- .02	.12	-162.2	B	153	-51	-54	170.1	-0.33	-18.5	0.45	15.0	21.40	E SY
72 HER	17 18.8	32 32	5.39	.62	.07	.08	-78.4	A	-26	-81	-64	106.5	-0.75	-37.0	0.32	10.2	18.40	E SY
ADS10638C	17 32.3	6 2	8.38	.58	- .05	.15	-144.0	C	149	-148	-171	270.8	-0.81	-39.2	0.65	12.2	11.70	E SY
W 10190	17 36.1	18 35	9.79	.48	- .10	.11	-242.0	B	160	-145	-98	237.1	-0.45	-24.4	0.65	12.7	12.00	E SY
W 10288	17 44.7	67 19	9.70	.70	.14	.11	-78.1	B	-71	-84	1	110.0	0.01	0.5	0.38	11.1	18.10	E SY
-9 4604	17 45.1	-9 35	9.68	.66	- .06	.34	-134.2		111	-92	-16	145.1	-0.11	-6.3	0.44	11.6	17.30	S2
+4 3509	17 45.3	4 58	8.92	.85	.46	.08	-93.1	B	60	-109	32	128.5	0.26	14.4	0.44	10.3	15.60	E SY
ADS10858AB	17 50.3	-7 54	7.64	.62	.07	.08	-124.0	C	98	-61	-28	118.8	-0.24	-13.6	0.33	11.7	20.40	E SY
G154-34	17 53.1	-16 24	11.30	.70	- .13	.45	-216.0		126	-371	-215	446.9	-0.55	-28.8	0.66	11.4	-10.60	SF
ADS10938AB	17 55.9	-13 5	9.64	.60	- .05	.18	188.0	B	-247	-192	36	314.9	0.12	6.6	0.87	19.5	7.30	E SY
-36 12201	18 2.6	-36 36	10.22	.57	- .19	.32	363.8	B	-355	-162	-8	390.3	-0.02	-1.2	0.96	86.0	10.30	E SY
GC 24647	18 3.2	4 39	6.79	.63	.04	.12	-123.5	B	75	-84	-37	118.5	-0.33	-18.2	0.36	10.7	18.10	E SY
HD166913	18 12.1	-59 25	8.26	.45	- .21	.22	-42.0		43	-40	65	87.6	1.11	47.9	0.15	10.4	22.50	E2
LTT 7321	18 21.4	-45 31	10.92	.50	- .15	.17	106.0	B	-60	-148	-86	181.4	-0.54	-28.3	0.59	10.5	11.70	E SY
GC 25190	18 25.2	46 3	8.31	.60	.04	.08	-86.0	B	47	-98	32	113.3	0.29	16.4	0.38	10.2	16.70	E SY
W 11060	18 33.4	28 40	11.30	.42	- .23	.23	-80.0	C	-182	-179	-109	277.6	-0.43	-23.1	0.78	14.3	8.60	E SY
HD 175606	18 54.9	-51 31	9.34	.44	- .23	.24	164.6		-93	-154	-119	215.7	-0.66	-33.5	0.63	11.1	11.10	E2
-66 3406	18 56.1	-66 15	8.61	.70	(1.75)	(.13)	-89.0	B	110	-4	13	110.8	0.12	6.7	0.33	15.8	26.10	E SY
GC 26124	18 58.5	19 1	10.08	.70	.09	.19	-19.0	C	-132	-131	-10	186.2	-0.05	-3.1	0.61	12.5	13.40	E SY
HD177095	19 1.0	-20 32	9.64	.62	.03	.12	78.2	B	-120	-143	-15	187.3	-0.08	-4.6	0.63	12.0	12.20	E2SY
HD177758	19 3.7	-11 58	7.23	.57	- .04	.10	0.0		-49	-116	0	125.9	0.00	0.0	0.47	10.4	14.90	E2
HD178149	19 6.1	-48 33	9.07	.67	.02	.19	-42.7		79	-140	-10	161.1	-0.06	-3.6	0.56	10.5	12.50	E2
W 11787	19 17.4	41 33	8.84	.85	.34	.36	-123.5	B	-30	-127	-58	142.8	-0.44	-24.0	0.60	10.2	13.80	E SY
HD181720	19 19.7	-33 0	7.85	.58	- .06	.16	-57.2		72	-142	-65	172.0	-0.41	-22.2	0.56	10.4	12.30	E2
-45 13178	19 20.2	-45 9	9.62	.46	- .22	.22	18.0	B	40	-288	-55	295.9	-0.19	-10.7	0.91	10.1	-2.30	E SY
31 AQL	19 22.6	11 50	5.15	.79	.40	.01	-100.6		122	-25	-23	126.6	-0.18	-10.5	0.35	14.6	24.00	S2
W 11949	19 29.6	36 3	10.20	.48	- .12	.13	-172.0	C	-221	-242	-168	368.3	-0.51	-27.1	0.95	16.3	2.30	E SY
+26 3578	19 30.5	26 17	9.36	.37	- .22	.28	-129.0	B	-7	-148	-49	156.1	-0.33	-18.3	0.57	10.0	11.70	E SY
GC 27027	19 31.6	33 5	6.60	.59	.01	.10	-163.3	B	63	-155	38	171.6	0.23	12.8	0.60	10.3	11.00	E SY
+16 3924	19 36.0	16 35	8.48	1.85		.25	-386.9		100	-422	-234	492.8	-0.54	-28.3	0.47	11.1	-15.70	S2
-42 14547	19 51.5	-42 46	10.12	.43	- .26	.26	-138.2	B	158	-218	16	269.7	0.06	3.4	0.86	12.1	4.70	E SY
G143- 17	19 52.8	10 36	8.83	.58	- .11	.22	-200.6		158	-119	64	207.9	0.32	17.9	0.59	13.0	14.60	S2
HD 189558	19 58.3	-12 23	7.74	.57	- .10	.21	-14.7		-73	-128	47	154.7	0.32	17.7	0.53	10.8	13.70	E2
GC 27820	20 1.6	29 46	5.70	.72	.38	-.10	-46.2	B	10	-47	-92	103.8	-1.91	-62.4	0.15	10.0	21.80	E SY
GC 27992	20 7.9	-36 14	5.31	.86	(1.95)	(.02)	-130.7	A	121	-58	45	141.5	0.34	18.5	0.38	12.8	20.70	E SY
-7 5235	20 13.9	-7 36	8.39	.58	- .03	.14	-109.8		105	-71	-20	128.3	-0.16	-9.0	0.37	11.8	19.40	S2
-3 4864	20 19.4	-3 22	10.20	.83	.43	.07	33.8		-63	-35	-31	78.5	-0.43	-23.3	0.24	11.9	23.00	S2
HD193901	20 20.6	-21 31	8.66	.55	- .13	.19	-175.0	B	154	-180	-19	237.6	-0.08	-4.6	0.74	12.1	8.50	E2SY
W 12754	20 22.6	24 54	10.82	.38	- .25	.27	-320.0	B	63	-337	8	342.9	0.02	1.3	0.74	10.3	-7.20	E SY
LTT 15972	20 22.8	41 20	9.10	.60	.10	.03	-162.2	B	-35	-172	6	175.6	0.03	2.0	0.66	10.2	9.30	E SY
-9 5491	20 30.1	-9 32	9.54	.65	.00	.21	-257.4		165	-159	121	259.1	0.53	27.8	0.70	12.7	10.60	S2
HD196761	20 37.3	-23 59	6.36	.72	.22	.06	-44.0		62	22	4	65.9	0.06	3.5	0.27	16.4	28.70	E2
ETA CEP	20 44.3	61 39	3.43	.92	.62	.08	-87.3	A	33	-97	10	102.9	0.10	5.6	0.37	10.1	16.80	E SY
GC 29020	20 46.4	-20 49	8.14	.60	(1.68)	(.06)	-85.0	C	83	-62	17	105.0	0.16	9.3	0.30	11.2	20.30	E SY
HD199288	20 54.5	-44 18	6.53	.60	- .05	.17	-8.2		-27	-116	51	129.6	0.43	23.2	0.45	10.2	14.90	E2
+71 1053	21 11.1	71 27	9.74	.54	- .02	.08	-22.1		133	-65	-3	148.1	-0.02	-1.2	0.42	13.2	20.00	S2
+45 3561	21 27.9	45 40	7.89	.76	.31	.06	-83.7	B	66	-84	1	106.8	0.01	0.5	0.35	10.5	18.10	E SY
-35 14849	21 30.7	-35 39	10.58	.40	- .22	.24	110.0	B	-152	-310	-56	349.8	-0.16	-9.2	0.87	12.6	-4.50	E2SY
HD205156	21 31.5	-50 1	8.14	.59	.00	.11	100.0	C	-125	-24	-24	129.5	-0.19	-10.7	0.42	16.5	24.10	E2SY
HD205650	21 34.5	-27 51	9.04	.51	- .28	.32	-102.1	B	121	-82	8	146.4	0.05	3.1	0.43	12.1	18.30	E SY
WOLF 1143	21 53.1	32 24	11.10	.63	- .08	.27	-177.9	B	326	-281	-180	466.5	-0.42	-22.7	0.98	29.4	-1.60	E SY
HD208998	21 58.3	-53 20	7.04	.58	.02	.08	-20.0		24	-116	39	124.7	0.33	18.2	0.45	10.0	14.90	E2
G126- 62	22 9.1	17 51	9.48	.43	- .24	.28	-272.8		224	-251	40	338.8	0.12	6.8	0.97	15.0	1.40	S3
GC 31171	22 14.8	12 39	7.03	.60	.08	.05	-29.9	B	95	-36	-32	106.5	-0.31	-17.5	0.28	12.4	22.90	E SY
GC 31267	22 19.4	-51 3	8.73	.85	(1.90)	(.08)	-0.4	B	12	-147	24	149.4	0.16	9.2	0.56	10.0	11.80	E SY
-42 15988	22 30.9	-42 19	9.64	.42	- .20	.22	47.0	B	-72	-119	-6	139.2	-0.04	-2.5	0.50	10.8	14.60	E SY
-46 14447	22 45.6	-46 19	10.05	.41	- .25	.28	-83.0	B	30	-180	102	209.1	0.56	29.2	0.68	10.0	8.50	E SY
GC 32040	22 57.0	68 45	8.74	.78	.42	-.02	-26.0	C	104	-73	-1	127.1	-0.01	-0.5	0.38	11.7	19.20	E SY
ADS16644AB	23 14.5	-14 6	8.17	.47	- .20	.21	10.1	B	-300	-258	-44	398.1	-0.11	-6.3	0.99	27.6	0.70	E SY
-50 13953	23 18.9	-49 46	10.15	.66	- .05	.35	72.0	B	8	-102	-59	118.1	-0.58	-30.0	0.39	10.0	16.30	E SY
+59 2723	23 24.2	60 20	10.47	.44	- .22	.22	-103.2		224	-206	-64	311.0	-0.21	-11.9	0.86	15.3	5.90	S2
GC 32800	23 33.0	30 44	6.85	.59	.07	.04	-103.0	C	44	-100	57	123.2	0.52	27.6	0.39	10.2	16.50	E SY
HD222766	23 40.9	-8 12	10.10	.60		.17E	-98.0		147	-160	22	218.4	0.10	5.8	0.68	12.0	10.50	E2
HD223713	23 49.5	-61 41	9.47	.78	.27	.16	-26.7		-1	-116	92	148.1	0.79	38.4	0.44	10.0	14.90	E2
-17 6856	23 56.8	-17 13	8.92	.77	.25	.16	-42.8	B	166	-102	-80	210.6	-0.41	-22.3	0.56	13.8	16.30	E SY

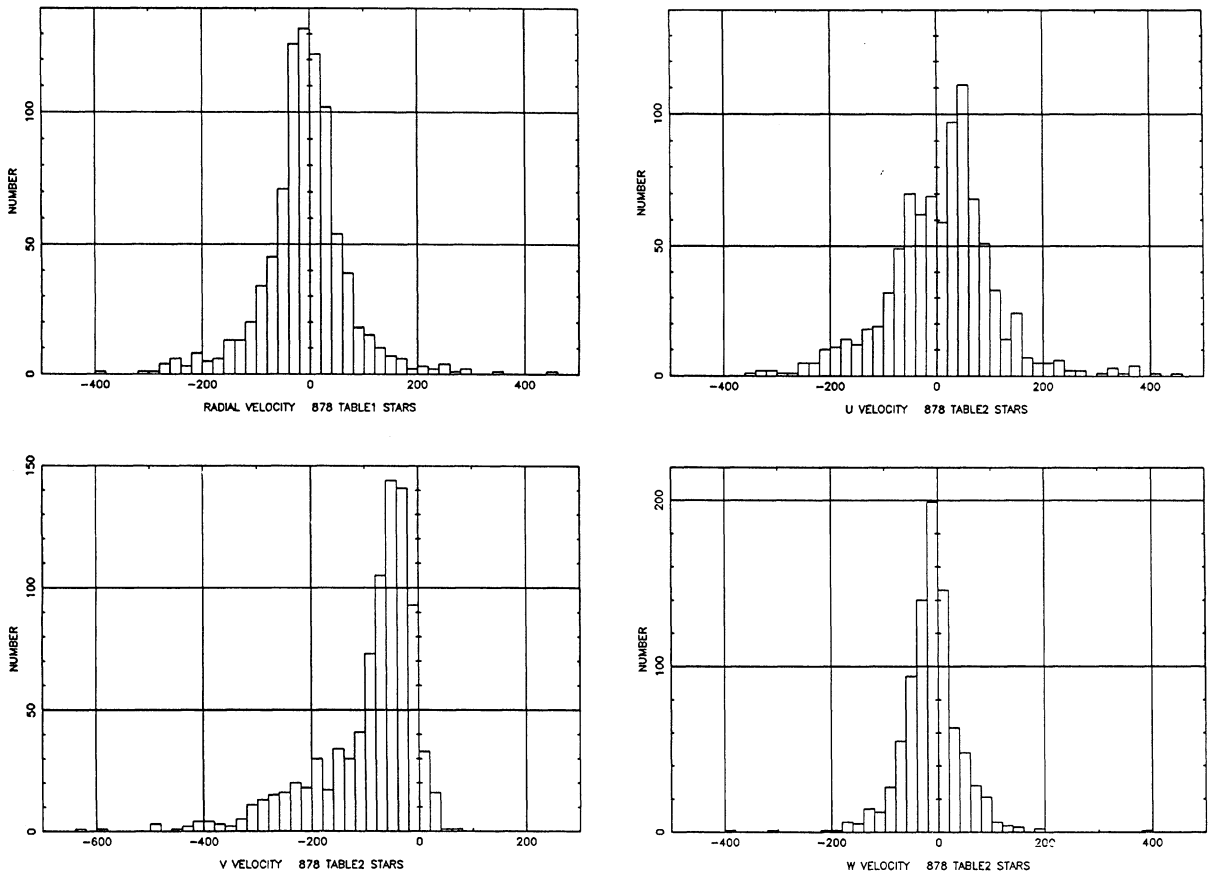

FIG. 1. Distributions of the measured radial velocity and of the calculated U, V, and W velocities for the 878 stars in Table II.

The most striking difference is the distribution in V, where much of the thick-disk component is absent (recall that it was not found in ELS) and the tail toward higher negative V velocities is stronger than in Fig. 1.

b) The Bottlinger Diagram as a Function of Metallicity

It was shown by Roman (1954) and then by ELS, and later, with more data, in Papers II and III, and again by Eggen (1979) that a stellar orbit's progressive departure from circularity about the galactic center is a strong function of [Fe/H]. This is true both in the projection of the orbit onto the galactic plane via the Bottlinger (1933) U, V velocity diagram (Schwarzschild 1952; Trumpler and Weaver 1953; Eggen 1964, Fig. 1; Sandage 1969, Fig. 3) and in the W velocity component as well.

The Bottlinger diagram for the 1125 star sample covering all metallicity values and the complete range of $B-V$ colors is shown in Fig. 3. The U and V values in Tables II and III have been reduced to the local standard of rest, assumed to be in circular orbit about the galactic center, by subtracting 10 km s^{-1} from the listed U and adding 15 km s^{-1} to the listed V (cf. Delhaye 1965, Tables 1 and 2).

The peculiar "indented" feature of the distribution seen where no points exist in Fig. 3 in a small circle centered at $U' = -10$ and $V' = +15$ is an artifact of the selection of only high-proper-motion stars. Stars with such small U' and V' velocities relative to the Sun have small enough proper motions to be excluded from the sample.

The two principal features to note in Fig. 3 are (1) the heavy concentration of points in the approximately rectangular area bounded by $-100 < V' < +50$, $-100 < U' < +100$, and (2) the more thinly spread, broader distribution outside this region, ranging to $V \sim -500$ km s^{-1} and $|U| \sim 350$ km s^{-1}. These two distributions will be seen repeatedly in different representations in what follows. As before, we believe the first to be the thick disk, and the second to be the extended-halo population.

Figure 4 shows how the distribution changes over the Bottlinger diagram for different ranges of metallicity, binned by ultraviolet excess. The concentration centered on $V' \simeq -30$, $U' \sim 0$ is present only in the two highest-metallicity bins of $\delta = 0$–0.09 and 0.10–0.15 in panels (a) and (b) (corresponding to the high-metallicity range of $0.17 >$ [Fe/H] > -0.82 from Table VII discussed later). The distribution in the lower two panels is progressively broader, both in V and in U. Here the metallicity range in panel (c) for δ between 0.16 and 0.20 is $-0.91 >$ [Fe/H] > -1.30 and the mean asymmetric-drift velocity is $\langle V \rangle \sim -155$ km s^{-1}. In panel (d) for the lowest-metallicity bin, which ranges between $-1.4 >$ [Fe/H] $\gtrsim -3.5$, the asymmetric drift has increased to $\langle V \rangle \sim -210$ km s^{-1} with a corresponding increase in the dispersion in the U velocity. This increase in $\sigma(U)$ is the "pressure" support of this kinematic subsystem

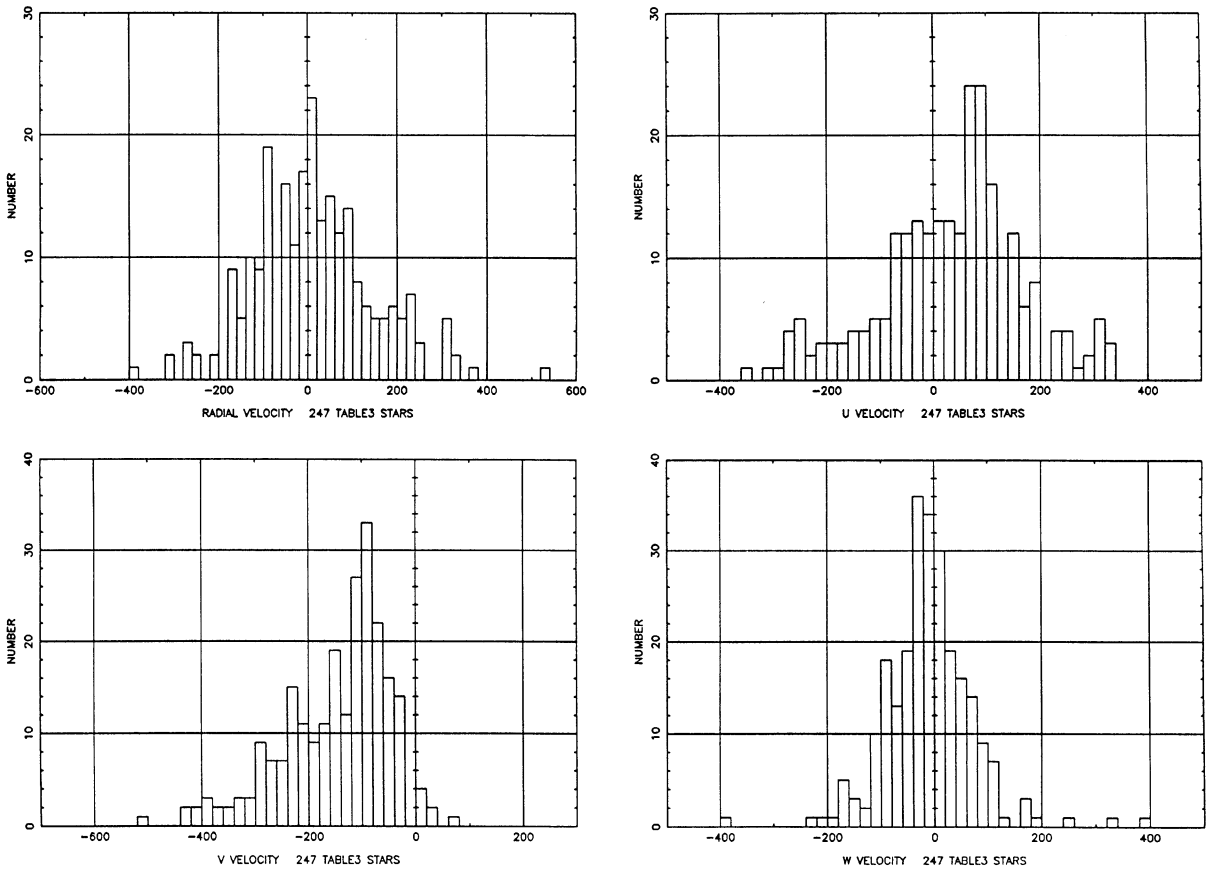

FIG. 2. Same as Fig. 1 but for the 247 star sample of Table III.

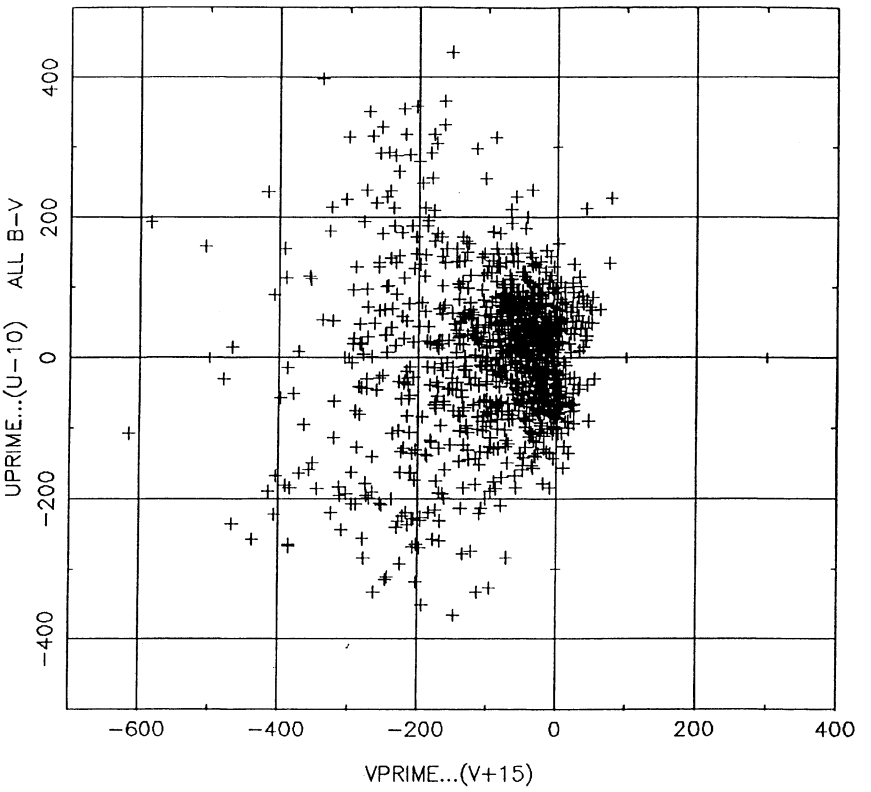

FIG. 3. The Bottlinger diagram, relative to the local standard of rest, for the total 1125 star sample of Table II plus Table III. Stars for the complete range of the metallicity are plotted.

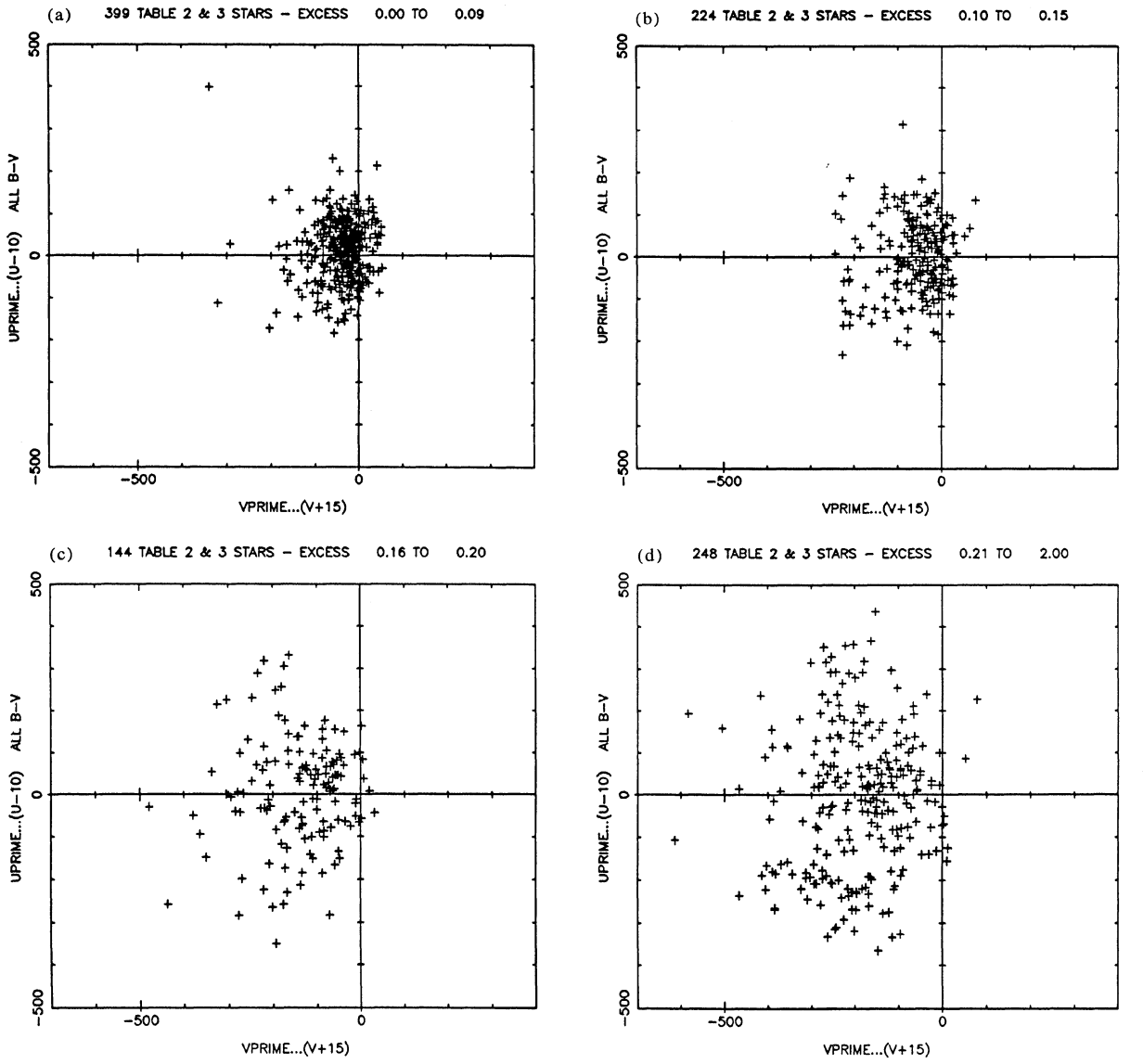

FIG. 4. Composite of four Bottlinger diagrams for stars of all colors in Tables II and III, divided into the excess groups of (a) $\delta = 0$–0.09, (b) 0.10–0.15, (c) 0.16–0.20, and (d) $\geqslant 0.21$.

in the absence of a high enough rotational velocity for centrifugal support—an empirical discovery by Strömberg (1924) with the theoretical explanation by Jeans. As the circular velocity decreases, its U component must increase to maintain the balance between kinetic and potential energy for each stellar orbit.

To test whether the binning by ultraviolet excess has been affected by using stars redder than $B - V = 0.8$ where the relation between δ and [Fe/H] is beginning to be guillotined (Sandage 1969, Table 1A), we restrict the sample in Figs. 5 and 6 to stars with $B - V \leqslant 0.8$. The resulting sample of 797 stars embraces $-0.10 < \delta \leqslant 0.33$ and shows the same features as Figs. 3 and 4 but with fewer stars. Clearly, the mean asymmetric-drift velocity $\langle V \rangle$ is a monotonic function of $\delta(0.6)$. The point is so central that we now inquire whether a similar pattern of dependence of kinematics on [Fe/H] holds for the W velocities perpendicular to the plane.

V. THE (W,V) VELOCITY CORRELATIONS

a) The Diagrams

Knowledge of how the W velocity distribution varies across the Bottlinger diagram is crucial for separating out the various kinematic subsystems. The σ's of these distributions give the scale heights of each of the Lindblad components if indeed they are discrete units. Even if not discrete but, rather, only a single kinematic continuum exists, the variation of $\sigma(W)$ with [Fe/H] gives information on the formation history of the halo as a whole during its collapse.

The $\sigma(W)$, [Fe/H] correlation is related to (1) whether a semicontinuous heavy-element enrichment occurred within the halo gas during most of its collapse time at all heights, or (2) whether the bulk of the enrichment occurred only during the last stages of the collapse when the remaining gas, not yet converted into stars, was close to what was to become (or

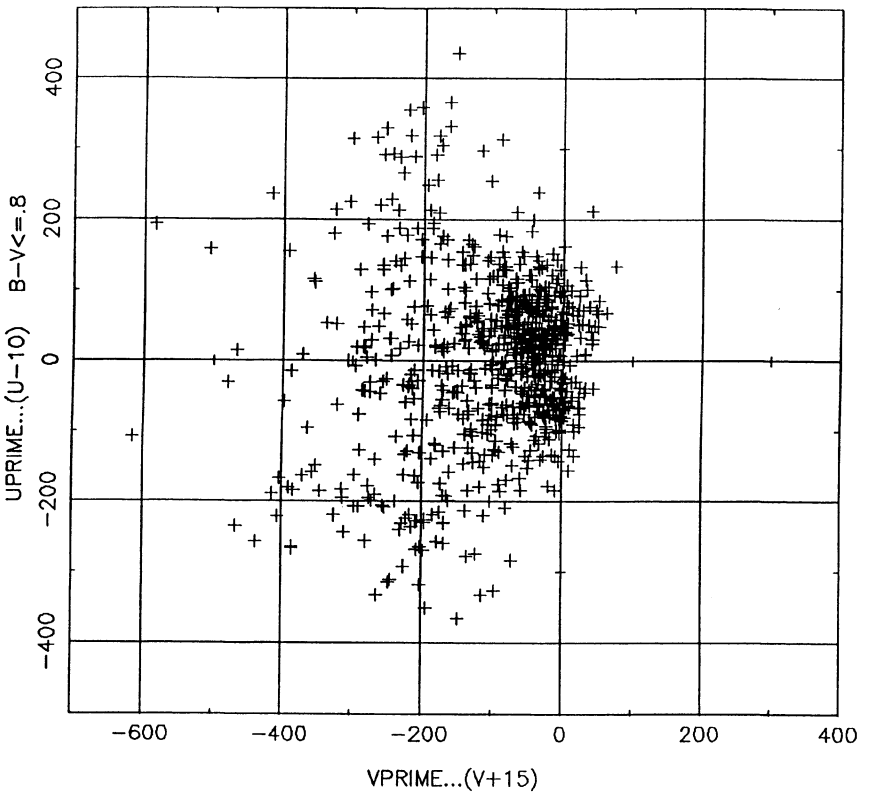

FIG. 5. Same as Fig. 3 but for the subset of the sample for stars with $B - V \leqslant 0.8$.

was becoming) the Galactic plane. In either of these two possible histories, for a plane (or indeed for a nonspherical bulge or a thick disk) to form, part of the Z energy of position above the eventual plane must be progressively destroyed by dissipation (i.e., cooling of the gas) during the collapse. Otherwise, no flattening would occur.

In the first of the two stated histories, a chemical gradient with height will exist in the present halo stars at all heights provided that gas-gas dissipation occurs as the gas falls toward the plane. Otherwise (if there is no dissipation), high-metallicity stars would exist in the high halo, put there again on their outward orbits after the gas been asterated, regardless of what height, because no energy of position would have been lost. The strength of the gradient depends on the *rate* of energy dissipation (the cooling rate) compared with the rate of metal enrichment. Obviously, this time ratio also determines the *distribution* of [Fe/H] at a given height now in the present equilibrium Galaxy.

In the second history, a chemical gradient would exist only in the lower halo, or, for the discrete Lindblad subsystem picture, in the bulge which may be the same as the Gilmore-Wyse thick disk.

The extremes of these two possibilities are whether the halo can be considered as a single evolving dynamical unit in the early times, as assumed by ELS, or merely as a collection of separate pieces each with their own individual collapse and enrichment histories, as advocated by Searle and Zinn (1978) and Norris (1986a).

One way to display the variation of the W velocity distribution across the face of the Bottlinger diagram would be to plot Figs. 3–6 separately for various binning intervals of W *for each bin in* δ. The number of such diagrams is very large. To cover the four ultraviolet-excess ranges displayed in Figs. 4 and 6 by binning $|W|$, using 20 km s^{-1} intervals from $|W| = 0$ to 300 km s^{-1}, requires 60 separate diagrams. We, in fact, proceeded in this way and did find the principal characteristics of the change of $\langle W \rangle$ and $\sigma(W)$ with V and δ by inspecting the very large number of plots. However, display of the data in this way would be prohibitive of space and quite confusing unless the diagrams were to be inspected in rapid succession, viewed by progressive flipping of the diagrams in order, like a motion picture. We have chosen two, more compact, representations of the U, V, W, δ parameter space which, together, display the main features of the distributions.

Figure 7 shows the V,δ distribution for the 797 star subset that has $B - V \leqslant 0.8$; the data are from Tables II and III. This is the same sample displayed in Fig. 5 and in the four panels of Fig. 6. The number of stars is slightly different between Figs. 6 and 7 (797 compared with 768) because the 29 stars in the high-metallicity interval of $\delta < 0.00$ are not used in Fig. 6 but are present in Fig. 7.

The concentration of stars in the velocity range $50 > V > -100$ in Fig. 5 is also present in Fig. 7 as the roughly rectangular distribution within this velocity range and bounded within the ultraviolet-excess range of $-0.06 < \delta < 0.15$. Clearly, these are the same stars shown in the U,V plane in panels (a) and (b) of Fig. 6.

The striking feature of Fig. 7 is the abrupt break in the number of stars at $\delta = 0.15$, with a much thinner distribution for $\delta > 0.15$. The progressive variation toward more negative V velocities beginning at this δ value is the second important point. The W distribution provides the clue that these two features are the signatures of the two separate

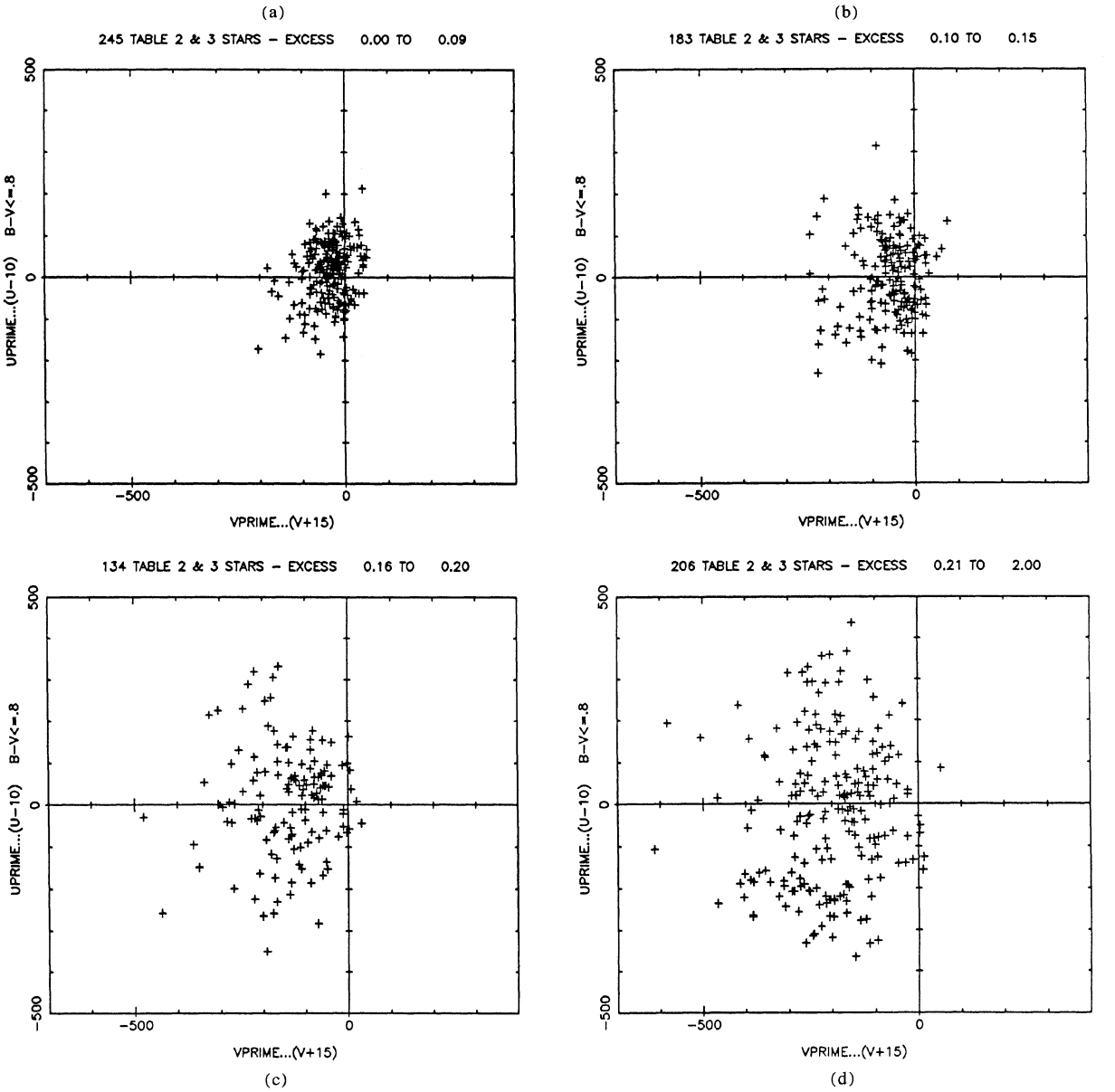

FIG. 6. Same as Fig. 4 for stars with $B - V \leqslant 0.8$.

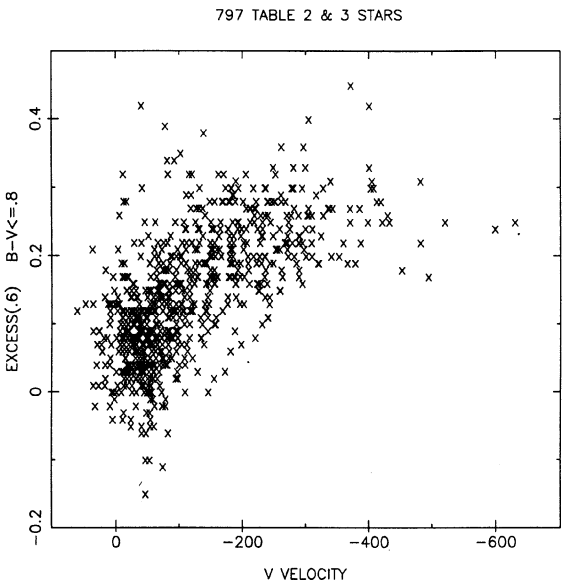

FIG. 7. V,δ diagram for the Table II plus Table III sample for stars with $B-V\leqslant 0.8$. The V velocity is heliocentric, not reduced to the local standard of rest.

Lindblad kinematic subsystems with different mean $\sigma(W)$ values—the thick disk and the extended halo—that we have been discussing.

Figure 8 shows the (W,V) distributions for five bins of the ultraviolet excess corresponding to the metallicity ranges of [Fe/H] between $+0.17$ and -0.32, -0.40 and -0.82, -0.91 and -1.30, -1.40 and -1.70, and -1.80 and -2.66, respectively. The progressive change of the W,V distributions among the five panels is the main feature of Fig. 8.

The upper left-hand panel for the highest-metallicity stars shows that the strong concentration near $\langle V\rangle = -40$ km s^{-1}—which contains the same stars as in Fig. 6(a)—are generally confined to $|W|$ values smaller than 60 km s^{-1}. The distribution in $|W|$ changes character at this velocity in panels (a) and (b). We interpret this to define approximately the division of the halo and the thick disk. We shall later use the criterion of $|W|\geqslant 60$ km s^{-1} as one definition of halo stars. The other definition of separation, which we shall also use, is based on the striking difference in Fig. 7 in the V distribution above and below $\delta = 0.15$ at $V > 100$ km s^{-1}. A justification for this cut is suggested in Fig. 8 by the disappearance of the thick-disk component between the middle and the upper right-hand panels, and by the corresponding

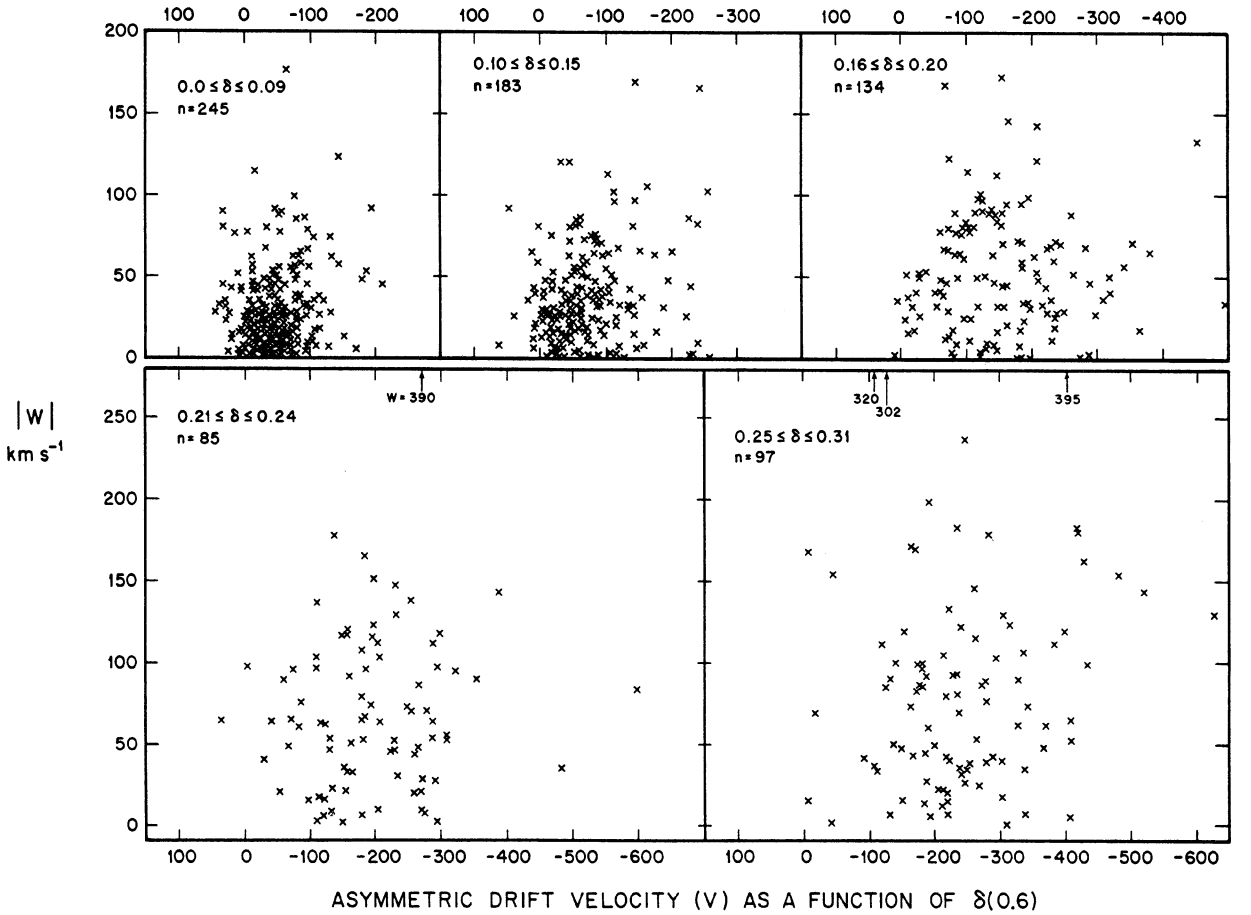

FIG. 8. V,W diagram of five intervals of $\delta(0.6)$ for stars in the sample with $B-V\leqslant 0.8$. The velocities are heliocentric.

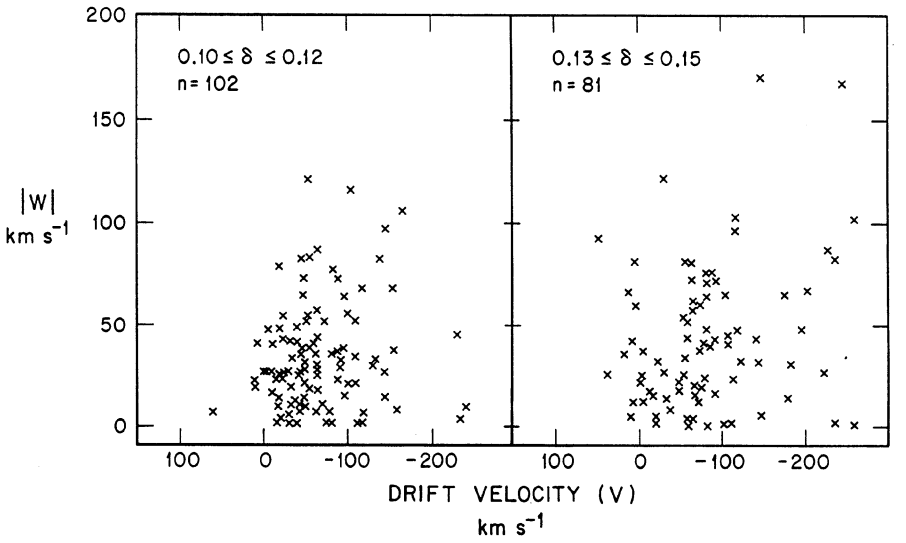

FIG. 9. V,W diagram for stars in the upper middle panel of Fig. 8 divided more finely in the $\delta(0.6)$ interval to show the progressive change in the character of the distribution near $\delta(0.6) \sim 0.15$.

striking difference in the W distribution, all occurring near $V = -100$ km s^{-1}.*

The three upper panels of Fig. 8 show again the suggestion from Fig. 7 that a fundamental change occurs in the kinematic and chemical abundance distributions in our sample near $\delta = 0.15$. Indeed, a detailed inspection of the number of stars in Fig. 7 in the interval $0.10 < \delta < 0.15$ suggests that the change is already occurring near $\delta = 0.12$. To test this, we divided the sample shown in the middle panel of Fig. 8 into the two abundance intervals of $0.10 \leqslant \delta \leqslant 0.12$ and $0.13 \geqslant \delta \geqslant 0.15$ (corresponding to [Fe/H] between -0.40 and -0.57, and -0.65 and -0.82, respectively). The result, shown in Fig. 9, is that the disk component still dominates in the first interval, shown in the left-hand panel, but has markedly decreased compared to the broader V distribution in the right-hand panel for lower-metallicity stars. This interval from $0.13 \leqslant \delta \leqslant 0.15$ contains relatively more halo stars, defined either by the $|W| > 60$ km s^{-1} or the $V < -100$ km s^{-1} criteria.

The final three panels of Fig. 8 for $\delta \geqslant 0.16$ clearly show a progressive kinematic variation in $\langle V \rangle$, $\langle W \rangle$, and $\sigma(W)$ as the data are divided into these three metallicity ranges. Nearly all trace of the thick-disk component has disappeared in the upper right-hand panel, which is the same conclusion to be drawn from Fig. 6(c). The mean asymmetric-drift velocity is $\langle V \rangle \simeq -155$ km s^{-1} and the dispersion in W is $\sigma(W) = 73$ km s^{-1}. For the next bin of lower metallicity in the bottom left-hand panel, where $-1.40 < [\text{Fe/H}] < -1.70$, these values increase to $\langle V \rangle = -195$ km s^{-1}, $\sigma(W) = 92$ km s^{-1}. They increase further for the lowest-metallicity sample in the lower right-hand panel of Fig. 8 in the range $-180 < [\text{Fe/H}] < -2.66$ to $\langle V \rangle = -237$ km s^{-1} and $\sigma(W) = 114$ km s^{-1}.

Figure 8 shows then that even for the predominantly halo stars in the three lowest metallicity bins the kinematic properties in V and W vary monotonically with [Fe/H] for stars in our kinematically selected sample. We discuss in Secs. VIII and IX the selection-bias properties of our sample to address the question of whether the data of Figs. 7 and 8 contradict the opposite statement of Searle and Zinn (1978) that "...there is no statistical evidence that the kinematics of subdwarfs more metal-poor than 1/10 of the solar metal abundance are correlated with their abundances." Searle and Zinn reached their conclusion from a small sample of globular clusters, divided into disk and halo, and by a reanalysis of the subdwarf sample studied in Paper II of the present series. A similar conclusion has been reached by Norris (1986a) from his sample of low-metallicity stars selected by nonkinematic methods.

The trends in Figs. 7 and 8 ae so obvious even among the high-velocity stars, which we are not biased against in our proper-motion sample, that the contradiction is fundamental, if the Norris, Zinn, and Searle claims indeed refer to halo stars. We do not inquire further in this paper into how the difference can be resolved by an appropriate definition of halo and disk except to flag the dependence of the results on the validity of our distance scale. Our purpose here is simply to analyze our sample so that a later inquiry can be made of relative merits of the present conclusions and those of Searle, Zinn, and Norris. To this end, it is important to list the statistics that arise from Figs. 3–8, and later to discuss the effects of the various selection biases (Sec. IX) in our sample.

*The separation of our data into discrete components is, of course, arbitrary using the set limits of $|W| = 60$ km s^{-1} and $V = 100$ km s^{-1}. If indeed two components exist rather than a continuum, the kinematic parameters we derive for them will be affected to some extent by their *overlapping* velocity distributions which cannot be completely separated by the arbitrary velocity cuts defined above. For example, if $\langle \sigma(W) \rangle \simeq 40$ km s^{-1} for the thick disk, then $|W| = 60$ km s^{-1} is only 1.5σ from it, and $\sim 13\%$ of thick-disk stars will be in the "halo" sample. A cut at $|W| = 80$ km s^{-1} reduces this fraction to 5% but, from Fig. 8, the number of stars to analyze then becomes small. This overlap between the thick disk and the halo (and indeed at the low-velocity end between the thin and thick disks) must be continuously kept in mind at appropriate places in the analysis of the text. Among these places will be the metallicity distributions in Fig. 10, where it may be that the unexpected high-metallicity tail in panel (d) contains mostly thick-disk stars from the upper two left-hand panels of Fig. 8. Another crucial place in the analysis is in the V_{rot}, [Fe/H] correlation for "halo stars alone" in Figs. 26 and 30 using the $|W| = 60$ km s^{-1} halo definition. However, from Fig. 8 it can be seen that in this case the decrease of V_{rot} with [Fe/H] is still valid in our data (using our distance scale) if a $|W| = 80$ km s^{-1} cut had been made. We are indebted to the referee for his suggestion to emphasize this problem of overlapping velocity distributions.

b) Mean Values and Standard Deviations of the Velocity Correlations

Statistics for the total sample are listed in Table IV, neglecting for the moment that this sample is made up of the two separate kinematic components isolated in Figs. 7 and 8. The format is similar to that of Table 4 of Paper II (Sandage 1969), except that we also list here the σ values in addition to the absolute mean values of $\langle|U|\rangle$, $\langle|V-\langle V\rangle|\rangle$, and $\langle|W|\rangle$ of the velocity distributions. The σ statistic for Gaussian distributions is $(\pi/2)^{1/2} = 1.25$ larger than the absolute values which is, in fact, approximately the ratio in columns 5, 7, and 9 in the second section of Table IV.

Two separate data subsets are listed in Table IV; one for all $B-V$ values containing the 1125 stars from Tables II and III and the other for stars with $B-V \leqslant 0.80$, also from Tables II and III.

The systematic variations of the kinematics with metallicity that are shown in Figs. 4–9 are contained in Table IV and the two tables which follow it. The simplest summary is that as the metallicity decreases from [Fe/H] $\sim +0.2$ to ~ -4 the mean asymmetric-drift velocity (column 6 of Table IV) becomes progressively more negative and the $\sigma(U)$ and $\sigma(W)$ dispersions increase monotonically with $\delta(0.6)$.

Statistics for the thick-disk component are listed in Table V. The data are from Tables II and III for stars with colors $B-V \leqslant 0.80$ and with V velocities greater than -100 km s^{-1}. The sample is divided into seven $\delta(0.6)$ ranges whose corresponding [Fe/H] values from the calibration in Table VII in the next section are in column 2.

Figures 4(a) and 4(b), 6(a) and 6(b), 7, and 8(a) and 8(b) show that the thick-disk kinematic unit is well defined for $\delta \leqslant 0.16$ but is not evident in our data for metallicities smaller than this. Again, the dramatic break between the top middle and top right-hand panels of Fig. 8 shows this. However, as we have no alternate criteria here other than $V > -100$ to define the thick-disk component, many halo stars are undoubtedly present in the Table IV statistics in the last three ultraviolet-excess bins of $\delta(0.6) \geqslant 0.16$. The increase of $\sigma(U)$ and $\sigma(W)$ with $\delta > 0.16$ shown in columns 5 and 9 is, therefore, contaminated by nondisk halo stars (cf. footnote in Sec. V*a*).

TABLE IV. Statistics of the velocity distributions from the total data sample in Tables II and III.[a,b,c]

δ(0.6)	<δ(0.6)>	n	<U>	<|U|> σ(U)	<V>	<|V-<V>|> σ(V)	<W>	<|W|> σ(W)
(1)	(2)	(3)	(4)	(5)	(6)	(7)	(8)	(9)
Total Sample (all B-V values); n = 1125								
≤-0.01	-0.040	110	7.9	47.6	-52.5	28.1	-13.5	24.2
0.00 to 0.09	0.049	399	21.7	59.5	-53.1	34.6	-10.8	28.1
0.10 to 0.15	0.124	225	11.5	73.9	-75.3	49.7	-16.1	38.7
0.16 to 0.20	0.179	143	17.2	100.3	-154.4	75.1	-9.9	55.0
0.21 to 0.33	0.251	199	-6.0	139.9	-213.0	84.0	-10.0	79.2
>0.21	0.275	248	2.6	136.2	-207.5	87.8	-12.2	75.6
Subsample with B-V ≤ 0.80; n = 796								
<-0.01	-0.044	29	-3.9	50.8 58.6	-42.3	23.1 29.4	-21.3	28.1 27.4
0.00 to 0.09	0.053	245	24.5	59.4 66.9	-49.9	31.2 41.9	-9.2	27.3 36.2
0.10 to 0.15	0.124	183	12.4	78.1 93.0	-73.5	47.4 61.3	-16.1	39.3 47.1
0.16 to 0.20	0.179	134	20.2	101.5 128.2	-154.8	73.2 93.8	-9.6	56.3 73.1
0.21 to 0.33	0.250	183	-7.9	145.1 173.0	-218.8	83.1 106.6	-11.3	81.1 103.9
>0.21	0.262	206	-5.9	142.5	-216.2	85.2	-12.3	79.9

[a] The combined data for the thick disk and the halo components.

[b] Velocity units are km s^{-1}.

[c] No σ(U), σ(|V - <V>|), nor σ(W) have been calculated for the first part of this table for all B-V values.

TABLE V. Statistics of the velocity distributions of the thick disk defined by stars with $V > -100$ km s^{-1}.[a,b]

δ (1)	[Fe/H] (2)	n (3)	<U> (4)	σ(U) (5)	<V> (6)	σ(V-<V>) (7)	<W> (8)	σ(W) (9)
≤-0.01	+0.30	29	-3.9	58.6	-42.3	29.4	-21.3	27.4
0.00 to 0.09	+0.17 to -0.32	223	+29.4	64.6	-41.1	31.0	-9.4	34.5
0.10 to 0.12	-0.40 to -0.57	81	+18.3	83.8	-44.6	30.5	-11.7	39.3
0.13 to 0.15	-0.65 to -0.82	55	+12.5	80.0	-44.1	36.9	-11.0	47.2
0.16 to 0.20	-0.91 to -1.30	42	+27.6	93.9	-58.3	31.7	-15.7	57.0
0.21 to 0.24	-1.40 to -1.70	12	+44.0	107.4	-51.9	38.4	-11.0	69.4
0.25 to 0.33	-1.80 to -2.99	8	-50.7	81.3	-38.3	33.9	-15.2	91.5

[a] Stars from Tables II plus III with B-V ≤ 0.8.

[b] Velocity units are km s^{-1}.

The main feature to be noted in Table V is the mean value of $\langle V\rangle \simeq -45$ for all excess bins. This is larger than the standard solar motion of -15 km s^{-1} relative to the local standard of rest, indicating a slight rotational lag of 30 km s^{-1} relative to the circular velocity at the solar circle. If the rotation of the local standard of rest at the solar circle is 220 km s^{-1}, our data give 190 km s^{-1} for the rotation of the thick-disk component.

From the first four rows of Table V, our best values for the thick-disk kinematics are then $\langle V\rangle_{\rm lag}^{\rm LSR} = 30$ km s^{-1}, $\langle$[Fe/H]$\rangle \simeq -0.6$ with a range of $\sim \pm 1$ dex, $\sigma(V) = 30$ km s^{-1}, $\sigma(U) = 70$ km s^{-1}, and $\sigma(W) = 37$ km s^{-1} corresponding to a scale height of $\sim$750. (The complete sample in Table V of 450 stars give $\sigma(W) = 42$ km s^{-1}, giving a scale height of $\sim$940 pc.)

Our thick-disk sample does not have the extreme kinematic characteristics described by Gilmore and Wyse (1985, Sec. IV*b*), who give $\sigma(W) = 60$ km s^{-1} (for a scale height of 1.3 kpc) and a lagging velocity *relative to the Sun* of $V \sim 40$–100 km s^{-1} (our value is 45 km s^{-1}). Yet, it seems clear that we are identifying the same component, but with slightly different numbers because of a different data set (note that our data may be contaminated by some low-velocity old thin-disk stars which would artificially decrease $V_{\rm drift}$; cf. footnote in Sec. V*a*). We show in the next section that the *metallicity* distribution for the component of our data defined by $V > -100$ is nearly identical to the distribution shown by Gilmore and Wyse (1985, their Figs. 4, 5, and 7) based on their data and on those of Hartkopf and Yoss (1982). Note also that our $\sigma(W) = 42$ km s^{-1} is nearly identical to that of Hartkopf and Yoss (1982, Fig. 8) for their "low" metallicity group of G and K giants in the pole.

Statistics for the extreme halo are listed in Table VI for our

TABLE VI. Statistics of the velocity distributions of halo stars in Tables II and III defined by two different velocity criteria.[a]

δ (1)	[Fe/H] (2)	n (3)	$\langle U\rangle$ (4)	$\sigma(U)$ (5)	$\langle V\rangle$ (6)	$\sigma(V-\langle V\rangle)$ (7)	$\langle W\rangle$ (8)	$\sigma(W)$ (9)
			Halo stars defined by $V<-100$ km s^{-1}					
0.00 to 0.09	+0.17 to −0.32	22	−25.2	71.3	−139.2	33.0	−7.1	51.8
0.10 to 0.12	−0.40 to −0.57	21	−35.3	91.7	−132.1	78.3	−14.2	53.9
0.13 to 0.15	−0.65 to −0.82	26	+32.3	133.0	−166.0	54.8	−42.3	58.7
0.16 to 0.20	−0.91 to −1.30	92	+16.8	141.4	−198.9	78.4	−6.8	79.4
0.21 to 0.24	−1.40 to −1.70	73	−6.6	153.8	−217.9	87.1	+2.8	94.4
0.25 to 0.33	−1.80 to −2.99	101	−11.6	198.1	−252.6	99.6	−20.9	115.8
		335						
			Halo stars defined by $\lvert W\rvert\geqslant 60$ km s^{-1}					
0.00 to 0.09	+0.17 to −0.32	25	+41.2	76.0	−67.2	55.9	—	—
0.10 to 0.12	−0.40 to −0.57	16	−8.4	73.6	−89.2	46.2	—	—
0.13 to 0.15	−0.65 to −0.82	25	−4.2	125.0	−102.0	83.7	—	—
0.16 to 0.20	−0.91 to −1.30	55	+9.8	130.0	−164.6	84.4	—	—
0.21 to 0.24	−1.40 to −1.70	47	+5.2	153.1	−193.0	108.7	—	—
0.25 to 0.33	−1.80 to −2.99	62	−1.9	200.3	−251.3	120.9	—	—
		230						

[a] Stars from Tables II and III with $B-V\leqslant 0.8$.

two definitions of what constitute halo stars. The format is the same as for Table V. All data are from Tables II and III for stars with colors of $B-V\leqslant 0.8$. The monotonic change of $\sigma(U)$ in column 5, $\langle V\rangle$ in column 6, and $\sigma(W)$ in column 9 with [Fe/H] in column 2 is the principal feature of the distributions. The scale heights implied from column 9 for $\sigma(W)$ vary between 300 pc and 5 kpc as [Fe/H] varies between $\delta(0.6)<-0.01$ and $+0.33$. The W,δ distribution and the change of $\sigma(W)$ with δ are the subjects of Sec. VII.

VI. THE METALLICITY DISTRIBUTIONS OF THE THICK DISK AND THE HALO COMPONENTS

The main theme of the ELS model, nevermind the details, is that various kinematical distributions are correlated with heavy-element abundance, and indeed, that [Fe/H] is the *principal variable* in the complex parameter space of the problem. We discuss in this section the [Fe/H] distributions inferred from the measured $\delta(0.6)$ values for the present program stars and compare them with earlier studies by others of the metallicity distribution of old-disk stars in the solar neighborhood.

The $\delta(0.6)$ value was converted to [Fe/H] for each star in the sample, using the calibration listed in Table VII. This is based on the original calibration by Wallerstein and Carlson (1960) and Wallerstein (1962), put in its modern version by Carney (1979a) and Cameron (1985). The relation by Carney stops at $\delta_{0.6}=0.3$, [Fe/H] $=-2.5$. It has been arbitrarily extrapolated for $\delta_{0.6}>0.3$ in Table VII. The resulting very low values of [Fe/H] in Fig. 10 are based on this extrapolation. They may be considered as suspect in their zero point. The [Fe/H] distributions for the old thin disk, the thick disk, and the halo are listed in Table VIII and are compared in Fig. 10, based on Table VII.

The two illustrated samples of *thin*-disk stars in the solar neighborhood in panels (a) and (b) of Fig. 10 are from Twarog (1980a, his Table 4, based on his large data sample: 1980b) and from the Gliese (1969) catalog of trigonometric parallax stars with $\pi\geqslant 0''.45$ that have colors between $B-V=0.30$ and 1.0. The [Fe/H] distribution of the Twarog sample of ~ 1000 stars is similar to those of Pagel and Patchett (1975, Fig. 6) and Eggen's (1978b, Table 8) earlier studies from smaller samples. The Gliese sample contains a very low-amplitude, low-metallicity tail that reaches [Fe/H] <-2, not contained in the Twarog sample. This is expected because many stars chosen for the determination of trigonometric parallaxes have very high proper motion. A nonrepresentative, large number of high-velocity (halo) stars passing through the solar neighborhood are contained in all parallax catalogs so chosen.

Panel (c) of Fig. 10 shows the [Fe/H] distribution for stars from the thick disk defined by $\lvert V\rvert<100$ km s^{-1} with the added restriction that W be in the range $40\leqslant\lvert W\rvert\leqslant 79$ km s^{-1}. The data are from column 4 of Table VIII. We chose this definition of the thick disk, restricted between values of $\lvert W\rvert$ that correspond to heights reached above the plane between ~ 700 pc and ~ 1.6 kpc, because the thick disk itself

TABLE VII. The adopted mean relation between UV excess and [Fe/H]$_\odot$.

$\delta(U-B)_{0.6}$ (1)	[Fe/H]$_\odot$ (2)	$\delta(U-B)_{0.6}$ (3)	[Fe/H]$_\odot$ (2)
−0.10	0.42	0.16	−0.91
−0.09	0.41	0.17	−1.00
−0.08	0.39	0.18	−1.10
−0.07	0.36	0.19	−1.20
−0.06	0.34	0.20	−1.30
−0.05	0.32	0.21	−1.40
−0.04	0.30	0.22	−1.50
−0.03	0.27	0.23	−1.60
−0.02	0.23	0.24	−1.70
−0.01	0.20	0.25	−1.80
0.00	0.17	0.26	−1.92
0.01	0.13	0.27	−2.05
0.02	0.09	0.28	−2.19
0.03	0.04	0.29	−2.34
0.04	−0.01	0.30	−2.50
0.05	−0.06	0.31	−2.66
0.06	−0.12	0.32	−2.82
0.07	−0.18	0.33	−2.99
0.08	−0.25	0.34	−3.17
0.09	−0.32	0.35	−3.34
0.10	−0.40	0.36	−3.51
0.11	−0.48	0.37	−3.69
0.12	−0.57	0.38	−3.87
0.13	−0.65	0.39	−4.07
0.14	−0.73	0.40	−4.27
0.15	−0.82	0.41	−4.47

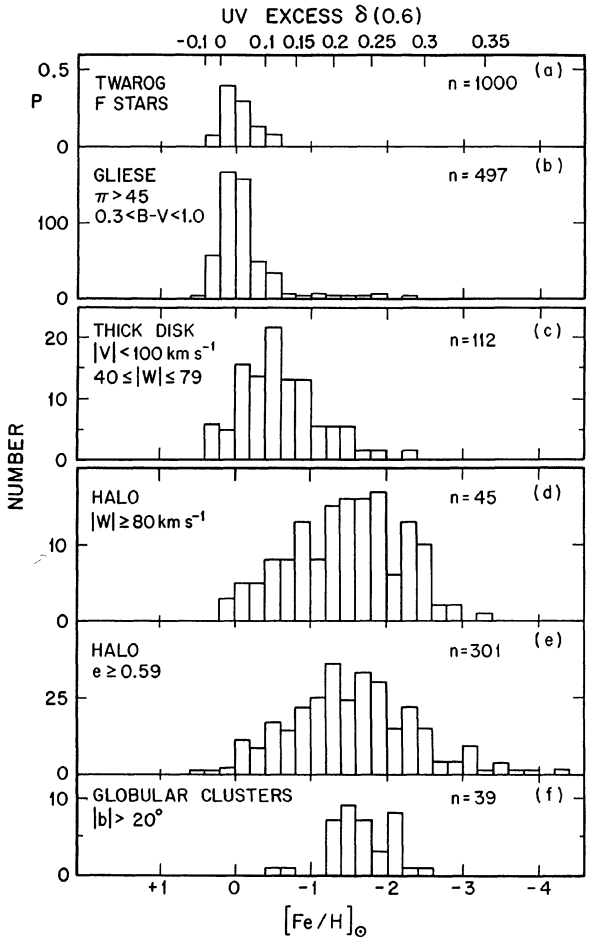

FIG. 10. Metallicity distributions for the old thin disk in (a) and (b), the old thick disk in (c), and the halo from three different samples in (d)–(f).

shows a variation of $|W|$ with $\delta(0.6)$ (cf. Figs. 16 and 23). By confining the $|V| < 100$ km s^{-1} sample to these high $|W|$ values, we find thereby the [Fe/H] distribution that is expected at a mean height of ~ 1 kpc due only to the thick disk. It is at this height that the comparison with the data of Hartkopf and Yoss (1982) can be made most securely (see Fig. 5(b) of Gilmore and Wyse 1985). This restriction in $|W|$ also eliminates the high-velocity tail of the *thin, old disk* population which undoubtedly contaminates the sample when the low $|W|$ velocity stars are included.

Panels (d), (e), and (f) of Fig. 10 show the [Fe/H] distribution of halo objects defined in three different ways. The 45 stars in panel (d) are stars from Tables II and III that have $B - V \leqslant 0.80$ and $|W| \geqslant 80$ km s^{-1}. The larger sample of 301 stars in panel (e) shows all stars from Tables II and III that have orbital "eccentricity" values of $(R_1 - R_2)/(R_1 + R_2)$, as defined by Schwarzschild (1952) and calculated by the method of ELS, greater than $e \geqslant 0.59$. Panel (f) is the distribution of 39 globular clusters with Galactic latitude $\geqslant 20°$ from data listed by Harris and Racine (1979), based in large measure on the work of Zinn (1978,1980). The [Fe/H] distribution (not shown) of the intermediate-velocity "Population II" Cepheids (Harris 1981), *obviously members of the thick disk*, is also nearly identical to Figs. 10(d), (e), and (f).

TABLE VIII. Summary of [Fe/H] distributions for the three identified Lindblad kinematic subsystems.

$[Fe/H]_\odot$	Old[a] Disk	Trig.[b] $\pi \geq 45$	Thick Disk[c]		Halo[d] $\|W\|>80$	$e \geq 0.59$	⊕
(1)	(2)	(3)	(4)	(5)	(6)	(7)	(8)
	P	Nr.	Nr.	Nr.	Nr.	Nr.	Nr.
0.60 to 0.41	0.00	3	0	4	0	1	
0.40 to 0.21	0.08	59	7	21	0	1	
0.20 to 0.01	0.40	168	5	70	3	2	
0.00 to -0.19	0.30	158	16	89	5	11	
-0.20 to -0.39	0.14	50	14	68	5	8	
-0.40 to -0.59	0.08	33	23	81	8	17	1
-0.60 to -0.79		9	13	37	8	14	1
-0.80 to -0.99		3	13	32	13	22	0
-1.00 to -1.19		6	6	16	8	25	0
-1.20 to -1.39		1	6	12	15	36	7
-1.40 to -1.59		1	6	9	16	24	9
-1.60 to -1.79		2	1	2	16	33	7
-1.80 to -1.99		3	1	3	17	30	3
-2.00 to -2.19		0	0	0	6	15	8
-2.20 to -2.39		1	1	2	13	22	1
-2.40 to -2.59				1	10	15	1
-2.60 to -2.79					2	4	
-2.80 to -2.99					2	4	
-3.00 to -3.19					0	9	
-3.20 to -3.39					1	1	
-3.40 to -3.59						3	
-3.60 to -3.79						1	
-3.80 to -3.99						1	
-4.00 to -4.19						0	
-4.20 to -4.39						2	

[a] Twarog's (1980a,b) field F star sample, no corrections.
[b] Gliese (1969) catalog using stars with $0.3 \leqslant B - V \leqslant 1.0$.
[c] Thick disk defined by stars in Tables II and III with $|V| < 100$ km s^{-1} and $40 \leqslant |W| \leqslant 79$ km s^{-1} in column 4 and merely by $|V| < 100$ in column 5.
[d] Three halo definitions. Columns 6 and 7 are data from Tables II and III. Column 7 data are for Galactic globular clusters with $|b| > 20°$ from Zinn's (1978, 1980) abundance scale as averaged with others by Harris and Racine (1979).

To simplify the detail of Fig. 10, the three principal panels are replotted in Fig. 11 for only one representation of the solar neighborhood (the Gliese sample), the thick disk (again using the $40 \leqslant |W| \leqslant 79$ km s^{-1} criterion), and the 301 star halo sample for stars with $e \geqslant 0.59$. The conclusion from these data is that the distribution over metallicity for each of the three kinematic components is fundamentally different. We show in the next section that the $|W|$ distributions of the three components are also fundamentally different, mirroring the different values of $\sigma(W)$ from Tables V and VI.

To make the distinction even clearer, we show in Fig. 12 only the two extreme distributions, one for the old thin disk in the solar neighborhood and the other for the $e \geqslant 0.59$ halo sample. The principal conclusion is that the range of [Fe/H] for the old *thin* disk is very small, confined almost entirely to $0.4 > [Fe/H] > -0.6$. The range in the lower panel of Fig. 12 for the halo is larger, embracing $\sim 0 > [Fe/H] \gtrsim -3.2$ for halo stars *now in the solar neighborhood*. This is not, of course, the range to be expected at any height *in situ* because the 301 halo stars of Figs. 10–12 cover a wide range of W and will therefore climb to different heights above the plane, causing phase mixing *and an artificially broad* [Fe/H] *now* at any given height *in situ* compared to what the [Fe/H] distribution was at formation.

VII. CORRELATIONS BETWEEN [Fe/H] AND W VELOCITY

a) The Total Sample

Figure 5 of ELS shows how $|W|$ varies with $\delta(U - B)$ for the small ELS sample. The wedge-shaped distribution has

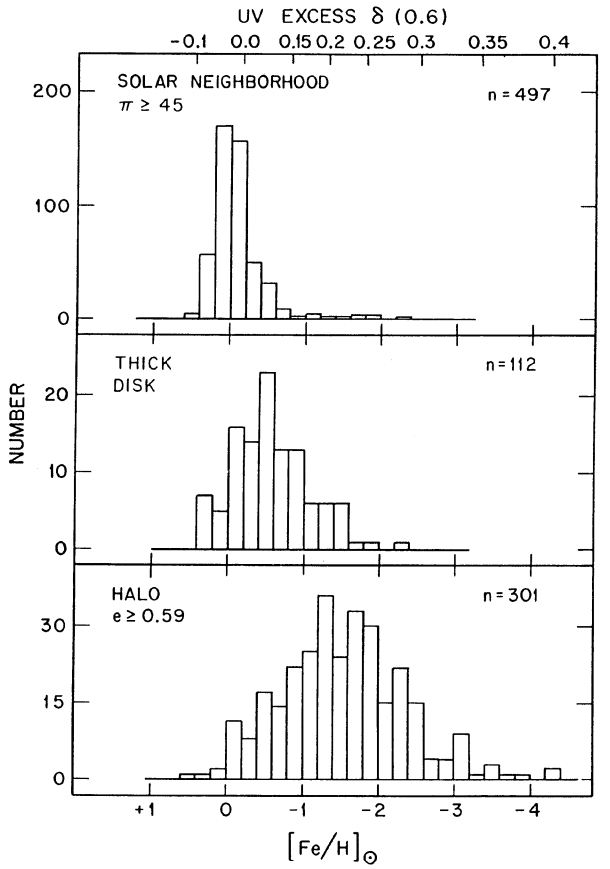

FIG. 11. Same as Fig. 10, in less detail.

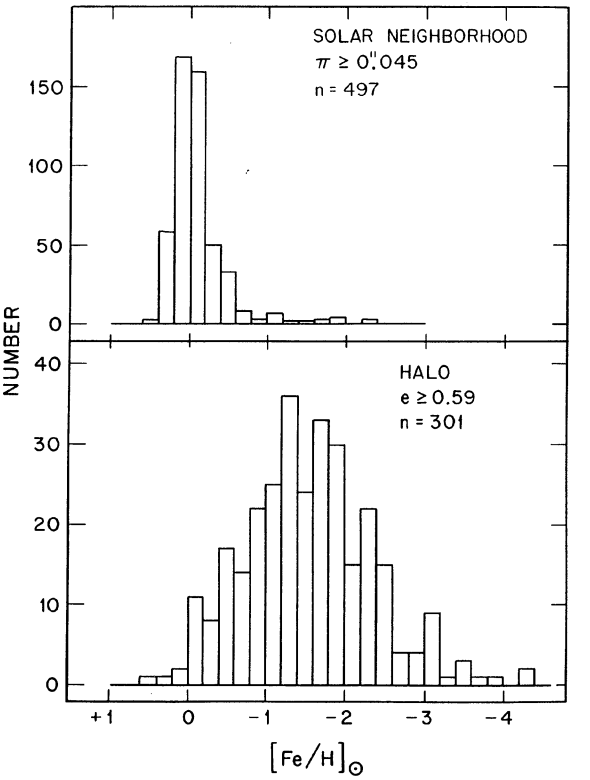

FIG. 12. Same as Figs. 10 and 11 for the old thin disk from stars within 22 pc of the Sun and for the halo defined by stars with planar eccentricities $e \geqslant 0.59$.

been taken at various times as evidence either for (1) a continuous variation of [Fe/H] with height above the plane (Sandage 1969, 1981), or (2) for a single, wide distribution of metallicity which is the same at every height (Searle and Zinn 1978). The issue evidently centers on (a) whether $\sigma(W)$ varies with $\delta(U-B)$, or (b) if two box-like distributions exist in the W,δ plane, one confined by $|W|<50$ km s^{-1} for $\delta(0.6)\leqslant 0.18$ and the other as a taller, flat-topped box that embraces all $|W|$ values from 0 to ~ 250 km s^{-1} for $\delta(0.6)\geqslant 0.18$ (e.g., Figs. 10–12 in Chap. 7 of Mihalas and Binney 1981).

The interpretation of the history of the halo was said to depend on which description of Fig. 5 of ELS is correct—more particularly, whether $\sigma(W)$ differs between the two intervals of $0.18\leqslant\delta\leqslant 0.25$ and $\delta > 0.25$ after selection bias is taken into account. One of the principal purposes of the present work has been to increase the small ELS sample of only one hundred stars to study this question.

b) The Present Sample

The (W,δ) diagram for the present sample of 878 high-proper-motion stars from Table II (all $B-V$ values included) is shown in Fig. 13. To be sure, stars of the thick-disk component are also present, confined mostly to $\delta \lesssim 0.16$ as emphasized repeatedly in Figs. 3–8. The thick disk is clearly seen as a discontinuity in the number of stars in Fig. 13 at $\delta \sim 0.16$.

Figure 14 shows the (W,δ) distribution for the 247 stars in

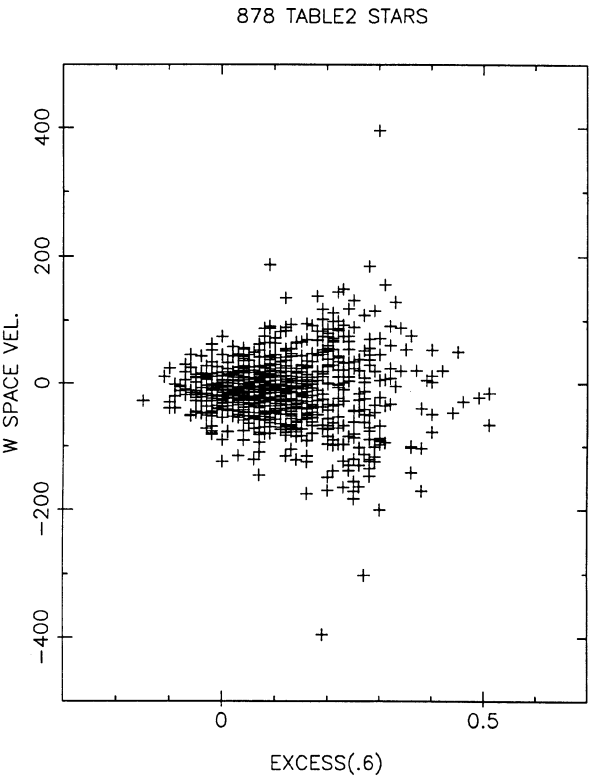

FIG. 13. W,δ diagram for the 878 stars in Table II. The W velocity is heliocentric, not reduced to the LSR.

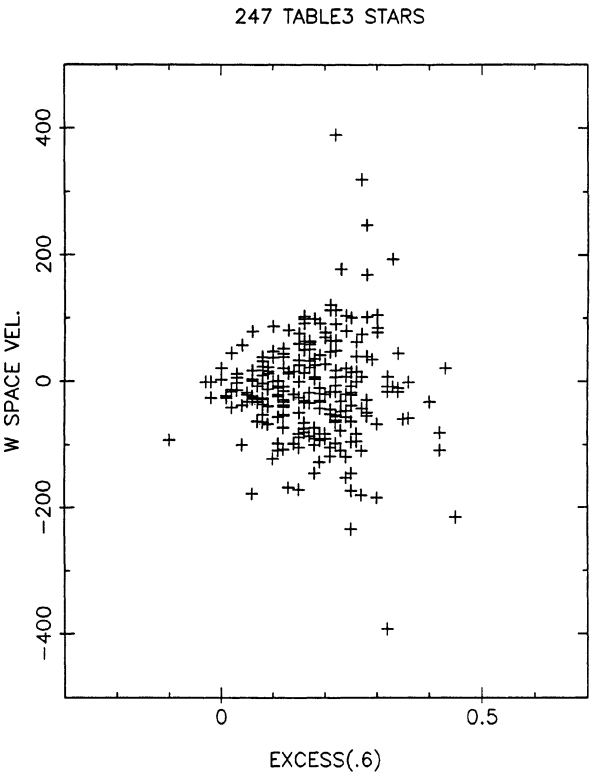

FIG. 14. Same as Fig. 13 for the 247 stars in Table III.

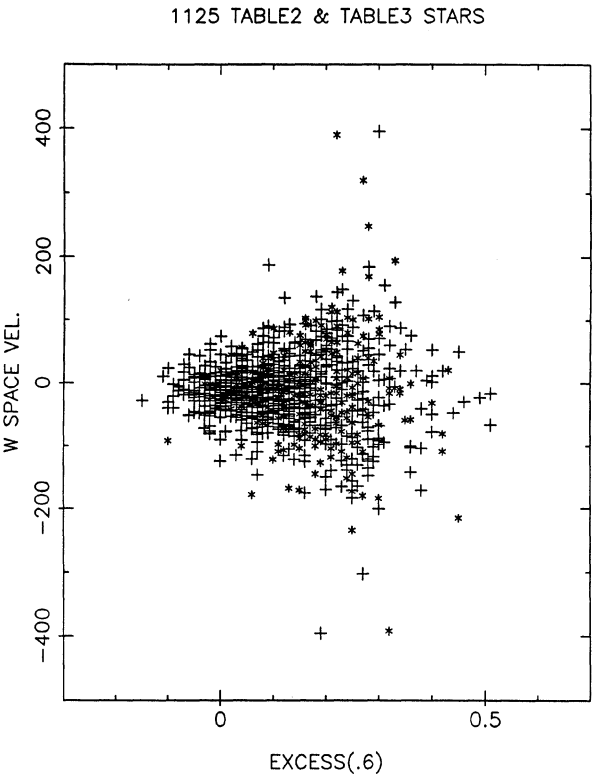

FIG. 15. W,δ for the total 1125 star sample of Table II plus Table III. Asterisks are stars from Table III.

Table III from the literature that are not contained in Table II. As mentioned before, the thick-disk component is much less pronounced in this sample than in Fig. 13. The combined data for the total 1125 star sample are plotted in Fig. 15. Crosses are the stars from Fig. 13; asterisks are from Fig. 14.

The question of whether $\sigma(W)$ increases with decreasing [Fe/H] for *the halo alone* cannot be answered from Fig. 15 until the thick-disk component is removed. We do this in a statistical way, again by dividing the sample into two bins separated at $V > 100$ km s^{-1}. The (W,δ) distribution for the *thick disk* is shown in Fig. 16 for stars with $B - V \leqslant 0.8$. The

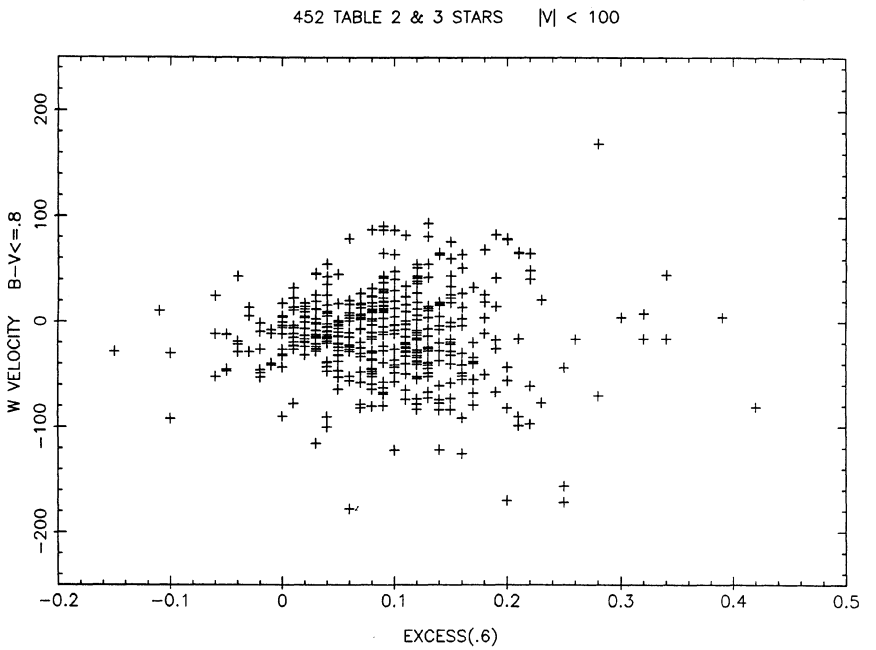

FIG. 16. W,δ distribution for stars of the thick disk alone, defined by $|V| < 100$ km s^{-1}. The data are for stars in Tables II and III with $B - V \leqslant 0.8$.

detailed statistics of this distribution have already been given in Table V. There is an increase in $\sigma(W)$ with δ for all δ bins except for $\delta_{0.6} \gtrsim 0.3$, where we suspect that $\delta_{0.6}$ is not a measure of [Fe/H] but rather signals photometric difficulties such as binarism or any number of other possibilities. Figure 16 shows that the effect is much smaller for the thick disk than that for the total distribution in Fig. 15. However, the $\sigma(W)$ variation in the thick-disk data is beyond doubt *in our sample* (see Sec. IX for a discussion of the observational bias). If real, it requires that a *chemical gradient exists within the thick disk itself*: those stars which climb highest above the plane in this bulge component have the lowest metallicity. The data are in agreement with the gradient over the first 2 kpc of the thick disk discovered by Hartkopf and Yoss (1982), as also discussed by Gilmore and Wyse (1985, their Figs. 4, 5, and 7–9). Such a gradient in the lower halo (or upper thick disk) is present in nearly all E and S0 galaxies, as shown by the variation of $U - V$ colors with photometric-aperture size (de Vaucouleurs and de Vaucouleurs 1972; Sandage and Visvanathan 1978). The gradient shown in Fig. 16 is therefore no surprise. We suggest a mechanism for its formation in Sec. XII, item 10.

With the stars of the thick disk removed from the $B - V \leqslant 0.8$ sample, the (W,δ) diagram for pure halo stars is shown in Fig. 17. There is no doubt that *in this sample* $\sigma(W)$ is a monotonic function of $\delta(0.6)$ over the entire range of $0 < \delta \lesssim 0.32$ (or $0.2 > [\mathrm{Fe/H}] \gtrsim -3$). The statistics have already been set out in Table VI, column 9, where indeed $\sigma(W)$ changes progressively. Again, if this apparent progressive variation of $\sigma(W)$ is not due to selection bias of the sample (Sec. IX), Fig. 17 requires a gradient of [Fe/H] *in situ* in the halo (Sandage 1981, Paper III), although, as mentioned before, at any height, phase mixing of the orbital motion perpendicular to the plane will *broaden* the observed [Fe/H] distribution at the present epoch after many Z oscillations (compared with the initial (formation) chemical gradient). At any height, stars from all higher heights (and hence with lower [Fe/H] values carried by such stars) will be passing through the slab at Z of thickness dZ and will intermingle with stars of higher [Fe/H] whose Z energy is just sufficient to bring them to height Z.

The detailed distribution of W for various bins of δ shown in Figs. 13–17 is shown in Fig. 18 for the disk-plus-halo sample of Fig. 15 (but for $B - V \leqslant 0.8$) and in Fig. 19 for the halo alone (Fig. 17), again for $B - V \leqslant 0.8$. The top panel of Fig. 18 is the W distribution for the unbiased sample of 420 stars in the direction of the Galactic pole ($b = 90°$) using new radial-velocity measurements discussed elsewhere (Sandage and Fouts 1987). The stars were chosen at random from the AGK2 catalog with no knowledge of their proper motions. The selection criteria were (1) spectral type between ~A5 and K0, (2) B magnitude brighter than ~10.5, and (3) the stars had to be within $\pm 5°$ of the $b = 90°$ direction. Similar unbiased radial-velocity data have been obtained for the U

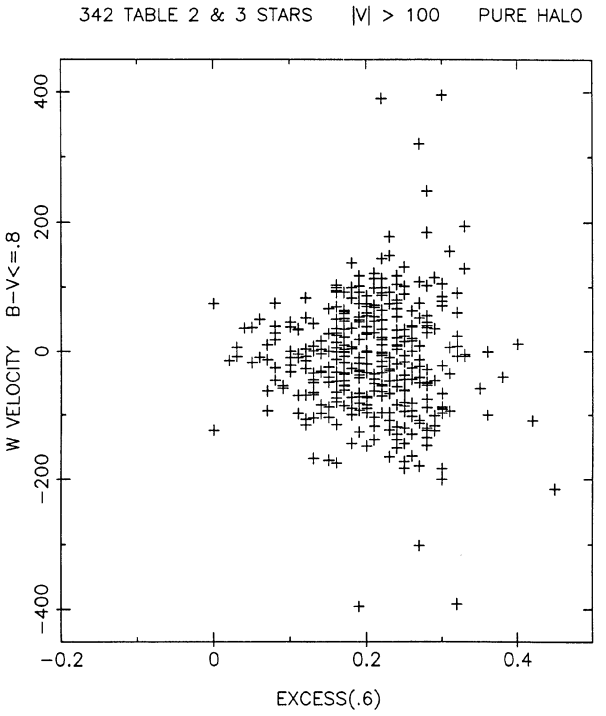

FIG. 17. W,δ distribution for the pure halo stars in the sample with $B - V \leqslant 0.8$. The thick-disk component has been removed from the total sample of Fig. 15 by the criterion $|V| > 100$ km s^{-1} to define the halo component.

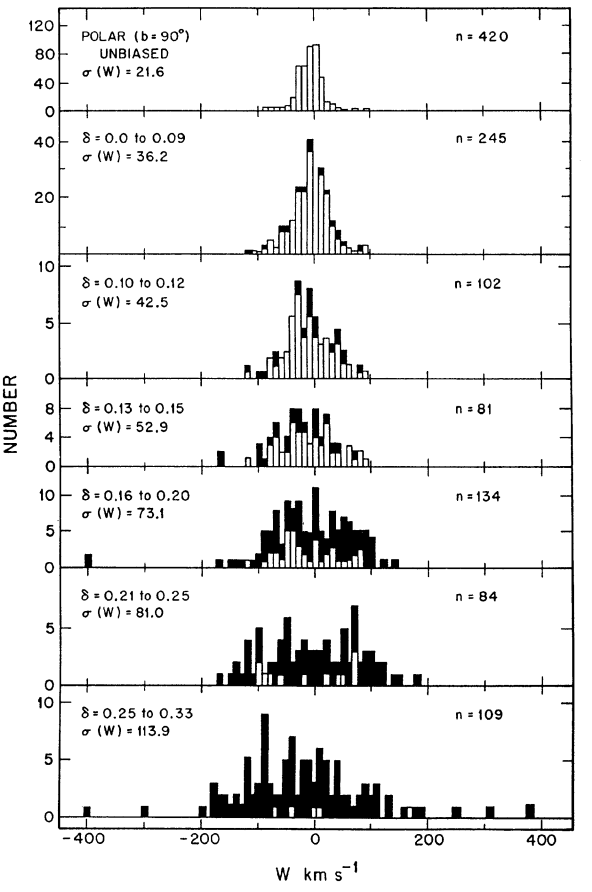

FIG. 18. Histogram of the W,δ distributions for the total sample with $B - V \leqslant 0.80$ shown in six $\delta(0.6)$ intervals. The top panel is from an unbiased radial-velocity survey of 420 stars near $b = 90°$ of spectral types F0 to K0 chosen without regard to knowledge of proper motion or metallicity (Sandage and Fouts 1987). Solid bars are halo stars defined by $|V| > 100$ km s^{-1}. Open bars are from the thick disk defined by $|V| < 100$ km s^{-1}.

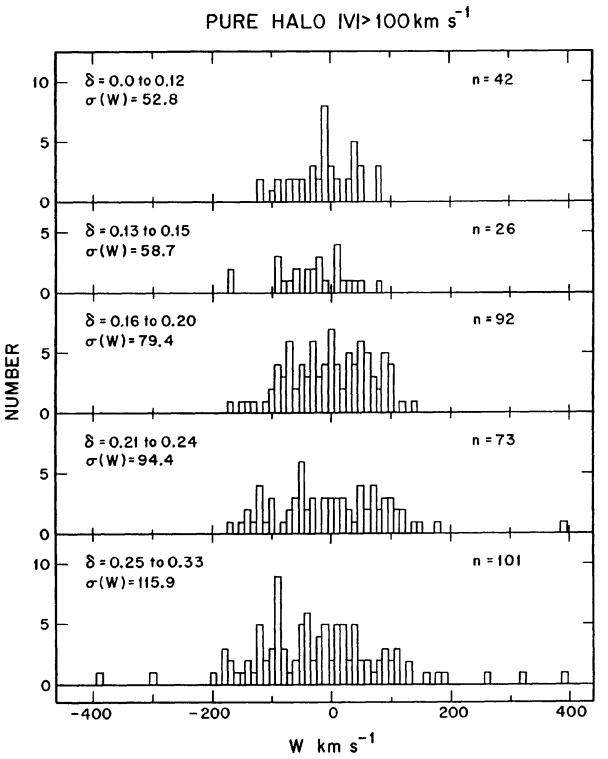

FIG. 19. Histograms of W,δ distribution of Fig. 17 for the pure halo stars alone.

direction ($l = 180°, b = 0°$) for 430 stars, and the V direction ($l = 90°, b = 0°$) for 445 stars. The purpose of this auxiliary, radial-velocity program has been to obtain the density normalization of the three kinematic components (the old thin disk, the thick disk, and the halo) from a kinematically unbiased sample.

The *old* thin-disk distribution in the top panel of Fig. 18 gives $\sigma(W) = 21.6$ km s^{-1}, which is close to the old-disk values that center around ~ 19 km s^{-1}, as summarized by Delhaye (1965, Tables 1 and 2), based on many previous determinations. Our value corresponds to a scale height of ~ 435 pc; the nominal value of 340 pc corresponds to $\sigma(W) = 19$ km s^{-1} for the old "thin" disk (cf. second footnote in Introduction).

The remaining six panels show the W distribution for the various bins of $\delta(0.6)$. The data are from those shown in Fig. 15, except for the $B - V \leqslant 0.8$ restriction. The listed $\sigma(W)$ values in Fig. 18 are from the second part of Table IV except that the interval from $\delta = 0.10$ to 0.15 has been divided into two parts from 0.10 to 0.12 and 0.13 to 0.15. The open bars in Fig. 18 are thick-disk stars ($V > -100$). Halo stars ($V < -100$) are the dark bars.

Figure 19 shows details of the halo distribution alone. The progressive widening of the distribution as [Fe/H] decreases is a different representation of the wedge-like nature of Fig. 17. The scale heights associated with each $\sigma(W)$ are given by that Z value where

$$\sigma^{-2} \int_0^Z g(Z)dZ = 1, \qquad (1)$$

obtained from

$$D(Z) = D(0)\exp\left[-\sigma^{-2}\int_0^Z g(Z)\,dZ\right] \qquad (2)$$

using the acceleration $g(Z)$ perpendicular to the plane which was previously adopted in Paper III (Sandage 1981), based in part on the function adopted by Saio and Yoshii (1979). From the $\sigma(W)$'s from Table VI shown in each panel of Fig. 19, the scale heights for the various δ bins vary from ~ 1 kpc in the upper panel for $0 \leqslant \delta \leqslant 0.12$ to 4.9 kpc for $0.25 \leqslant \delta \leqslant 0.33$. This is the most direct prediction of a true chemical gradient to be expected in the first ~ 15 kpc of the high halo itself (the thick-disk component has been removed from the data). Although controversial, it has often been suggested from other data *in situ* in the halo that a true gradient does indeed exist (Harris and Canterna 1979 with earlier references; Sandage 1981, Sec. VI; Zinn 1985, Fig. 11), but the idea has been challenged by others (cf. Searle and Zinn 1978; Butler, Kinman, and Kraft 1979; Norris 1986a) in support of their picture of the formation of the Galactic halo and disk.

VIII. EVIDENCE FOR COLLAPSE

a) The ELS Data

The principal evidence that led ELS to the notion of collapse was the strong correlation between metallicity and the shape of a stellar orbit projected onto the galactic plane. In their Fig. 4, the correlation was presented as the eccentricity, ultraviolet-excess diagram from their total sample, taken from two separate catalogs. The variation appeared to be monotonic for all e and δ values.

The eccentricity of a star's orbit remains the same as that of the gas cloud out of which it was formed, provided only that the gravitational potential of the Galaxy changes slowly over an orbital period of the star. Hence, the existence of stars on highly plunging orbits signals that the parent gas clouds themselves must have been plunging either inward or outward, at the time when these particular stars were formed. Because Fig. 4 of ELS suggested that the lowest-metallicity stars have the most elongated orbits, and because [Fe/H] is an increasing function of the time, the conclusion was that the earliest dynamical phase of the galaxy was one of collapse. As the collapse continued, dissipation formed flattened Lindblad subsystems, first the thick disk and then the thin disk, each in turn with higher [Fe/H] values. (Of course, at a later time, gas in the present old thin disk must continuously be puffed up in the Z direction by energy input in the ISM; otherwise, gas-gas dissipation would collapse the disk into a much thinner sheet than is now observed.)

This time sequence of increased [Fe/H] values with elapsed time, together with energy dissipation of the gas causing a flattened disk and a decay of noncircular gas orbits which were initially nonradial, has been the explanation both of the (W,δ) and the (e,δ) diagrams of ELS (their Figs. 4 and 5). A different representation of the (e,δ) diagram leading to the same picture of collapse is the angular momentum, δ diagram (Fig. 6 of ELS). All the ELS diagrams have the appearance of a continuous variation of each of the kinematic parameters with δ.

However, as previously mentioned, the ELS data have also been interpreted not as a *continuous* variation of $|W|$, $|V|$, e, and h with δ, but rather as two box-like distributions, each with a fixed spread of [Fe/H] (Mihalas and Binney 1981, Figs. 7–10 and 12), *neglecting the fact that two sepa-*

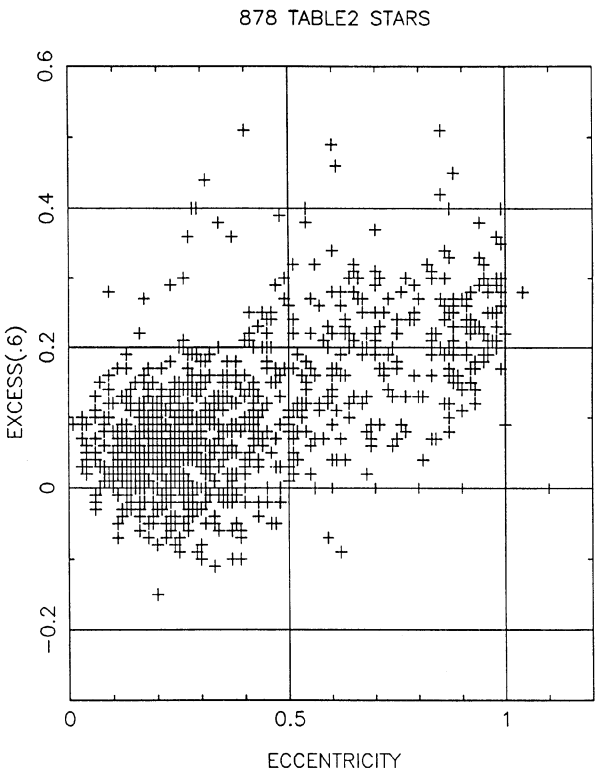

FIG. 20. e,δ distribution for the total sample of the 878 stars in Table II.

rate catalogs were used by ELS with different bias characteristics.

b) Evidence from the Present Sample

We have already discussed the W,δ correlation in Figs. 13–17 using our new sample. There is no suggestion of a two-box distribution, but a continuum suggesting collapse with dissipation.

However, to test the collapse picture more directly, the most important diagram is the eccentricity, δ distribution. The 878 star sample from Table II for all $B-V$ values with $B-V \leqslant 0.8$ is shown in the e,δ plane in Fig. 20. The diagram differs from Fig. 4 of ELS in two respects. (1) The thick-disk component is present in Fig. 20, dominating the distribution in the region $e<0.4$, $\delta<0.18$. (2) The few stars in the upper left-hand part of Fig. 20 with large excess but small projected eccentricity are low-metallicity stars in nearly circular orbits in the U,V plane. These are the type of stars discussed by Bond (1980), Norris, Bessell, and Pickles (1985), and Norris (1986a) in their nonkinematically selected samples. No stars of this type appear in Fig. 4 of ELS, undoubtedly because the sample size was too small; ELS was *not* biased against them because the low-velocity catalog of Eggen (1964) that was used was complete but the number per unit volume is so small that the ELS low-velocity sample contained none.

Including all $B-V$ colors from Tables II and III, we have 27 such stars (16 from Table II and 11 from Table III) with $e \leqslant 0.4$ and $\delta \geqslant 0.20$. Norris *et al.* (1985) and Norris (1986b) estimate that such stars constitute $\sim 20\%$ of their low-metallicity group. We conclude by the following two arguments that the number is too small to affect the systematic variation of kinematics with metallicity.

(1) Detailed data for the 27 stars are listed in Table IX. The distances in column 9 are based on the assumption that the stars are on the main sequence, appropriate to their metallicity, not evolved subgiants. Because subgiants must exist in our sample, it is certain that at least some of the stars in Table IX have actual e values greater than 0.4 since putting them at greater distances will increase the space velocity and therefore the planar eccentricity. Furthermore, the listed e values are for the projected orbit using only the U and V velocity values, neglecting W. Many of the W values in column 10 of Table IX are high, giving true eccentricities larger than their projected (planar) values.*

(2) The second argument is more powerful. The thick-disk component can be removed from our sample using either of the two definitions of $V < -100$ km s^{-1} or $|W| > 60$ km s^{-1} for the halo stars. The removal can be seen by plotting the e,δ diagram of Fig. 20 in various bins of increasing $|W|$. Four such intervals of $|W|$ are shown in Fig. 21. In the upper left-hand panel, with $25 \leqslant |W| \leqslant 50$ km s^{-1}, the distribution is still dominated, as in Fig. 20, by the thick disk with $\langle \delta(0.6) \rangle \sim 0.06$, $\langle e \rangle \sim 0.25$. The true halo distribution begins in the upper right-hand panel for $50 \leqslant |W| \leqslant 75$ km s^{-1} and continues in the lower two panels for $75 \leqslant |W| \leqslant 100$ and $|W| > 100$, respectively. From panels (b), (c), and (d), it is evident that (1) e varies continuously with δ *for the halo stars*, and (2) that very few stars exist in the upper left-hand part of the e,δ plane for panels (b), (c), and (d), where $|W| > 50$ km s^{-1}. We take this to be a direct demonstration of the *real* paucity of such stars because our kinematically selected sample *will* contain stars with these high W values. They will appear above the 0.27 arcsec yr^{-1} PM level if they are in low Galactic latitude and are closer than 40 pc from the Sun if $|W| = 50$ km s^{-1} with correspondingly higher distances for higher W velocities. The point is that $|W| \geqslant 50$ km s^{-1} is high enough so that part of our sample in low latitudes is not biased against such stars and therefore that the very small number of small e, high δ stars in Figs. 21 (b–d), relative to higher-metallicity stars with the same e values, is real.

The conclusion from Fig. 21 is, then, that the e,δ distribution in Fig. 17 is monotonic rather than two box-like distri-

*Norris' (1986c) point concerning the low e, low [Fe/H] stars centers on the ELS time scale of collapse. ELS argued that the preponderance of high e orbits for the oldest stars requires a rapid collapse; the collapse time must be *shorter* than the Galactic rotation period of the particular parent gas cloud out of which any individual star formed, otherwise the orbit would be nearly circular. Said differently, the velocity component toward the Galactic center must be high compared with the circular velocity if e is to be high. Norris argues that the presence of low e, low [Fe/H] stars violates this argument, vitiating the ELS collapse rate, and therefore their picture. There are two ways to counter this suggestion. (1) Even if the number of low e, low [Fe/H] stars is as high as 20% of the low [Fe/H] sample, as claimed by Norris, Bessell, and Pickles (1985), 80% of this sample remain with high eccentricities, requiring a rapid collapse for them. (2) There is a hierarchy of collapse times depending on the initial density, as $t_c \sim (G\rho)^{-1/2}$, and on the dissipation history. The stars found by Norris, Bessell, and Pickles could then be those formed slightly later in the collapse phase, where dissipation has slowed the collapse and the orbits begin to circularize. As there is a broad distribution of [Fe/H] at any epoch, albeit with a trend of $\langle$[Fe/H]$\rangle$ with time, these stars would be those on the low-metallicity tail of formation at a slightly later epoch. The picture is, of course, not changed if all halo stars were, in fact, formed in globular clusters which later evaporated. One needs only to substitute the word *clusters* for *stars* in the above paragraphs.

TABLE IX. Stars with nearly circular orbits ($e \leqslant 0.40$) and low metallicities ($\delta \geqslant 0.20$; i.e., [Fe/H] < -1.30).

Name (1)	R.A. (2)	Dec. (3)	$B-V$ (4)	$\delta(0.6)$ (5)	D(pc) (6)	e (7)	U (8)	V (9)	W (10)
				Stars from Table II					
G74-5	02 07.5	29 34	0.58	0.20	43	0.25	53	−61	−43
G102-20	05 37.3	12 09	0.65	0.21	69	0.26	23	−72	66
G43-26	10 02.7	12 15	0.53	0.22	333	0.16	25	−482	35
G57-19	11 45.3	15 10	0.86	0.44	90	0.31	110	−22	−47
G14-32	13 05.8	−07 02	0.94	0.28	16	0.09	−7	−32	70
G14-33	13 06.2	−03 42	0.66	0.21	106	0.40	126	−60	−90
G63-46	13 37.5	12 50	0.58	0.20	58	0.26	−66	−39	−56
G64-34	13 57.3	−05 08	1.01	(0.40)	75	0.28	66	−65	53
G21-25	18 45.6	−05 08	0.76	0.28	51	0.09	−19	−16	−70
L15637	19 12.7	10 29	0.52	0.20	70	0.34	38	−88	79
G23-7	19 33.2	01 37	0.96	0.40	22	0.29	44	−75	2
G23-14	19 49.3	05 29	0.74	0.30	60	0.26	−67	−41	4
G18-14	21 58.4	09 42	0.98	0.20	41	0.25	−55	−50	−72
G28-48	23 10.4	01 31	0.88	0.29	62	0.23	−62	−16	−35
G30-2	23 33.4	08 13	1.02	(0.38)	92	0.34	−21	−87	−104
G30-31	23 55.3	08 20	1.16	(0.36)	50	0.27	20	−73	−103
				Stars from Table III					
G30-52	00 09.9	14 17	0.81	0.25		0.08	33	−21	−21
−17°219	01 11.7	−16 42	0.72	0.42	51	0.14	34	−40	−81
CD −31 622	01 30.0	−30 56	0.63	0.28		0.22	−59	−12	169
−13°482	02 31.8	−12 36	0.45	0.22		0.30	11	−81	−61
HD 17288	02 42.8	−60 16	0.57	0.22		0.27	57	−66	49
55°1362[a]	10 01.4	54 35	0.70	0.32	34(525)	0.17	−41	−11	−16
−21°3420[b]	11 53.0	−22 06	0.52	0.20	100(263)	0.36	27	−95	−82
G62-52	13 33.5	01 28	0.67	0.22		0.33	−54	−75	−97
HD 120559	13 48.4	−57 11	0.66	0.23		0.36	69	−86	−77
HD 166913	18 12.1	−59 25	0.45	0.22		0.15	43	−40	65
−50°13953	23 18.9	−49 46	0.66	0.35		0.39	8	−102	−59

[a] Could be a globular cluster subgiant at 525 pc distance.
[b] Could be a subgiant at 263 pc distance.

butions as in Fig. 7.11 of Mihalas and Binney (1981). A similar conclusion can be reached from a h,δ diagram (not shown) similar to Fig. 6 of ELS but made from our present sample. When the h,δ data are divided into W intervals as in Fig. 21, the evidence is again for a continuous variation of h with δ for all values of $|W|$, not a box-like distribution as in Fig. 7.12 of Mihalas and Binney. Therefore, we cannot confirm the hypothesis that the presence of large numbers of low-velocity, low [Fe/H] stars which we have missed changes the conclusion (Figs. 17 and 21) that the kinematics and [Fe/H] are monotonically related for halo stars over the entire range of metallicities, if the halo is defined *spatially* as we have done via the V and $|W|$ cuts, rather than *chemically* as is done by Norris.

IX. THE SYSTEMATIC VARIATION OF U AND V WITH [Fe/H]

The point just made from the e,δ diagram can be verified in a different way from the V,δ diagram of Fig. 7 and from the U,δ diagram, the thick-disk stars being removed from each.

a) The Thick Disk Defined in the U, δ and U, W Diagrams

In a way similar to identifying the thick-disk component from the V,δ and V,W diagrams of Figs. 7 and 8 from the discontinuity in the distribution at $\delta(0.6) \sim 0.15$, we see the same phenomenon in the U,δ diagram set out in Fig. 22. The data are from Tables II and III for stars with $B-V \leqslant 0.8$. The U value is relative to the Sun, not corrected to the local standard of rest.

The distribution is wedge shaped but clearly has two components, again signaled by the discontinuity in numbers at $\delta \sim 0.15$. The identification of the thick disk in this way is confirmed in the U,W diagram of Fig. 23, where the sample is restricted to $|V| < 100$ km s^{-1}, based on the transition found in Fig. 8 between the top middle and top right-hand panels there. The $\sigma(U) = 75$ km s^{-1} and $\sigma(W) = 42$ km s^{-1} values shown in Fig. 23 are close to the values listed before for the thick disk. That we are dealing with a rather discrete kinematic entity is emphasized by the box-like distribution of the U,δ diagram for stars with $|V| < 100$ shown in Fig. 24. Most stars assigned to the thick disk in this way have $\delta < 0.16$, or [Fe/H] $\gtrsim -0.9$, seen also from Figs. 8, 10, and 11.

b) The V,δ Distribution for Halo Stars: Spin-Up

Figure 25 shows the V,δ distribution for stars in Tables II and III with $B-V \leqslant 0.8$ whose $|W|$ values are larger than 60 km s^{-1}. This is Fig. 7 with the thick-disk component (defined now by $|W| \leqslant 60$ km s^{-1}) removed. The statistics for this distribution of the halo sample, defined in this way, are those listed previously in the second part of Table VI.

The obvious feature of Fig. 25, and the one central to the ELS picture of galaxy collapse with continuous dissipation in the halo, is the *monotonic variation of V with δ*. The statistics of this variation are repeated in Table X. Column 4 is the Strömberg mean drift velocity reduced to the local standard of rest (LSR) by adding 15 km s^{-1} to column 6 of Table VI. (The first entry in Table X is the assumed mean metallicity of the *young* disk with assumed zero lag.) Column 5 is column 4 subtracted from an assumed rotation velocity of the LSR of 220 km s^{-1}. The quoted errors in columns 4 and 5 are $\sigma\langle V - |V|\rangle/\sqrt{n-1}$ as taken from columns 3 and 7 of

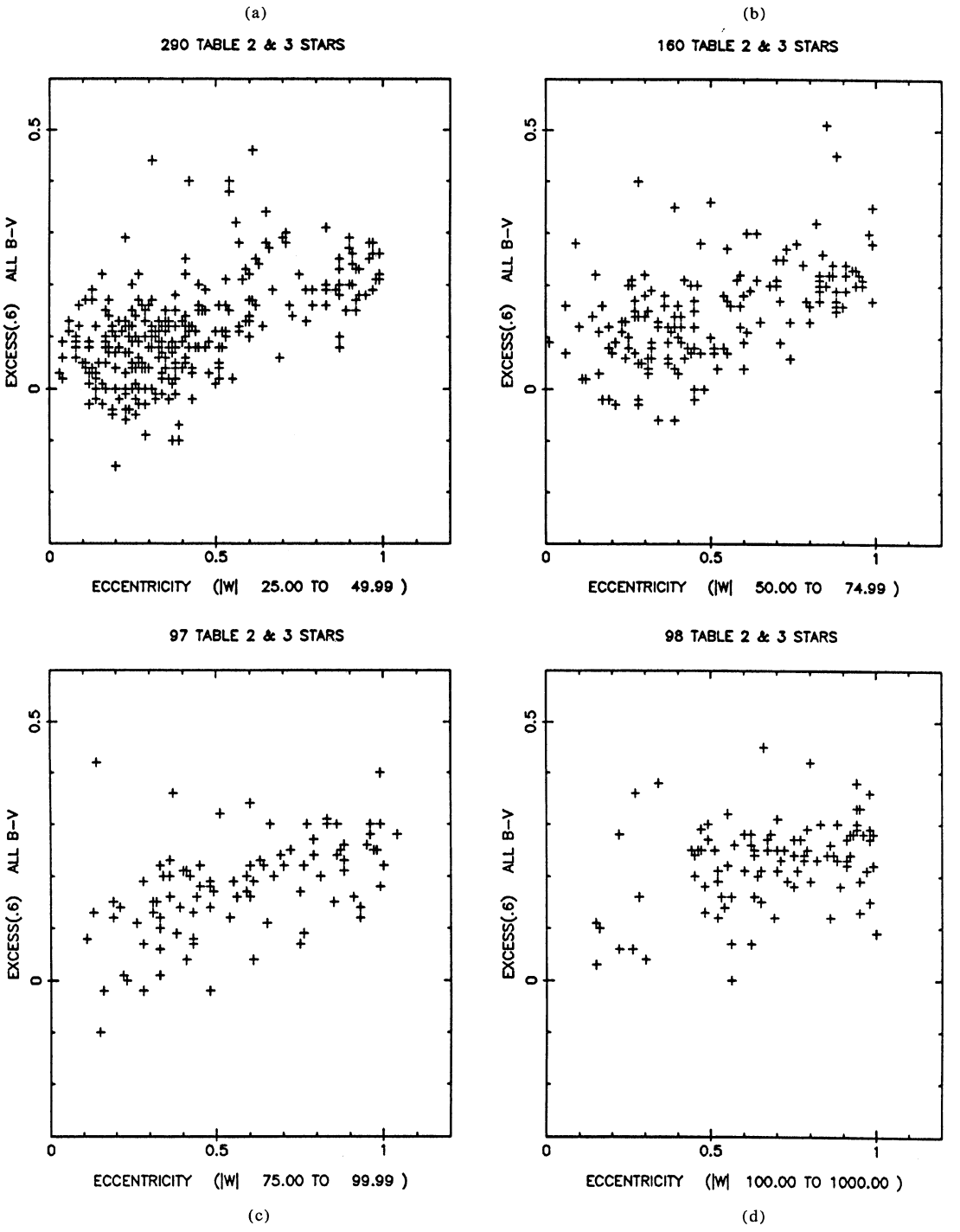

FIG. 21. e,δ distribution broken into four intervals of W to see the effect of removal of the thick-disk component. The data are from Tables II and III.

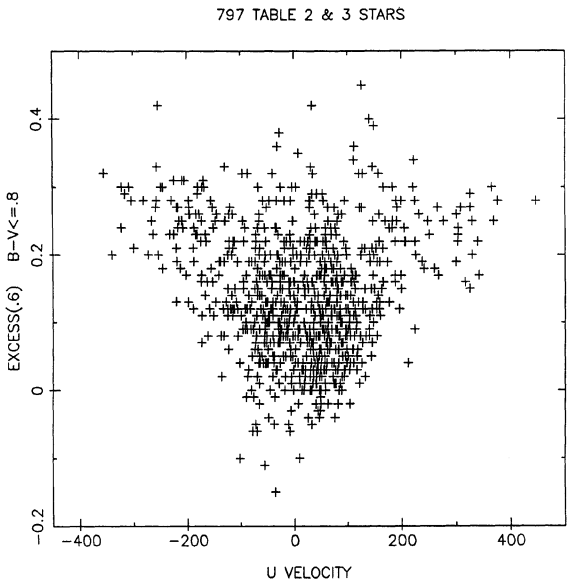

FIG. 22. U,δ for the complete sample from Tables II and III for $B-V\leqslant 0.8$.

Table VI. The $\sigma(U)$ values in column 6, to be used in the next section, are from column 5 of the second half of Table VI.

The data in columns 1, 2, and 5 of Table X are plotted in Fig. 26, showing the monotonic decline of the rotational velocity for halo stars in our sample as $\langle$[Fe/H]$\rangle$ changes from ~ 0 to ~ -2.6.

c) Is the Contradiction with the Data of Norris Concerning Rotation of the Halo Due to Bias in Our Kinematically Selected Sample?

Two arguments show that it is not. (1) The first is the one used before in Sec. VIII*b* concerning the reality of the lack of stars in the upper left-hand quadrant of the e,δ diagrams of Figs. 20 and 21. Our sample in Fig. 25 *contains only high W velocity stars*, which, as explained before, we are not totally biased against. There are, indeed, six stars in Fig. 25 with $V> -100$ and $\delta > 0.22$, but their number is insufficient to counter the very large trend toward highly negative V values in this diagram as δ progressively becomes larger than 0.22. The lower envelope, sloping upward to the right in Fig. 25, is beyond doubt real, because our sample is surely *not* biased against the high-velocity stars but, on the contrary, favors them. For the claims of Norris and of Searle to be correct requires that so many low V, high δ halo stars exist in the upper left of Fig. 25 so as to keep $\langle V\rangle$ constant with δ. That $V_{\rm rot}$ actually does vary with δ for $\delta \lesssim 0.22$ or [Fe/H] as low as -1.6 is proved by a second, more powerful argument.

(2) Suppose, indeed, that the Strömberg asymmetric-drift velocity is *not* related to $\langle$[Fe/H]$\rangle$ for stars more metal poor than [Fe/H] $= -1.0$. If $\langle V\rangle$ were, in fact, constant for $\delta \geqslant 0.16$, then $\sigma(U)$ *must not vary* with δ in this same [Fe/H] interval. As mentioned in Sec. IV*b*, this is because of the empirical result of Strömberg (1924), which is the theoretical Newtonian requirement for dynamical stability, that the smaller the rotational velocity, the smaller is the centrifugal acceleration and the larger must be the U velocity for dynamical equilibrium. Consequently, all that is required to show that the variation of $\langle V\rangle_{\rm rot}$ with $\langle$[Fe/H]$\rangle$ shown in Fig. 26 is not caused by our kinematically selected sample (which, after all, is not biased on the high-velocity end) is to show that $\sigma(U)$ is also a monotonically increasing function of decreasing [Fe/H]. The proof of dynamical stability is that the Strömberg lag velocity V(lag) in column 4 of Table X should vary with the dispersion $\sigma(U)$ according to Jeans' equation. The data to test this variation from our sample are set out in Figs. 27–29.

The U,δ data for halo stars, defined by the $|V|>100$ km s^{-1} criteria (accepting all W values), are shown in Fig. 27. This is the same as Fig. 22 with the thick-disk component of Fig. 24 removed. The progressive increase of $\sigma(U)$ with δ is evident by the wedge-shaped distribution. Again, the cor-

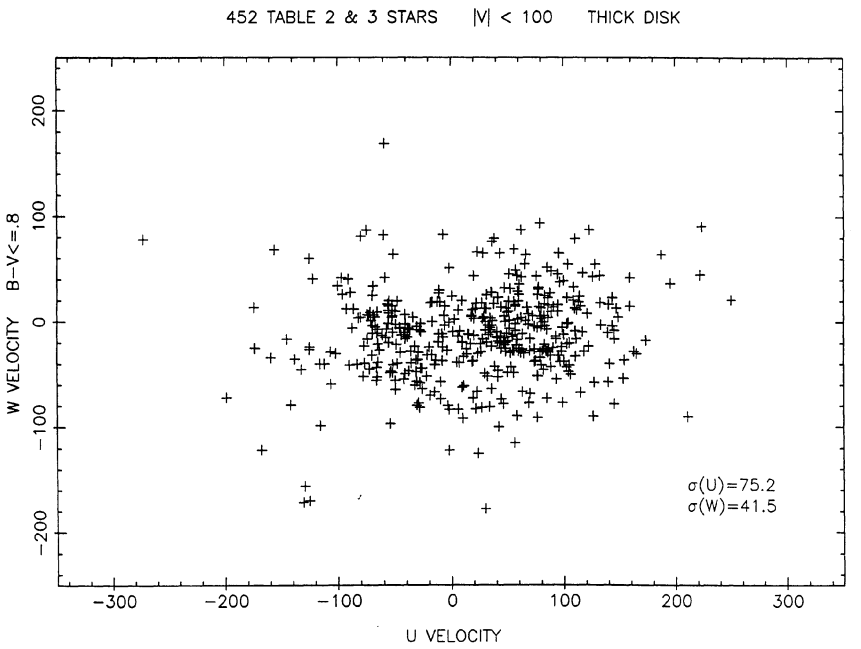

FIG. 23. U,W diagram for stars in Fig. 22 for the thick-disk component defined by $|V|<100$ km s^{-1}.

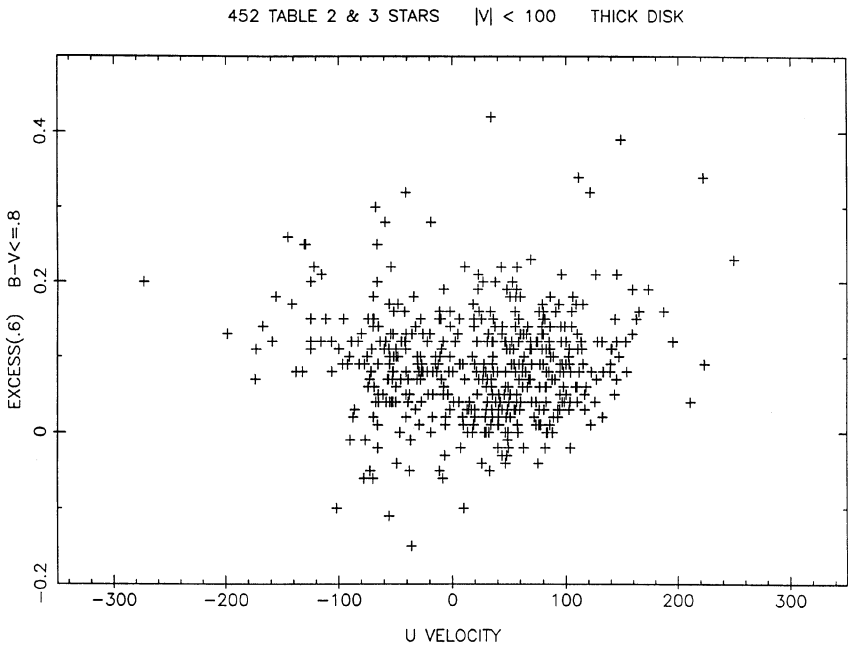

FIG. 24. U,δ diagram for the same stars in Fig. 23.

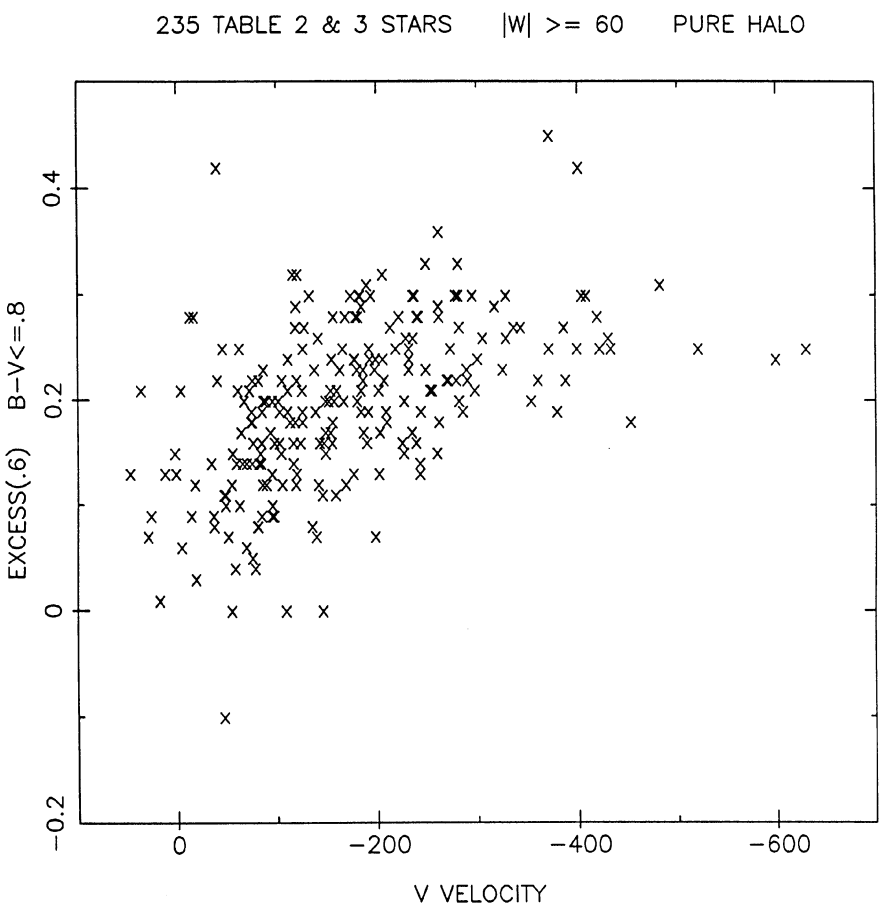

FIG. 25. The V,δ diagram of Fig. 7 with the thick-disk stars removed. The sample contains stars from Tables II and III with $|W| \geqslant 60$ km s^{-1} and $B - V \leqslant 0.8$.

TABLE X. Mean V(lag) and V rotational velocities for halo stars defined by $|W| \geq 60$ km s^{-1}.

<δ>	[Fe/H]	n	LSR V(lag)	LSR V(rotation)	σ(U)
			km s^{-1}		
(1)	(2)	(3)	(4)	(5)	(6)
0	+0.2	Large	0±0	220±0	35
0.045	-0.03	25	-52±11	168±11	76.0
0.11	-0.48	16	-74±12	146±12	73.6
0.14	-0.73	25	-87±17	133±17	125.0
0.18	-1.10	55	-150±11	70±11	130.0
0.225	-1.55	47	-178±16	42±16	153.1
0.29	-2.34	62	-236±15	-16±15	200.3
		Thick Disk			
0.08	-0.25	-200	-30	190	65

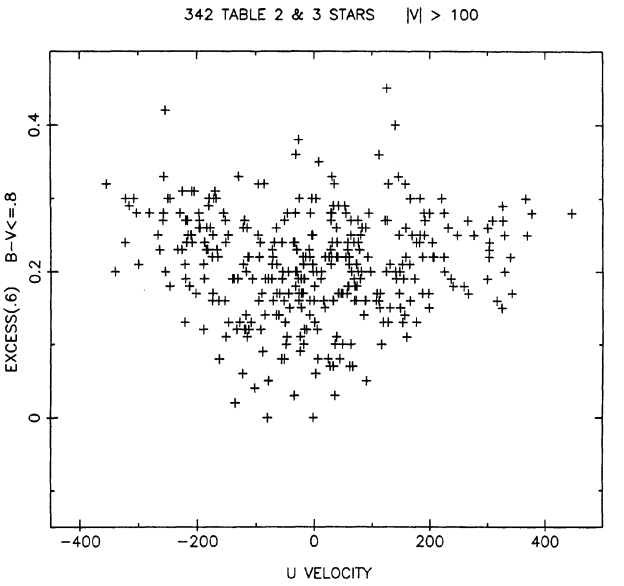

FIG. 27. U,δ diagram for halo stars from Tables II and III with $B - V \leqslant 0.8$ that have $|V| > 100$ km s^{-1} with no restriction on the W values.

relation cannot be destroyed by the kinematic bias of our sample because we miss only stars with small U values. Adding any number of low U velocity stars will not change the distribution of high $|U|$ values evident in Fig. 27. The high-velocity region for which our sample is not biased shows upward-sloping boundary lines of increasing $|U|_{max}$ as δ increases.

The same conclusion follows from Fig. 28, which defines the halo differently by the criterion of $|W| \geqslant 80$ km s^{-1}, including all V values. The same wedge-shaped distribution occurs, giving an increase of $\sigma(U)$ with increasing δ. Again, this cannot be destroyed by adding any number of a postulated large population of low-velocity, metal-poor stars to the sample.

Figure 29 shows the relation between the Strömberg lag velocity from column 4 of Table X and the square of the dispersion in U, calculated from column 6. The two light circles are data from low-velocity stars as discussed by Mihalas and Binney (1981, Fig. 6.7).

The theoretical expectation from the Jeans equation is that V_{lag} should vary nearly as $\sigma^2(U)$ for small values of the lag velocity, but should increase with no increase in $\sigma(U)$ for large values of the lag. The basic Jeans equation is discussed, for example, by Freeman (1975, Eq. (36)), which, for small

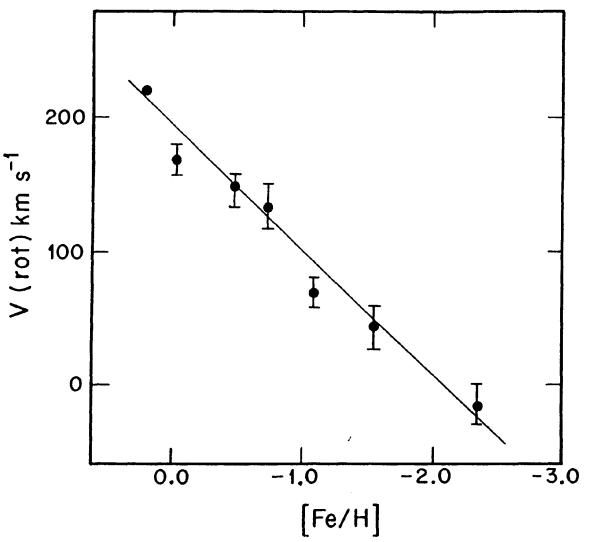

FIG. 26. Variation of V_{rot} with [Fe/H] from the data in Table X.

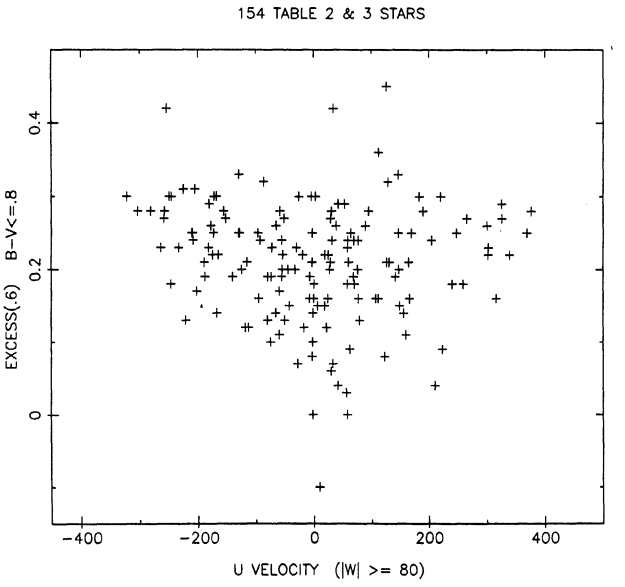

FIG. 28. Same as Fig. 27 but for the different sample of halo stars defined by $|W| \geqslant 80$ km s^{-1} with no restriction on V.

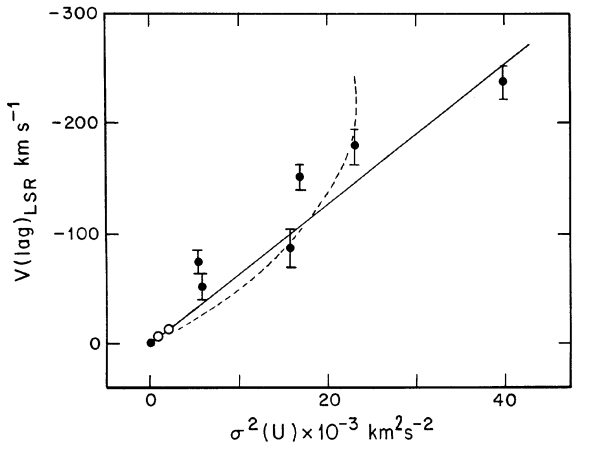

FIG. 29. Lag velocity in V as a function of $\sigma^2(U)$ for the halo stars in Figs. 25–28. The light circles are data from the solar neighborhood summarized in Fig. 7 of Mihalas and Binney (1981). The dashed line is the theoretical expectation from Eq. (3). The solid line is the linear relation in $\sigma^2(U)$ put through the data by eye.

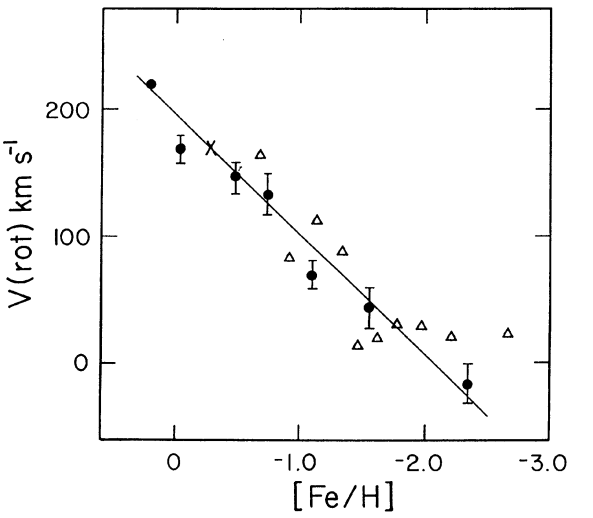

FIG. 30. Same as Fig. 26 but with the data of Norris added as triangles. Except for the last point of lowest metallicity at [Fe/H] ~ -2.6, the agreement between the two data sets is good.

$V_{\rm lag}$, reduces to Freeman's Eq. (38). For large $V_{\rm lag}$, Oort's (1965) Eq. (37) becomes

$$V_{\rm drift} = \frac{C\sigma^2(U)}{2V_c - V_{\rm drift}}, \qquad (3)$$

where C is a constant, $V_{\rm drift} = -V_{\rm lag}$ (using the sign convention in Fig. 29), and V_c is the circular velocity of the local standard of rest.

Equation (3) for small $V_{\rm drift}$ (relative to V_c) is approximately quadratic in $\sigma^2(U)$. For large values of $V_{\rm drift}$, Eq. (3) has a vertical asymptote such that $\sigma(U)$ does not continue to increase with increasing $V_{\rm drift}$. The dashed curve in Fig. 29 is Eq. (3) fit to all data points but the last, by eye. The agreement is satisfactory except for the last point at $\sigma(U) = 200$ km s^{-1} rather than 150 km s^{-1} expected from Eq. (3) with $C = 2.1$ obtained from the lower-velocity points. The increase in $\sigma(U)$ for this last data point is not expected from the Jeans theory. The good fit of Eq. (3) for the [Fe/H] > -1.6 data points could be taken to support Fig. 26, being correct for this metallicity range. But then we must explain the unexpectedly large $\sigma(U)$ for the last point.

A distance error for stars with [Fe/H] smaller than ~ -1.7 (our last bin in Figs. 26 and 29) could explain the anomaly if our distances in Tables II and III were too large for these stars. However, this would conflict with the theoretical models (VandenBerg and Bell 1985, Fig. 4) and with the direct test (Eggen and Sandage 1962). A test using radial velocities alone, independent of distances (Hartwick 1987), could be decisive. (We are indebted to Freeman, to Gilmore, and to Norris for discussions on the points raised in this section.)

The conclusion from these two arguments is that the monotonic change in $V_{\rm rot}$ with [Fe/H] shown in Fig. 25 is real at least for [Fe/H] $\gtrsim -1.6$ if our distance scale is not in error. Evidently, the halo has progressively spun up as it progressively collapsed as a unit, enriching itself as it fell.

The difference with Norris is, in fact, not so great in the basic data. Figure 30 shows the $V_{\rm rot}$, [Fe/H] plot of Fig. 26, but with the Norris data added as triangles. The cross is our value for the thick disk from Table X. The agreement is excellent (everywhere within 0.3 dex from the mean curves), except for the last data point of lowest metallicity by Norris. As repeatedly mentioned above, we are *not* kinematically biased in this region of high motion relative to the Sun. However, they *are* sensitive to distance errors as a function of [Fe/H] in our own data. If the correct calibration of ΔM_v below the fiducial ZAMS as a function of [Fe/H] differs from what we used in Papers IV and V, i.e., if there is a smaller saturation of the ΔM_v depression for [Fe/H] $\lesssim -1.7$ than we have assumed and which agrees with the theoretical expectation for [Fe/H] $\lesssim -1.7$ (VandenBerg and Bell 1985, Fig. 4), our distances to stars of the lowest [Fe/H] may be too great, giving an incorrectly large space motion. This problem of calibration cannot be solved until trigonometric parallaxes of subdwarfs are available or, as previously mentioned, until our data can be analyzed in terms of radial velocity alone. Judgment on the difference between our results and those of Norris should be suspended until this radial-velocity analysis (Hartwick 1987) is complete. In any case, what is clear is that the difference is not due to our sample being kinematically selected.

X. INTERESTING STARS SELECTED FROM THE KINEMATIC DISTRIBUTIONS

The important subsample of possible low-velocity stars relative to the Sun that have low metallicities has been discussed in Sec. VIII and is set out in Table IX. Because many of the stars are likely to be subgiants and therefore would be more distant than we have assigned them by our main-sequence assumption, stars in this table may not have their low listed velocities. They would not then necessarily present a problem for the ELS picture. Special observations are required to measure their absolute magnitudes.

We can, however, isolate two other classes of stars, one of which presents an unanswered problem, and the other which was expected to exist by ELS but was not found, perhaps because the ELS sample was so small.

TABLE XI. Stars with elongated orbits ($e \geqslant 0.59$) and high metallicity ($\delta_{0.6} \leqslant 0.09$).

Name (1)	R.A. (2)	Dec. (3)	$B-V$ (4)	$\delta(0.6)$ (5)	D(pc) (6)	e (7)	U (8)	V (9)	W (10)
				Stars from Table II					
G70-31	01 00.9	04 48	0.74	0.02	169	0.68	−136	−155	−15
G3-22	01 47.2	05 32	0.91	0.04	155	0.81	−126	−203	−13
G272-125	01 54.2	−14 25	0.38	0.09	168	0.76	223	27	91
G37-34	03 16.5	33 25	0.85	0.07	44	0.69	−51	−178	−5
G79-63	03 41.3	09 47	0.83	0.07	111	0.83	143	−212	8
G80-31	03 50.4	00 51	0.72	0.09	102	0.60	−89	−145	−58
G6-41	03 53.9	24 30	0.79	0.06	129	0.69	2	−181	50
G38-25	04 02.9	32 49	0.97	0.06	42	0.74	166	−175	−54
G7-31	04 13.3	07 46	0.76	0.09	123	0.71	−25	−187	−54
G101-25	06 09.6	38 55	0.82	−0.09	115	0.62	−36	−160	−2
G90-32	07 53.6	30 32	0.70	0.08	216	0.87	−163	−219	−46
G51-20	08 34.5	31 43	0.76	0.07	148	0.75	33	−197	−94
G41-5	08 50.6	09 36	0.77	0.04	113	0.61	211	−58	−90
G49 38	10 07.7	21 56	0.81	0.04	120	0.63	119	−150	21
G12-20	12 08.5	12 25	0.81	0.09	143	0.69	240	−75	23
G65-29	14 08.4	07 07	0.92	0.04	122	0.60	45	−156	−52
G66-18	14 35.7	−00 37	0.86	0.09	207	1.00	408	−354	187
G16-34	16 09.7	05 37	0.94	0.08	101	0.77	−103	−335	−12
G19-11	17 02.0	03 48	0.96	−0.07	94	0.59	69	−151	17
G19-26	17 23.7	03 32	0.97	0.07	138	0.84	38	−307	1
G128-36	23 06.4	26 44	0.90	0.07	115	0.62	−73	−154	−109
G68-29	23 32.5	25 07	0.81	0.08	82	0.68	35	−180	−22
				Star from Table III					
LTT 15972	20 22.8	41 20	0.60	0.03		0.66	−35	−172	6

a) A Problem Distribution: Stars with Plunging Orbits ($e \geqslant 0.59$) with High Metallicity ($\delta_{0.6} \leqslant 0.09$)

Such stars are most easily identified by inspecting the sloping lower boundary of the e,δ diagram of Fig. 20. Data for the 23 most extreme cases are listed in Table XI, taken as a subset from Tables II and III using the stated e and δ parameters. The eccentricities, of course, are high because of the large U and/or V values. These stars are either an unexplained part of the ELS picture or the metallicities inferred from the $\delta(0.6)$ values are incorrect, due either to incorrect photometry in the basic catalog (SK) or because of spectral peculiarities which would make $\delta(0.6)$ a poor indicator of [Fe/H] in these cases. Note that most of the stars in Table XI are redder than $B-V=0.8$, making $\delta(0.6)$ a less precise indicator of [Fe/H] than for bluer stars.

b) Stars that Lead the LSR by $(V+15) > 50$ km s^{-1}

The escape velocity from the Galaxy at the solar circle is at least $\sqrt{2}V_{\rm rot}$. This would be the exact value if the edge of the mass distribution of the Galaxy stopped at the solar circle. If $V_{\rm rot} = 220$ km s^{-1}, the minimum escape velocity would then be 310 km s^{-1}. All indications are that it is larger than this, some estimates being as large as 650 km s^{-1} (Caldwell and Ostriker 1981). Because $V_{\rm rot}$ can hardly be put larger than 250 km s^{-1}, giving a *minimum* escape velocity of 350 km s^{-1}, the evidence then requires that the mass distribution continue beyond the solar circle—no great surprise.

However, there should be stars from this outer region with high angular momenta which would lead the LSR by V velocities that approach the value V (escape) − V(rotation). Hence, even if V(escape) was as low as 310 km s^{-1} for $V_{\rm rot} = 220$ km s^{-1}, there should be stars which lead the LSR by at least ~90 km s^{-1}. No such stars are known. Their absence has always presented a major problem.

There are only six stars from Table II and two from Table III which have V velocities (relative to the Sun) greater than +35 km s^{-1}, which means V relative to the LSR greater than 50 km s^{-1}. They are listed in Table XII, where the entries are self-explanatory. The "eccentricity" is in column 9, the angular momentum h in column 10, and the apogalacticum distance $R_{\rm max}$ is in column 11. As in Tables II and III, these are calculated following ELS, using $R_\odot = 10$ kpc and $V_{\rm rot} = 250$ km s^{-1}.

TABLE XII. Stars with $V > 35$, leading the LSR by $V' \geqslant 50$ km s^{-1}.

Name	RA	Dec	B-V	δ(0.6)	U	V	W	e	h	R_{max}
(1)	(2)	(3)	(4)	(5)	(6)	(7)	(8)	(9)	(10)	(11)
				From Table II						
G33-31	00 58.7	14 58	0.87	0.38	237	63	-171	0.94	32.8	239
G97-43	05 26.1	04 45	0.74	0.01	78	36	32	0.37	30.1	20
-5° 1355	05 37.5	-05 04	0.64	0.09	59	36	29	0.33	30.1	19
G87-3	06 42.8	32 36	0.95	0.04	-20	39	-59	0.31	30.4	19
G14-23	12 58.8	-09 11	0.54	0.13	79	48	94	0.43	31.3	23
G26-20	21 35.5	-11 07	0.60	0.13	59	36	-28	0.33	30.1	19
				From Table III						
GC 4690	03 51.0	52 17	0.68	0.12	145	61	-8	0.65	32.6	41
-14° 3322	11 23.6	-15 26	0.58	0.21	96	37	65	0.42	30.2	22

The most extreme case is G33-31, with $e = 0.94$, $h = 33$, and $R_{max} = 240$ kpc. The V_{LSR} of G33-31 is $63 + 15 = 78$ km s^{-1}, which is the largest in our sample, but is still far below what is expected.

The inferred [Fe/H] value for G33-31 is very low at ~ -4 from $\delta(0.6) = 0.38$ but, except for $-14°3322$ in the second part of Table III with $\delta(0.6) = 0.21$, the δ values for the remaining six stars are smaller than 0.14. Hence, although we do have a few stars not seen in the ELS data that lead the Sun by more than ~ 35 km s^{-1}, the V(max) limit is still far too small to be at the escape velocity in the $+V$ direction. (Note the small values of e for all stars in Table XII except G33-31.)

The sample, of course, has a built-in bias against many such stars for the three reasons explained in Paper III (Sandage 1969). What we are looking for here are stars with very large values of h and e. These necessarily have large values of R_{max}. Their rarity is seen most clearly in the h, e diagram of Fig. 31. This is the same type of diagram as in Fig. 8 of ELS, except that retrograde orbits are shown explicitly by plotting h rather than $|h|$.

The sharp boundary lines, sloping between $|h| = 25, e = 0$ and $h = 0$, $e = 1$ for both positive and negative h are the locus of $R_{max} = 10$ kpc. The void space inside these boundary lines is the domain of stars whose apogalactic distance R_{max} is less than $R_\odot$. Such stars can never reach the solar neighborhood and are therefore not in the sample.

Stars with $e > 1$ are unbound in the adopted ELS model galaxy. Only one star in the 1125 star sample exceeds the *model* escape velocity with $e = 1.04$. The star is G18-40, which has the nominal listed values of $U = 446$, $V = -167$, and $W = -76$ in Table II. Its UV excess is $\delta(0.6) = 0.28$. Note, however, the large sensitivity of U to the distance given by the listed $dU/dr = 1.6$ km s^{-1} pc^{-1} in Table II; the U value is uncertain for this star because of this sensitivity to the distance.

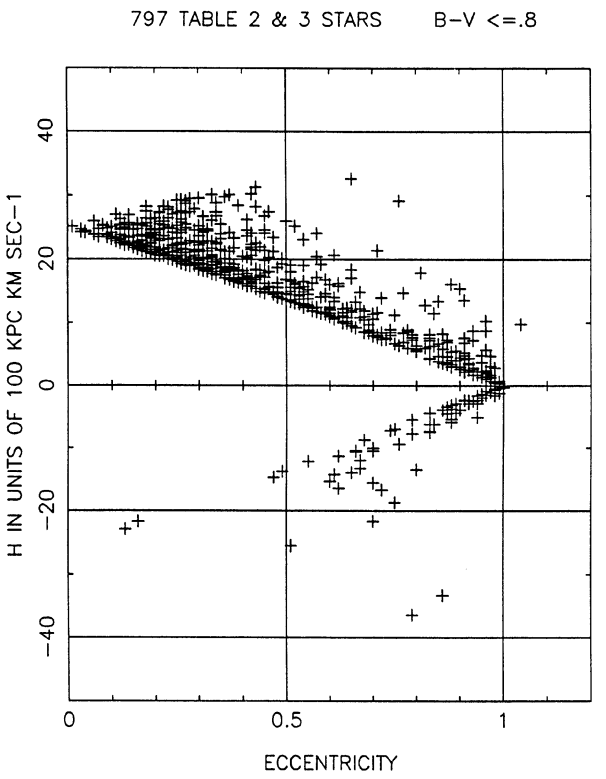

FIG. 31. Angular momentum, e distribution for the total sample with $B - V \leqslant 0.8$.

The stars that lead the Sun should crowd the $e = 1$ line in the domain of large positive h values. Virtually no stars exist in this region. The one isolated star there is, in fact, G33-31, discussed above but not shown in Fig. 31 because $B - V \geqslant 0.8$ for this star. The other star of note at $e = 0.76$ and $h = 29.2$ is G272-125 with $U = 223$, $V = 27$, $W = 91$ (relative to the Sun), and $\delta(0.6) = 0.09$.

The next largest e value for $h > 30$ is for GC 4690 listed in the second part of Table XII with $e = 0.65$, $h = 32.6$, $R_{max} = 41$ kpc, $\delta(0.6) = 0.12$, and with $U,V,W = (145, 61, -8)$. These three stars are the three most extreme isolated points in the Bottlinger diagram of Fig. 3 for $V > 35$ and $U > 100$. Figure 3 and Fig. 31 are, of course, equivalent, being merely different representations of the same phenomena.

The main point to be noted in Fig. 31 is the general lack of stars with $e > 0.5$ and $h \geqslant 25$. This limits R_{max} to being less than ~ 40 kpc (with very few exceptions in Tables II and III), pointing to a possible explanation for the lack of high $+V$ stars: they simply do not exist with the necessarily high e value in the Galaxy, never having been formed in numbers beyond this radius. *The edge of the stellar distribution in the Galaxy may occur at this* radius. We return to this point in the next section.

The metallicity distribution with Fig. 31 is of interest because of the variation of $\delta(0.6)$ over the Bottlinger diagram, which has been the main theme of this paper. The subsample of Tables II and III for all $B - V$ values for stars with $\delta(0.6) \geqslant 0.21$ is shown in Fig. 32. The strong concentration for $e > 0.50$ and the very thin distribution for $h > 20$, $e < 0.5$ is evident, consistent with the e,δ distributions of Figs. 20 and 21.

XI. THE ESCAPE VELOCITY

The mass of the Galaxy inside the solar circle is $M(R_\odot) = R_\odot V_{rot}^2/G$, but mass must exist outside because the rotation curve is flat to at least twice $R_\odot$. If the escape velocity at the Sun could be determined, we would have a direct measurement of the total mass of the Galaxy. Assuming a potential $\phi(R) \propto \ln(R)$ which gives a flat rotation curve and assuming spherical symmetry gives the well-known relation

$$V_{E,R_\odot}^2 = 2V_{rot,R_\odot}^2 \left[1 + \ln M_T/M_{R_\odot}\right], \quad (4)$$

where $V_{E,R_\odot}$ is the escape velocity at the solar circle, $V_{rot,R_\odot}$ is the circular rotation velocity also at the solar circle, M_T is the total mass, and $M_{R_\odot}$ is the mass inside the solar circle.

One of the reasons the present data were obtained was to "measure" $V_{E,R_\odot}$ so as to find M_T for the Galaxy. We do not discuss this problem here in the way it must be discussed later, star-by-star so as to eliminate distance errors, and thereby put the zero-energy surface properly through the data. We propose to do this eventually with our own data in combination with data from the other surveys now in progress (Carney and Latham 1985; Yoss 1986) but are satisfied here only to show the present data as they stand.

If all the distances, proper motions, and radial velocities in Tables II and III were precise and if we have sampled *all* of the relevant phase space using only the stars passing through

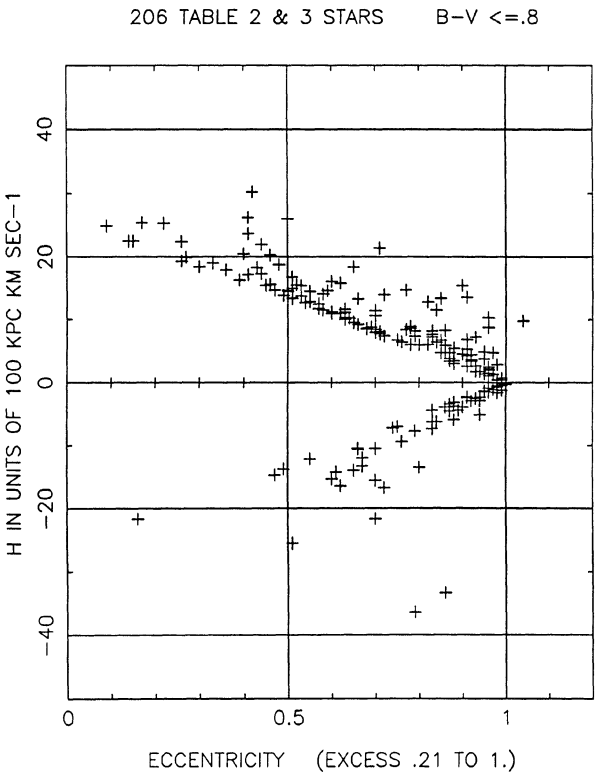

FIG. 32. Same as Fig. 31 but for metal-poor stars with $\delta(0.6) \geqslant 0.21$ in the total sample with $B-V \leqslant 0.8$.

the solar neighborhood, the escape velocity could be found from the envelope that encompasses all the points in Fig. 33. The V velocity (relative to the Sun) is plotted versus $(U^2+W^2)^{1/2}$ (neglecting the small correction to the LSR). The loci of constant kinetic energy in this diagram are circles centered on the V axis at $V^{\rm LSR}_{{\rm rot},R_\odot}$. This is because the square of the radii of such circles is $[(V^{\rm LSR}-V_{\rm rot})^2+U^2+W^2]^{1/2}$, which is twice the kinetic energy of any individual star at the solar circle referred to the inertial frame of the Galactic center. The representation in Fig. 33 is due to Toomre (1980).

The maximum radius that encloses all the points represents the highest kinetic energy of stars in the sample. However, our data are not complete in the stated sense because part of the total phase space is denied us by the selection bias. It is necessary to discuss which of the crucial stars never reach the solar neighborhood and therefore would not be in a sample no matter how large the sample may be. Hence, it is not clear if $V_{E,R_\odot}$ can ever be found in this way but, for illustration, we show two circles in Fig. 33 centered at $V_{\rm rot}=220$ km s^{-1}, which is $V+15=-235$ in the diagram as drawn. One circle has a radius of 400 km s^{-1} and the other has 450 km s^{-1}.

Almost all of our data are confined within the 450 km s^{-1} circle. It should be recalled that our distances are based on the main-sequence assumption for the absolute magnitudes, hence our velocity values are generally lower limits. We therefore derive in this way a *lower limit* to the escape velocity at the Sun of $\sim$450 km s^{-1}, the same as estimated in Papers IV (SK) and V (FS). This is higher than the value derived by Isobe (1974a,b) using Fricke's (1949a,b) method, but is lower than the preliminary value of 550 km s^{-1} by Carney and Latham (1985). If $V_{{\rm rot},R_\odot}=220$ km s^{-1}, Eq. (1) gives $M_{\rm T}/M_{R_\odot}=3$ using $V_{E,R_\odot}=450$ km s^{-1}. If $V_{E,R_\odot}=550$ km s^{-1}, then $M_{\rm T}/M_{R_\odot}=8$.

If $V_{{\rm rot},R_\odot}=220$ km s^{-1} and $R_\odot=8$ kpc, then the mass inside $R_\odot$ is $8.7\times10^{10}\,M_\odot$. If, then, $V_{E,R_\odot}=450$ km s^{-1} as our data suggest, $M_{\rm T}=2.6\times10^{11}\,M_\odot$. On the other hand, if $V_{E,R_\odot}$ is, in fact, as high as 550 km s^{-1}, then $M_{\rm T}=7\times10^{11}\,M_\odot$ which, when added to twice this value for M31, would give $M_{\rm T}$ (M31 + Galaxy) $=2\times10^{12}\,M_\odot$. This is close to

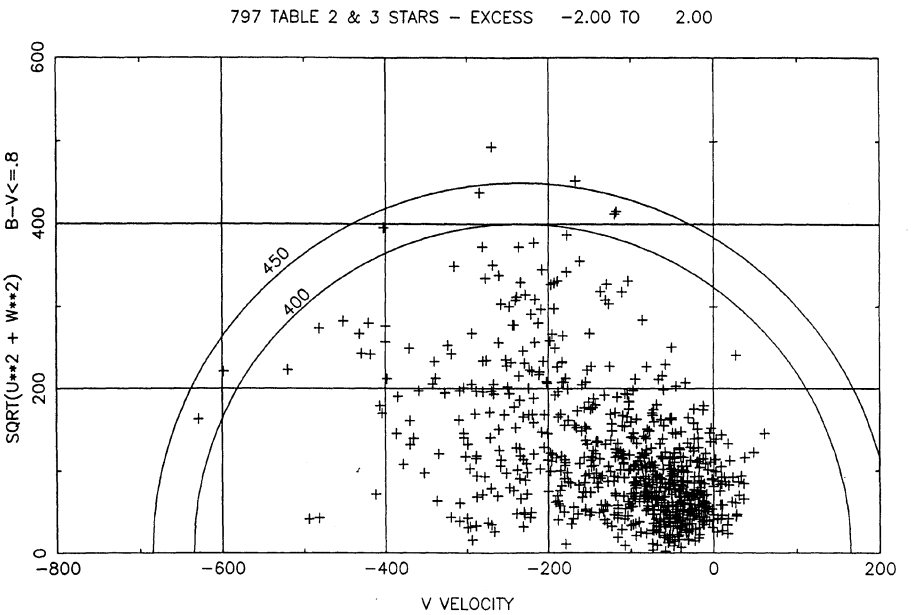

FIG. 33. $V,(U^2+W^2)^{1/2}$ Toomre energy diagram for the 797 stars in Tables II and III with $B-V \leqslant 0.8$ (all δ values included). The V velocity is heliocentric, not reduced to the LSR. The two circles of radii 400 and 450 km s^{-1} are centered at $V=-220-15=-235$ km s^{-1}, which is assumed to be the heliocentric velocity of rotation.

the value obtained from the Kahn-Woltjer (1959) timing test and is at the upper limit obtained from the deceleration test of the Hubble expansion by the Local Group (Sandage 1986), suggesting that 550 km s^{-1} is possible but perhaps somewhat high. The extreme escape velocity of 650 km s^{-1} suggested by Caldwell and Ostriker (1981) requires $M_T/M_{R_\odot} = 29$ or M_T (Galaxy) $= 2.5\times10^{12}\ M_\odot$ which, when added to the nominal M31 mass (as double the Galaxy), gives M_T (Local Group) $= 7.5\times10^{12}\ M_\odot$, which is well beyond the limit set by the deceleration and the Kahn-Woltjer tests. From this argument we consider 650 km s^{-1} to be impossibly high.

XII. SUMMARY AND DISCUSSION

The principal conclusions are:

(1) The distribution of data points in the Bottlinger diagrams of Figs. 3, 4(a), 4(b), 5, 6(a), and 6(b), and the V,δ diagram of Fig. 7, the V,W diagram of Fig. 8, the W,δ diagram of Fig. 15, the e,δ diagram of Fig. 20, and the U,δ diagram of Fig. 22 show the presence of two kinematic components. Figures 8 and 23 show that the large concentration of points centered at $\langle V\rangle = \simeq -40 (U) \simeq +20$ shown in Figs. 3 and 5 has the small mean W dispersion of $\sigma(W) \sim 42$ (Table V) corresponding to a scale height of ~ 1 kpc. We identify this to be part of the Gilmore-Reid-Wyse thick disk in our sample. Our values for its kinematic properties are $\sigma_U = 75$ km s^{-1}, $\sigma_V = 35$ km s^{-1}, $\sigma_W = 42$ km s^{-1}, $\langle V\rangle = -42$ relative to the Sun. The metallicity distribution in Figs. 10 and 11 is intermediate between that of the halo and of the thin disk in the solar neighborhood.

(2) There is a metallicity gradient with height in the thick disk shown in Fig. 16 by the wedge-shaped W,δ distribution. The distribution of [Fe/H] in the upper thick disk, defined by stars that are now close to the Galactic plane in the solar neighborhood that have $40 \leqslant |W| \leqslant 79$ km s^{-1}, is shown in Figs. 10 and 11. It spans the metallicity range $0.2 \gtrsim$ [Fe/H] > -2 with a mean near [Fe/H] ~ -0.5.

(3) The second kinematic component is the extreme halo. Figures 4(c), 4(d), 6(c), 6(d), 8(c), 8(d), and 8(e) show a monotonic variation of both $\sigma(W)$ and the Strömberg asymmetric-drift velocity $\langle V\rangle$ with [Fe/H] for halo stars, defined either by $|V| > 100$ km s^{-1} or by $|W| \geqslant 60$ km s^{-1}. The distribution of [Fe/H] for such stars, defined separately by $|W| \geqslant 80$ km s^{-1} and by $e \geqslant 0.59$, is shown in Fig. 10 to be similar to that of halo globular clusters, centered near [Fe/H] ~ -1.7 but spanning the entire metallicity range from $+0.2$ to -4 (Fig. 12).

(4) This large range in [Fe/H] is not present, however, at every height, but decreases markedly with increasing $|W|$. Figure 17 shows the W,δ diagram for halo stars alone, the thick-disk stars having been removed from Fig. 15. The wedge-shaped distribution, similar to Fig. 5 of ELS (however, now containing only halo stars) suggests again that low-metallicity stars can form at any height but, as the metallicity increases, $|W|$ decreases. As in ELS, this is interpreted to mean that because [Fe/H] increases with time, stars formed later will have higher [Fe/H] values on the average. Since from Fig. 17 they are observed to have smaller $|W|_{max}$ values, *collapse* of the parent-gas distribution is evident. However, to prevent such stars from rising to the large starting height of the outermost region of the original gas cloud, there must be dissipation even at these early epochs within the halo gas at heights corresponding to $\sim |W| = 300$ km s^{-1} (Fig. 17) corresponding to ~ 30 kpc (cf. Fig. 4 of Saio and Yoshii 1979 or Fig. 3 of Paper III).

(5) The distribution in the W,δ diagram of Fig. 17 is not affected by observational bias in our kinematically selected sample because the empty regions of $|W| \geqslant 100$ km s^{-1} for $\delta < 0.1$ are just those high-velocity parts of the diagram which our sample is best suited to study. Hence, the $\langle\delta\rangle = f(W)$ correlation in Fig. 17 is not a result of selection in our sample and suggests that, *in situ* at any height sampled by the W values present in our data (Z to 20 kpc), the mean value of [Fe/H] is expected to decrease, as also should its range, albeit the distribution is still broad.

(6) The increasing $\sigma(W)$ values for increasing $\delta(0.6)$ shown in Table VI and Fig. 19 for the halo show that the scale height of what appears to be a continuum halo kinematic distribution changes from ~ 1 kpc in the metallicity range of $0 < \delta < 0.12$ to 5 kpc in the range $0.25 \leqslant \delta \leqslant 0.33$, again suggesting that a chemical gradient should be seen in the halo to heights perhaps as high as ~ 20 kpc.

(7) Figure 25, which is Fig. 7 with the thick-disk component removed leaving only halo stars, suggests that the Strömberg asymmetric-drift velocity increases monotonically with $\delta(0.6)$. The mean lag velocity and hence the mean rotation about the center listed in Table X is plotted in Fig. 26 as a function of [Fe/H], suggesting that spin-up has occurred for halo stars as the collapse proceeds. This conclusion is opposite from that reached by Norris (1986a) from a different sample, but Fig. 30 shows that the present data and those of Norris are nearly identical except for the lowest-metallicity, highest-asymmetrical-drift bin of Norris, which is the bin in which our data are *least* biased because the stars there have the highest velocity. One must, however, be cautious because the result depends on the validity of our distance scale.

(8) We have argued in several ways that the difference is not due to bias in our kinematically selected sample because the trend is toward *higher* velocities in Fig. 25 where our sample is optimal for discovery. To counter the increased $\langle V\rangle$ with δ for $\delta \geqslant 0.16$ we must be missing enough stars in the semiblank region of $|V| < 100$ km s^{-1} and $\delta > 0.24$ in Fig. 25 to keep $\langle V\rangle$ constant over the entire range $0.16 \leqslant \delta \leqslant 0.32$ if Norris is correct. A stronger argument that the progressive change of $\langle V\rangle$ with $\langle\delta\rangle$ in Fig. 26 is real at least for [Fe/H] > -1.6 is the increase of $\sigma(U)$ with δ (Figs. 27 and 28), following the required Strömberg $V(\text{lag}) \sim f[\sigma(U)^2]$ relation shown in Fig. 29.

(9) The escape velocity cannot be estimated easily from our sample until a star-by-star analysis is done to assess the effect of distance errors on the derived space velocities and until the phase-space bias is estimated. Figure 33 suggests that the *minimum* escape velocity at the solar circle is ~ 450 km s^{-1} from our data alone. The deeper sample of Carney and Latham suggests a higher value near 550 km s^{-1} which would require that ~ 8 times more mass is outside the solar circle than within it. Our value of 450 km s^{-1} requires that ratio to be ~ 3. A value as high as 650 km s^{-1} requires M_T (Local Group) $\simeq 8\times10^{12}\ M_\odot$ which contradicts the Kahn-Woltjer and the deceleration tests.

(10) The principal new results compared with ELS are (a) the presence of the strong Gilmore-Reid-Wyse thick-disk component of intermediate metallicity in our kinematically selected sample, (b) a strengthening of the evidence for a W,δ correlation for halo stars alone, requiring a chemical gradient in the high halo, and (c) the progressive change of

$\langle V \rangle_{lag}$ with increasing $\delta(0.6)$, suggesting spin-up with increasing collapse factor.

We can only conjecture how the thick disk formed, keeping within the general outline of the ELS picture. The intermediate [Fe/H] value for the thick disk is perhaps the central clue to its formation. We conjectured in Sec. V*a* that the strength of the gradient, and consequently the mean value of [Fe/H] at any height, depends on the ratio of the *ratio* of the dissipation rate (i.e., decay rate of the Z energy of position of the parent gas clouds) to the rate of metal enrichment. If there is no dissipation but only freefall, there will be no gradient, as emphasized by Searle and Zinn (1978).

Because there *is* a gradient in the high halo for $\delta \geqslant 0.16$ (Fig. 17) and a wide distribution of [Fe/H], and a much more collapsed spatial structure and a higher $\langle$[Fe/H]$\rangle$ for the thick disk, we conjecture that a nonlinear dissipation process took place—the closer to the plane the parent gas had plunged, the higher became pressure support and therefore the greater the dissipation rate, and hence the larger was [Fe/H] at a given height *late* in the collapse phase. To produce a semidiscrete structure such as a true thick disk separated from the halo phase requires a discontinuity in the dissipation rate, occurring when the scale height of the parent gas out of which the thick disk formed was at ~ 1 kpc. One can suggest that at the time when the collapse had proceeded to ~ 1 kpc height above the structure that was becoming the Galactic plane the collapse rate slowed *relative to the metal enrichment rate* (due to increased pressure support), permitting *higher* values of [Fe/H] at any height $Z \lesssim 1$ kpc than would have been obtained if the ratio of dissipation rate to enrichment rate had remained constant. The physics of the cooling rate is now the unaddressed issue in this paper.

These ideas are, of course, only the most general outline, consistent with the metallicity, spatial, and kinematic data relating to the thick disk. They are similar in kind to earlier discussions of the formation of the thick disk, for example, by Jones and Wyse (1983), Gilmore (1984b), and Gilmore, Reid, and Hewett (1985) with extensive prior references.

It is a pleasure to thank Kenneth Freeman, Gerard Gilmore, and John Norris for helpful discussions. Gilmore's detailed refereeing of the paper resulted in improvements and clarification of essential points. We are also grateful to Norris for his critical reading and suggestions concerning an original draft, and to Freeman and Gilmore for correcting an early error. It is a pleasure to thank Maria Anderson for her expert preparation of the manuscript in its many drafts.

This paper constitutes part of the last phases of the Mount Wilson Halo Mapping Project, which has been supported by NSF grant AST 82-15063 in the last semesters, for which we are grateful.

Finally, it only remains to acknowledge our debt to Olin J. Eggen and D. Lynden-Bell, who, over the past quarter of a century, have inspired the work on subdwarfs through the belief that the correlation of kinematics and chemical composition holds the essential clue, no matter how the details are debated among the protagonists, to the formation history of the Galaxy.

REFERENCES

Bahcall, J. N., and Soneira, R. M. (1980). Astrophys. J. Suppl. **44**, 73.
Bahcall, J. N., and Soneira, R. M. (1984). Astrophys. J. Suppl. **55**, 67.
Becker, W. (1970). Astron. Astrophys. **9**, 204.
Bond, H. E. (1980). Astrophys. J. Suppl. **44**, 517.
Bottlinger, K. F. (1933). Veröff. Berlin-Babelsberg **10**, No. 2.
Butler, D., Kinman, T. D., and Kraft, R. P. (1979). Astron. J. **84**, 993.
Caldwell, J. A. R., and Ostriker, J. P. (1981). Astrophys. J. **251**, 61.
Cameron, L. M. (1985). Astron. Astrophys. **146**, 59.
Carney, B. (1979a). Astrophys. J. **233**, 211.
Carney, B. (1979b). Astrophys. J. **233**, 877.
Carney, B., and Latham, P. (1985). Preprint.
Delhaye, J. (1965). In *Galactic Structure*, edited by A. Blaauw and M. Schmidt (University of Chicago, Chicago, IL), Chap. 4.
de Vaucouleurs, G., and de Vaucouleurs, A. (1972). Mem. R. Astron. Soc. **77**, 1.
Dressler, A., and Sandage, A. (1983). Astrophys. J. **265**, 664.
Eggen, O. J. (1962). R. Obs. Bull. No. 51.
Eggen, O. J. (1964). R. Obs. Bull. No. 84.
Eggen, O. J. (1978a). Astrophys. J. Suppl. **37**, 251.
Eggen, O. J. (1978b). Astrophys. J. **222**, 191.
Eggen, O. J. (1979). Astrophys. J. **229**, 158.
Eggen, O. J., Lynden-Bell, D., and Sandage, A. (1962). Astrophys. J. **136**, 748.
Eggen, O. J., and Sandage, A. (1962). Astrophys. J. **136**, 735.
Fenkart, R. (1967). Z. Astrophys. **66**, 390.
Fouts, G., and Sandage, A. (1986). Astron. J. **91**, 1189 (Paper V).
Freeman, K. C. (1975). In *Galaxies and the Universe*, "Stars and Stellar Systems," edited by A. Sandage, M. Sandage, and J. Kristian (University of Chicago, Chicago, IL), Vol. 9.
Fricke, W. (1949a). Astron. Nachr. **277**, 241.
Fricke, W. (1949b). Astron. Nachr. **278**, 49.
Gilmore, G. (1984a). In *Science from Measuring Engines* (Royal Greenwich Observatory, East Sussex, England) (in press).
Gilmore, G. (1984b). Mon. Not. R. Astron. Soc. **207**, 223.
Gilmore, G., and Reid, N. (1983). Mon. Not. R. Astron. Soc. **202**, 1025.
Gilmore, G., Reid, N., and Hewett, P. (1985). Mon. Not. R. Astron. Soc. **213**, 257.
Gilmore, G., and Wyse, R. F. G. (1985). Astron. J. **90**, 2015.
Gliese, W. (1969). Veröff. Astron. Rechen-Instituts, Heidelberg, No. 22.
Greenstein, J. L. (1965). In *Galactic Structure*, "Stars and Stellar Systems," edited by A. Blaauw and M. Schmidt (University of Chicago, Chicago, IL), Vol. 5, p. 361.
Harris, W. E. (1981). Astron. J. **86**, 719.
Harris, W. E., and Canterna, R. (1979). Astrophys. J. Lett. **231**, L19.
Harris, W. E., and Racine, R. (1979). Annu. Rev. Astron. Astrophys. **17**, 241.
Hartkopf, W. I., and Yoss, K. M. (1982). Astron. J. **87**, 1679.
Hartwick, F. D. A. (1987). In preparation.
Illingworth, G. (1977). Astrophys. J. Lett. **218**, L43.
Isobe, S. (1974a). Astron. Astrophys. **36**, 327.
Isobe, S. (1974b). Astron. Astrophys. **36**, 333.
Jones, B. J. T., and Wyse, R. F. G. (1983). Astron. Astrophys. **120**, 165.
Jones, D. H. P. (1962). R. Obs. Bull. No. 52.
Kahn, F. D., and Woltjer, L. (1959). Astrophys. J. **130**, 705.
Kapteyn, J. C. (1922). Astrophys. J. **55**, 302.
Keenan, P. C., and Keller, G. (1953). Astrophys. J. **117**, 241.
Kormendy, J., and Illingworth, G. (1982). Astrophys. J. **256**, 460.
Lindblad, B. (1925a). Uppsala Medd. No. 3.
Lindblad, B. (1925b). Ark. Mat. Astron. Och. Fysik. **19a**, No. 21.
Lindblad, B. (1959). In *Handbuch der Physik*, edited by S. Flügge (Springer, Berlin), Vol. 53, p. 21.
Mihalas, D., and Binney, J. (1981). *Galactic Astronomy* (Freeman, San Francisco).
Norris, J. (1986a). Astrophys. J. Suppl. **61**, 667.

Norris, J. (1986b). Astrophys. J. **307**, 123.
Norris, J. (1986c). Private communication.
Norris, J., Bessell, M. S., and Pickles, A. J. (1985). Astrophys. J. Suppl. **58**, 463.
Oort, J. H. (1965). In *Galactic Structure*, "Stars and Stellar Systems," edited by A. Blaauw and M. Schmidt (University of Chicago, Chicago, IL), Vol. 5.
Pagel, B. F. J., and Patchett, B. E. (1975). Mon. Not. R. Astron. Soc. **172**, 13.
Roman, N. G. (1954). Astron. J. **59**, 307.
Roman, N. G. (1957). Astron. J. **62**, 146.
Saio, H., and Yoshii, Y. (1979). Publ. Astron. Soc. Pac. **91**, 553.
Sandage, A. (1969). Astrophys. J. **158**, 1115 (Paper II).
Sandage, A. (1981). Astron. J. **86**, 1643 (Paper III).
Sandage, A. (1986). Astrophys. J. **307**, 1.
Sandage, A. (1987). Astron. J. (in press).
Sandage, A., and Fouts, G. (1987). Astron. J. (in press).
Sandage, A., and Kowal, C. (1986). Astron. J. **91**, 1140 (Paper IV).
Sandage, A., and Visvanathan, N. (1978). Astrophys. J. **223**, 707.
Schwarzschild, M. (1952). Astron. J. **57**, 57.
Searle, L., and Zinn, R. (1978). Astrophys. J. **225**, 357.
Spitzer, L. (1942). Astrophys. J. **95**, 329.
Strömberg, G. (1924). Astrophys. J. **59**, 228.
Strömberg, G. (1925). Astrophys. J. **61**, 363.
Toomre, A. (1980). Private communication.
Trumpler, R. J., and Weaver, H. F. (1953). *Statistical Astronomy* (University of California, Berkeley, CA), Chap. 6.3.
Twarog, B. A. (1980a). Astrophys. J. **242**, 242.
Twarog, B. A. (1980b). Astrophys. J. Suppl. **44**, 1.
VandenBerg, D. A., and Bell, R. A. (1985). Astrophys. J. Suppl. **58**, 561.
Wallerstein, G. (1962). Astrophys. J. Suppl. **6**, 407.
Wallerstein, G., and Carlson, M. (1960). Astrophys. J. **132**, 276.
Wilson, R. F. (1953). *General Catalogue of Stellar Radial Velocities*, Carnegie Institution of Washington Publication No. 601 (Carnegie Institution of Washington, Washington, DC).
Woolley, R. V. d. R. (1957). Mon. Not. R. Astron. Soc. **117**, 198.
Wyse, R. F. G., and Gilmore, G. (1986). Astron. J. **91**, 855.
Yoshii, Y., Ishida, K., and Stobie, R. S. (1987). Astron. J. (in press).
Yoss, K. (1986). In preparation.
Zinn, R. (1978). Astrophys. J. **225**, 790.
Zinn, R. (1980). Astrophys. J. Suppl. **42**, 19.
Zinn, R. (1985). Astrophys. J. **293**, 424.